Sudan University of science and Technology

Collage of Graduate Studies

Investigation of Toxic Molecules in some Artificial Sweeteners using Raman Spectroscopy

الكشف عن الجزيئات السامة في بعض المُحلِيات الصناعيه بإستخدام مطيافيه رامان

A Thesis Submitted in Fulfillment of the Requirements for the Degree of Ph.D. in Laser Applications in physics

By

Ahmed Abubaker Mohamed Taher

Supervised by:

Prof. Dr.Abul Moneim. M. Awad elgied

CO. supervisor:

Dr. Sohad Saad Elwakeel

July 2019

الآيه

(وَلَا تَقْفُ مَا لَيْسَ لَكَ بِهِ عِلْمٌ ۚ إِنَّ السَّمْعَ وَالْبَصَرَ وَالْفُؤَادَ كُلُّ أُولَٰئِكَ كَانَ عَنْهُ مَسْئُولًا)

(36)الإسراء

صدق الله العظيم

Dedication

I dedicate this work

To

My parents, Brothers, teachers And All my Family members

Acknowledgement

First of all thanks to god for guiding me to conduct this study secondly I would like to thank my supervisor ***DrAbdulmuniem. Awadelgied*** *,* ***Dr.sohadsaadAlwakeel*** *and my X-supervisor* ***Prof.Dr.Nafie .A.Almuslut****.they have always been there for me ,helping me encouraging me ,and made me believe in myself and in my work . I am grateful to have a supervisor who is so passionate about the field of laser science; discussion with them has always been a source of inspiration for me. Also am heartily thankful to Dr.****Abdu Elsakhy Mohamed*** *–Elneelin University and* ***Mohamed ahmed Baba*** *–sudan university of science and technology.*

This research was performed using facilities at Micro and Nano Characterization Facility (MNCF), CeNSE, IISc, funded by Ministry of Electronics and Information Technology, and Department of Science and Technology Govt. of India'

Ahmed

Abstract

The field of this research was materials characterization using Raman spectroscopy technique. The aim of this research is to investigate the toxic molecules in some artificial sweeteners using Raman spectroscopy.

Six samples of artificial sweeteners (Tropicana slim, Steviana and süssina) were used in this study as follows; one powder and one liquid sample of each of the three brands of sweeteners (Tropicana slim ,Steviana and süssina) was prepared

HCl acid was used as a solvent for the samples to study the effect of the acidity, as well as to study the effect of temperature on the structure of the sweeteners. The samples were collected from commercial markets in Khartoum.

The analysis of the Raman spectra were performed for the Raman peaks of the three powder samples (Tropicana slim ,Steviana and süssina) at wavenumber values ; (263.0, 342.0, 415.0, 599.0, 642.0, 773.0, 1446, 876.0, 936.0, 1054.0, 1091.0, 1129.4, 1250.0, 1325.0,and 1369) cm^{-1} , these Raman peaks are attributed to the natural sweetener (sorbitol) ($C_6H_{14}O_6$).

The analysis of the Raman spectra were performed for Raman peaks of the powder sample (süssina) at wavenumber values; (622.4, 818.0 cm^{-1}) these Raman peaks are attributed to the toxic artificial sweetener (Aspartame) ($C_{14}H_{18}N_2O_3$), and Raman peaks at (711.0, 1032, 1154.0, 1300.0 cm^{-1}) these Raman peaks are attributed to the toxic artificial sweetener (saccharine) ($C_7H_4NNaO_3S$).

It was found that Tropicana Slim powder and Steviana powder contain natural sorbitol molecules ($C_6H_{14}O_6$) with high concentration and do not contain any of the toxic artificial Aspartame ($C_{14}H_{18}N_2O_3$) and saccharin ($C_7H_4NNaO_3S$) molecules.

Whereas it was found that (süssina) powder contains molecules of toxic artificial sweetener Aspartame ($C_{14}H_{18}N_2O_3$) and Saccharine ($C_7H_4NNaO_3S$) molecules with high concentration.

From Raman spectral analysis of the dissolved samples (Tropicana slim and steviana) was found that they contain natural molecules of sorbitol

with low concentration but it disappeared in the dissolved sample (süssina). However, the result of Raman spectral analysis of dissolved sample (süssina) revealed that it contains magnesium carbonate ($MgCO_3$) at the wavenumber value (1117.0) cm^{-1} which is nontoxic molecule with low concentration, while it disappeared in the other samples.The results obtained in this study were in good agreement with the literature.

المستخلص

يُعد هذا البحث ضمن مجال توصيف المواد بإستخدام تقنية مطيافية رامان. يهدف هذا البحث الى الكشف عن الجزيئات السامة في بعض المُحليات الصناعية باستخدام مطياف رامان. أُستخدمت في هذه الدراسة ستة عينات من المُحلِيات الصناعية في شكل مواد سائلة وصلبة (تروبيكانا سليم ، ستيفانا وسوسينا) على النحو التالي ؛ تم تحضير عينة صلبه وعينة مُذابة من كل عينة من المُحليات الثلاث (Tropicana slim ,Steviana and süssina)والتي تم جمعها من الأسواق التجارية بالخرطوم.أُستخدِم حمض الهيدروكلوريك كمذيب للعينات لدراسة تأثير الحموضة وكذلك دراسة أثر درجة الحرارة على بنية هذه المُحلِيات الصناعية.
تم إجراءالتحليل لأطياف رامان على قمم عينات المسحوق الثلاث (تروبيكانا سليم ، ستيفيانا وسوسينا) عند قيم الاعداد الموجيه ;(263.0 ، 342.0 ، 415.0 ، 599.0 ، 642.0 ، 642.0 ، 773.0 ، 1446 ، 876.0 ، 936.0 ، 1054.0 ، 1091.0 ، 1129.4 ، 1250.0 و 1325.0 و 1369) سم $^{-1}$ ، تُنسب هذه الاعداد الموجيه إلى جزيئات السكر الطبيعي السوربيتول ($C_6H_{14}O_6$).
ومن ثم تم إجراء التحليل الطيفي لقمم رامان في عينة المسحوق :(süssina) عند قيم الاعداد الموجية (622.4 ، 818.0 سم $^{-1}$) وتُعزى هذه الاعداد الموجيه إلى جزيئات المُحلى الصناعي الساماالأسبارتام ($C_{14}H_{18}N_2O_3$) كما تم رصد قمم رامان عند الاعداد الموجية (711.0 ، 1032 ، 1154.0 ، 1300.0) سم $^{-1}$والتي تنسب إلى جزيئات المحلى الصناعي السام السكرين ($C_7H_4NNaO_3S$)

وقد وُجد ان مسحوق تروبيكانا سليم ومسحوق إستيفيانا يحتويان على (جزيئات) السوربيتول الطبيعية($C_6H_{14}O_6$) و بتراكيز عاليه ولا تحتويان علي اي من جزيئات المُحليات الصناعيه السامة الأسبارتام ($C_{14}H_{18}N_2O_3$) والسكرين($C_7H_4NNaO_3S$) .

بينماوُجد ان مسحوق الُمحلى الصناعي (süssina)يحتوي علي جزيئات المُحلى الصناعي السامة الأسبارتام($C_{14}H_{18}N_2O_3$) وجزيئات المُحلى الصناعي السامة السكرين ($C_7H_4NNaO_3S$)بتركيز عالي جدا.

كما وُجد من تحليل طيف رامان للعينات المُذابه من عينات التروبيكانا سليم والاستيفياناأنهما يحتويان على جزيئات السوربيتول الطبيعي ولكن بتراكيز منخفضه بينما إختفت جزيئات مادة السوربيتول في عينه محلول السوسينا، كذلك وُجد من تحليل طيف رامان لعينة محلول (الاستيفيانا)انها تحتوي علي جزيئات ماده كربونات الماغنيزيوم غير السامة ($MgCO_3$) بتركيز منخفض عند قيمة العدد الموجي (1117.0 cm^{-1}), والذي ينسب لجزيئة كربونات الماغنيزيوم بينما إختفت في محلول عينتي التروبيكانا والسوسينا.

النتائج التي تم الحصول عليها في هذه الدراسه كانت تتفق بصورة جيدة مع الدراسات السابقه.

Table of Contents

Chapter One

1.1 Introduction:

Spectroscopy is the branch of science that dealing with the study of interaction of electromagnetic radiation with matter.The mostimportant consequence of such interaction is absorption or emission by the matter in discreteamounts called quanta. The ways in which the measurement of radiation frequency (absorbed or emitted) made experimentally, and the energy levels deduced from these, comprise the practice of spectroscopy.

The various branches of spectroscopy generally involve measurements of two experimental parameters:

- The energy of radiation absorbed or emitted by the system
- Intensity of the spectral lines

  In most branches of spectroscopy, the system interacts with the electric component of the light. However, in case of magnetic resonance spectroscopy it interacts with the magneticfield. Spectroscopy is one of the most powerful tools available for the study ofatomic and molecular structure and is used in the analysis of awide range of samples(Ayden R. wood, 2008).

1.2Molecular spectra:

When a molecule emits or absorbed a photon, its energy decreased or increased and one or more of the vibrational or rotational quantum numbers change. The important possibilities are:

i. Rotational spectra arise when the rotational quantum numbers changed and occur in the far infrared and microwave regions.
ii. Electron spin resonance involves achange in the direction of the resultant spin in the presence of the magnetic field.

iii. Nuclear magnetic resonance involves a change in the direction of nuclear spin quantum number in presence of magnetic field. When nuclei or electrons of certain elements are subjected to a strong magnetic field, additional quantized energy levels are produced as aresult of magnetic properties of these elementary particles. With nuclei ,waves ranging from 10- 200 MHz are normally employed (NMR) nuclear magnetic resonance , while for electrons; microwaves with frequencies between (1000 - 2500) are observed (ESR) electron spin resonance.

iv. electron spectra occur in visible and ultraviolet regions and arise when the electronic energy levels changes ,normally accompanied by changes in the rotational and vibrational energy levels.

v. vibrational rotational spectra arise when the vibrational quantum number(v) change, possibly with simultaneous change in the rotational quantum number(J) .these spectra are found in near infra region .

Raman spectra involve change in the vibrational and rotational energy levels (Ayden R.wood.et.al., 2008).

1.3Molecular energy levels and spectroscopy:

1.3.1 Translational energy levels:

The translational energy levels of amolecule are usually taken to be those of aparticle in athree- dimensional box

$$E(n_x, n_y, n_z) = \left(\frac{n_x^2}{I_x^2} + \frac{n_y^2}{I_y^2} + \frac{n_z^2}{I_z^2}\right), \qquad (1.5)$$

In general separation of the translational energy levels is many orders of magnitude smaller than KT, even for abox with dimensions on the order

of molecularsizes. The translationalbehavior of the molecules therefore appears to be classical.

1.3.2 Rotational energy levels –Diatomic molecules:

For the purposes of studying the rotational spectra of molecules it is essential to classify them according to their principal moments of inertia

The moment of inertia ***I*** of any molecule about any axis through the centre of gravity is given by

$$I = \sum m_i r_i^2 \qquad (1.6)$$

Where$\boldsymbol{m_i}$and$\boldsymbol{r_i}$are the mass and distance of atom***i***from the axis. There is one of these axes,conventionally labeled the***c***axis, about which the moment of inertia has its maximum valueand a second axis, labeledthe***a***axis, about which the moment of inertia has its minimumValue. It can be shown that the***a***and***c***axes must be mutually perpendicular. These, togetherwith a third axis, the ***b***axis, which is perpendicular to the other two, are called the principalaxes of inertia and the corresponding moments of inertia$\boldsymbol{I_a}$, $\mathbf{I_b}$ and$\mathbf{I_c}$are the principalmoments of inertia. In general, according to convention,

$$I_c \geq I_b \geq I_a, \qquad (1.7)$$

For a linear molecule, such as HCN in figure1.3(a)

$$I_c = I_b > I_a = 0\,, \qquad (1,8)$$

Where the **b** and the **c** axis may be in any direction perpendicular to the inter nuclear ***a***axis. Considering the nuclei as a point masses on the **x**axis, it is clear that $\mathbf{I_a}$must be zero since all the$\mathbf{r_i}$in equation (1.6) are zero.

For asymmetric rotor, or symmetric top as it is sometimes called, two of the principal moments of inertia are equal and the third is non-zero .

If the molecule is a prolate symmetric rotor figure1.3 (b) .

$$I_c = I_b > I_a \ , \qquad (1,9)$$

Figure1.3(b) shows the example of methyl iodide.

Since the heavy iodine nucleus makes no contribution to I_a

a, which is therefore relativelysmall, the molecule is a prelate symmetric rotor. The benzene molecule, shown in Figure1.3 (c), is an oblate symmetric rotor for which

$$I_c > I_b = I_a \ , \qquad (1,10)$$

As for I_c and$I_b$in methyl iodide, it is not immediately obvious that $I_b$and$I_a$in benzene areequal, but simple trigonometry will prove this.

A symmetric rotor must have either $C_n$axis with $n > 2$,or anS_4axisMethyl iodide has aC_3axis and benzene aC_6axis and, therefore, theseare symmetric rotors whereas allene, is also a symmetric rotor sinceit has an S_4axis which is theaaxis: allene is a prolate symmetric rotor.A spherical rotor has all three principal moments of inertia equal:

$$I_c = I_b = I_a \ , \qquad (1,11)$$

as is the case for methane and sulphur hexafluoride, shown in Figures 1.3(d) and 1.3 (e). Infact, all molecules belonging to either the T_d

orO_h point group are spherical rotors.

An asymmetric rotor has all principal moments of inertia unequal:

$$I_c \neq I_b \neq I_a \ , \qquad (1,12)$$

An example of an asymmetric rotor, a category which includes the majority of molecules, isformaldehyde, shown in Figure 1.3 (f). However, for many asymmetric rotors, either:

$$I_c \backsimeq I_b > I_a \ , \qquad (1{,}13)$$

And the molecule is known as a prolate near-symmetric rotor, or:

$$I_c > I_b \backsimeq I_a \ , \qquad (1{,}14)$$

When it is known as an oblate near-symmetric rotor (J.MichalHollas. 2004).

An example of the former is s-trans-acroleinFigure 1.3 (g)) and an example of the latter is pyrazineFigure 1.3 (h).

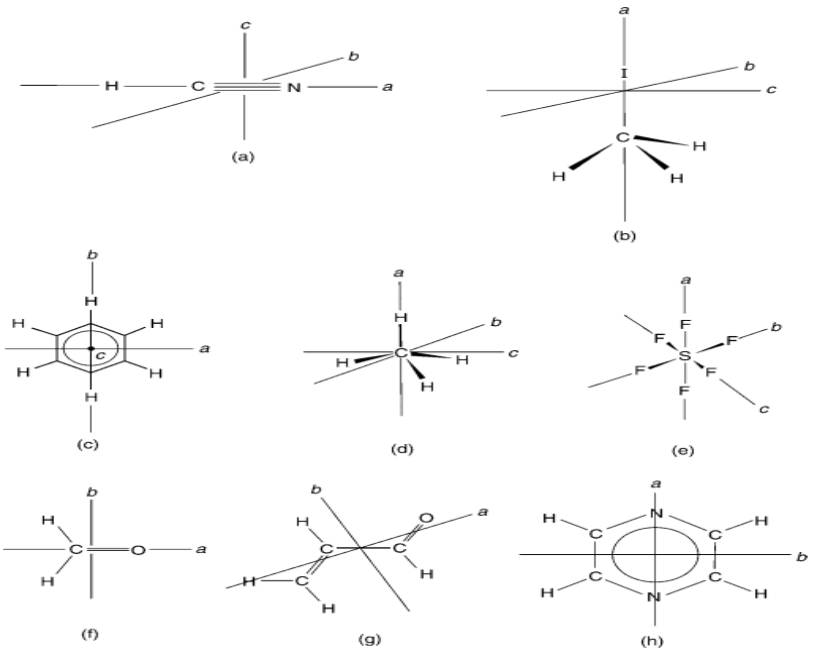

Figure (1.1)Principal inertial axes of (a) hydrogen cyanide, (b) methyl iodide, (c) benzene, (d) methane, (e) sulphur hexafluoride, (f) formaldehyde, (g)s-trans-acrolein and (h) pyrazine(John R. Ferraro, 2003).

1.3.3Rotational energy levels- poly atomic molecules:

Polyatomic molecules may rotate about the ,x ,y, and z axes or some combination of the three. They have moments of inertia,I_x,I_y ,I_z .Associated with each axes. And also corresponding rotational constantsA,Band C $\left[A = \frac{h}{(8\pi^2 cI_x)} \ , B = \frac{h}{(8\pi^2 cI_y)} , C = \frac{h}{(8\pi^2 cI_Z)}\right]$

The general equation for moment of inertia is

$$I = \sum_i m_i r_i^2 \qquad (1.15)$$

Where the sum is over the atoms in the molecule,m_i is the mass of atom*i* and r_i its distance from the rotation axis.

In general, the rotational constants A, B, and C may all be different and a molecule for which this is true is called an asymmetric top. The spectroscopy of such a molecule is quiet complicated. Instead, we will look atsymmetric top molecules, such as CH_3F,CH_3Cl,CCl_3H or benzene, for which two of the rotational constants are equal. Symmetric tops may be divided into prolatetops,for which B >A,C (e.g. CH_3F,CH_3Cl) and oblate tops, for which B < A.C,(e.g CCl_3H , benzene).

The rotational motion of asymmetric top molecule is described by three quantum numbers:

- J- is the total angular momentum
- K- is the projection of J onto the principal axis of the molecule
- M_J-is the projection of J onto some chosen lab-frame z axis (often just written M).Regardless of which category the molecules falls into ,the rotational energy is given approximately by

$$(J, K) = B_J(J + 1) + (A - B)K^2 \qquad (1.16)$$

When centrifugal distortion is included this becomes.

$$E\ (J,K) = B_J(J+1) + \ (A-B)K^2 - D_J J^2(J+1)^2 - D_J K_J (J+1)K^2 - D_K K^4 \quad (1.17)$$

The selection rules for asymmetrictop molecule are, $\Delta J = \pm 1$, $\Delta K = 0$

Transition energies and line separations may be calculated in a similar way to that worked through above for diatomic molecules by determining - $E(J+1.K) - E(J,K) \ldots etc$ (1.17)

1.3.4 Vibrational spectroscopy of diatomic molecules:

To a first approximation. The vibrational energy levels $E_V$of a diatomic molecule, treated in the harmonic oscillator approximation, are given by

$$E(V) = \left(V + \frac{1}{2}\right) h\nu \ , \qquad (1.18)$$

Where the vibrational quantum number v = 0,1,2,3,…. The classical vibrational frequency isv related to the reduced mass μ ,

$\mu = \left[\frac{m_1+m_2}{m_1 m_2}\right]$and the force constant K by $\nu = 1/2\pi(k/\mu)$The force conistant can be regarded as ameasure of the strength of the spring in the ball and spring model for molecular vibration[3].

$$E(V) = \left(V + \frac{1}{2}\right) \omega_e \ , \qquad (1.19)$$

This is usuallya fairly good approximation near the bottom of the potential well where the potential closely resembles that of aharmonic oscillator. However, real molecules have an harmonic potentials, and this is taken into account by rewriting the energy as aseries expansion, with successively higher order correction terms:

$$E(V) = \left(V + \frac{1}{2}\right)\omega_e - \left(V + \frac{1}{2}\right)^2 \chi_e \omega_e + \left(V + \frac{1}{2}\right)^3 y_e \omega_e + \cdots \qquad (1.20)$$

Often the firstcorrection term. Involvingω_e , $\chi_e$will be used, but note that the course of differences in calculated and measured properties involving vibrational energy levels is frequently neglected of higher order terms.note that every vibration has azero point energy ($Z\ P\ E$) found by substituting v = 0 into the above equation

$(ZPE) = E(0) = \frac{1}{2}\omega_e - \frac{1}{4}\chi_e\omega_e$. The energy levels in anharmonicoscillator are equally spaced by an energy ω_e .

The effect of anharmonicityis that the levels get increasingly closer together as the vibrational quantum number v increases until eventually there is no difference in energy between successive quantum states and the energy levels form a continuum.the energy at which this occurs consides with the point at which the potential energy function reaches zero and the molecule is no longer bound(this is the reason why the energy levels are no longer quantized). The dissociationenergy may be measured either from the bottom of the potential .in which case it is called D_e. Or from the zero point energy, in which case itcalled D_0.

$$\left(\frac{dE}{dV}\right) = 0 = \omega_e - 2\left(V_{max} + \frac{1}{2}\right)\chi_e\omega_e \rightarrow \left(V_{max} + \frac{1}{2}\right)^2 = \frac{\omega_e}{2\chi_e\omega_e} \ldots \quad (1.21)$$

Substituting back into the energy expression above gives

$$\mathrm{D_e} = \mathrm{E}(V_{max}) = \frac{\omega_\mathrm{e}^2}{4\chi_\mathrm{e}\omega_\mathrm{e}} (1.22)$$

D_e and D_0 related to$D_0 = D_e - E(0)$.

Physically the strength of the spring representing the bond which is affected by asubtle balance of nuclear repulsions, electron repulsions and electron nuclear attractions. None of these is affected by nuclear mass and therefore *K* is not affected by isotopicsubstitution (J.MichalHollas, 2004)

1.4.5 Rovibrationalspectroscopy:

In many aspects the vibration- rotationtransition of linear polyatomic molecules closely resembles those of polyatomic molecules. The molecular symmetry of linear poly - atomic molecules is either$D_{\infty h}$ or $C_{\infty V}$and there are $3N-5$ modes of vibrations. The numbers and types of normal modes can be quietlydetermined for all linear molecules. If they are N atoms, then there will be $N-1$stretching frequencies and

$\frac{((3N-5)-(N-1))}{2} = N-2$ Bendingfrequencies.

In the case of symmetric molecules of,$D_{\infty h}$symmetry the g or *u* labels need to be added by symmetrizing the stretching of bonds or the bending of the molecule.

The fundamental vibrational transitions of linear molecules are either of the $\sum - \sum$(parallel) type for stretching modes or of the $\pi - \sum$(perpendicular) type for bending modes. For symmetric linear molecules, which belong to $D_{\infty h}$ point group, g and u subscripts are needed.

The terms parallel and perpendicular are used because the transition dipole moment is either parallel (μ_z)or perpendicular$\mu_x$andμ_y to the molecular z axis , allowed parallel transitions arise from the $\mu_z$component of the transition dipole moment with σ_u^+symmetry,while allowed perpendicular transitions arise from μ_x andμ_y components, the $\sum - \sum$transitions can have P and R branches only , so that the appearance of the spectrum closely resembles that of the infrared spectrum of a diatomic molecule.

The rotational energy levels associated with the Π state of doubly degenerated because L = ± 1, where 1 is the quantum number of vibrational

angular momentum. As the molecule begins to rotate, the two components for agiven J begin to split slightly because of the interaction of the rotational angular momentum (J) with vibrational angular momentum (L).

The splitting Δv is proportional to$L$ and q is called the L- type bonding constant. It is useful to use parity labels to distinguish the two nearly degenerate levels for each$J$ .There are many different types of parity, but the two most common varieties are total parity and$\frac{e}{f}$parity (Peter F ,Bernath, 2005).

$$E(V,J) = \left(V+\frac{1}{2}\right)^2 \omega_e - \left(V+\frac{1}{2}\right)^2 \chi_e\omega_e + B_V J(J+1) - D_J J^2(J+1)^2 \ldots \quad (1.23)$$

Transition between the $E(V,J)$ levels in which v changes correspond to absorption of energy in the infrared region of the spectrum.

The gross selection rules for a vibrational transition is $d\mu dt \neq 0$, if the vibrations are approximated as simple harmonic oscillators, the specefic selection rule is $\Delta v = \pm 1$. Since real vibrations are anharmonic,in reality there are contributions from $\Delta V = \pm 2, \Delta V \pm 3$, etc, a change in vibrational quantum number v is often accompanied by a change in rotational quantum number J, according to the selection rule $\Delta J = 0, \pm 1$so, we talk about rovibrational (or vibrational) transitions, rather than simply vibrational transitions, this could arise from a bending vibration or from the electronic angular momentum of an unpaired electron(e.g OH,NO) .

Transition between two vibrational states gives rise to avibrational band ,made up of P,Q and R branches, corresponding to transitions between rotational states with $\Delta J = -1, 0$ (if allowed) and populations of energy levels and spectral line intensities- the Poltzman distribution the intensities of lines in spectrum depend up on aline strength factor related

to the overlap between the wave functions of the two states, the light intensity, and the population of the lower state. Within a givenrotational or vibrational spectrum, the lower state populations are usually the dominant factor. Under thermal condition these are given by the Poltzman distribution

$\frac{n_i}{n_0} = g_i \exp\left(-\frac{E_i}{kt}\right)$. Where$g_i$ is the degeneracy andE_i is the energy (relative to the ground state) of the state i . as aconsequence, we can predictthe most intense peak in arotational or rovibrational spectrum by maximizing the postman distribution to find the most highly populated rotational state at giventemperature. For rotational lines, the above equations becomes

$$n_J/n_0 = (2J+1)\exp\left[-\frac{B_J(J+1)}{kT}\right] \qquad (1-24)$$

Setting the first derivativeequal to zero and solving for J_{max} .

$$j_{max} = \frac{1}{2}\sqrt{\frac{2kt}{B}}\frac{1}{-2} \qquad (1.25)$$

1.5molecularabsorption spectroscopy:

Transitions within the molecules are usually studied by the selective absorption of radiation passing through them and less commonly by emission processes such as fluorescence and phosphorescence. When molecules absorb energy and get excited than either of the following energy changes occur:

(a) Transition of one electron to high energy level.

(b) Change in the intermolecular vibrations of the molecule.

(c) Change of moment of inertia of the molecule around its center of gravity.

(d) Transitions between electronic levels are found in the ultra violet and visible regions.

(e) Transitions between vibrationallevels, butwithin the same electronic levels are found in near and mid infrared regions.

(f) Transition between neighboring rotational levels are found in far infra-red and microwave regions.

Electronic transitionsinvolvejumps and to from the various sublevels and the resulting UV absorption spectra are observed in the form of aband because of the superimposition of vibrational and rotational energies on electronic energy, but its fine structure is also frequently observed.

Fore still fine structures gaseous samples are preferred over liquid samples or else the samples should be cooled within the help of liquidnitrogen.

The absorption of X-Ray results into transitions between inner shell electrons of the atoms while only valance electrons are involved in the transitions when visible or UV region is absorbed. In case of lighter elements X-Ray absorption spectra is independent of the element is in the free or combined state. However, visible and UV spectra are effected by the environment around the element(DR.H.Kaur, 2001).

1.6 Problem statement:

there is an urgent need to investigate the components of the Artificial sweeteners, which are now being used extensively especially by diabetes and obesity and have entered most of the food industries, some of them contain natural sweet compounds, Others contain artificial sweet chemical additives .these artificial chemical additives are now being banned by many countries because these materials are dangerous and harmful to health and still under study because they contain toxic chemical additives, also in markets there are pure sweeteners or sweeteners mixed with these industrial chemical additives.

1.7 Objectives Of the research:

The main objectives of this study:

- Characterization the commercial artificial sweeteners (Tropicana slim, Steviana and*süssina*).
- Investigation of artificial sweet chemical additives molecules (Aspartame, saccharine, Maltodextrin , Acesulfame K,

  and Dextrose) in some artificial sweeteners using Raman spectroscopy. The efficiency of this technique is the detection of change in the structure can be used as an indication of the toxic molecules as a fast, sensitive and accurate diagnostic technique for such molecules.

1.8 Research Methodology:

The methodology in this research:

the characterization will be done for Six samples of artificial sweeteners (Tropicana slim ,Steviana and süssina) using laser Raman Microscope

spectrometer Model Horiba Lab RAMHR 3D with laser wavelength is 532 nm and output power of 6 mW in the range from 50 to 4000 cm^{-1}.

as follows ; two samples of Tropicana slim (powder and liquid), two samples of Steviana (powder and liquid) and two samples of süssina (powder and liquid). HCl acid (25 mL) with (PH 3.I) and boiled mineral water (25mL) were used as a solvent for the samples to study the effect of the acidity and temperature on the structure of the sweeteners,

Then the spectroscopic analysis will be done for the obtained peaks of the wavenumbers from the materials under study .then the matching will be done by using the Molecular spectroscopy Database and the previous research and studies and the matching the results to make the characterization and investigation for the materials under study .

1.9 Thesislayout:

This thesis contains four chapters:

Chapter one presents the introduction of spectroscopy, the spectroscopic techniques, problem statement, Objectives Of the research. Chapter Two discuss the fundamentals and applications of Raman spectroscopy in classical and quantum images, Raman spectrometers, types of Raman

Spectroscopy, applications of Raman spectroscopy, The Artificial sweeteners and literature review.

Chapter Three covers the practical side, methods of collection of samples, Raman setup and procedure. Chapter Four deals with the obtained results, the analysis of Raman spectra, the discussion of the results, the comparison with other results, conclusions and recommendations.

Chapter two

Raman Spectroscopy

2.1 Introduction:

In 1922, ChandrasekharaVenkata Raman an Indian professor of physics, at the University of Calcutta, working on light interaction with liquids published the first of a series of papers with his collaborator K. SKrishnan. The first paper entitled ‘‘Molecular Diffraction of Light’’ ultimately led to his famous discovery on 28 February 1928. A week earlier, two Russian professors – G. S. Landsberg and L. I. Mandelstam – working at Moscow State University on light interaction with crystals since 1926 reported, independently the same phenomenon. The observed phenomenon indicated that when light is scattered by matter a small percentage of the scattered light will have a frequency that is different from the frequency of the incident light.The observed shift in the scattered frequency is the result of a combination between the frequency of the incident light and the frequency of molecular motion of the interacting material. In Russian literature, the phenomenon is known as combinatorial scattering of light. In the rest of the world, the phenomenon is known as the Raman Effect.C. V. Raman received the Nobel Prize in Physics in 1930. Seventy years after its discovery, in 1998, the Raman Effect was designated by the American Chemical Society as a National Historical Landmark in recognition of its significance as a tool for analyzing materials systems(Maher .S. Amer, 2010).

Sir Raman used sun light as the source and a telescope as the collector; theDetector was his eyes. That such a feeble phenomenon as the Raman scattering was detected was indeed remarkable.

Rotational and Vibrational Frequencies of a molecule can be adjunct to electronic and infrared spectra. Raman Effect may be defined as a phenomenon due to which the scattering of light has slightly different frequency from that of incident light and there occurs a change in the atomic oscillations within the molecule. Raman Effect has been important as a method for the elucidation of molecular structure, for locating functional groups or chemical bonds in the molecules.

Raman spectrum can be used for finger print identification like the IR spectrum. In this technique sample preparation requires careful filtration to remove all traces of suspended matter.Fluorescent impurities must be excluded if a blue source is used.Temperature control is not usually required but spectra of cooled samples may give a fine structure. Transformation of energy is considered in terms of stokes and anti- stokes lines in Raman spectroscopy (Peter F .Bernath, 2005).

2.2 Basic Considerations:

Raman scattering may be regarded as an inelastic collision of an incident photon $\hbar\omega_i$with a molecule in the initial energy levelE_i (Fig. 3.1a-c). Following the collision, a photon$\hbar\omega_s$ with lower energy is detected and the molecule isfound in a higher-energy level $E_f$as shown in Eq(2.1a)

$$\hbar\omega_{\mathrm{i}} + \mathrm{M}(\mathrm{E_i}) \rightarrow \mathrm{M}^{*}(\mathrm{E_f}) + \hbar\omega_{\mathrm{s}}\,, \quad \hbar(\omega_{\mathrm{i}} - \omega_{\mathrm{s}}) = \mathrm{E_f} - \mathrm{E_i} > o. \qquad (2.1a)$$

The energy difference$\Delta E = E_f - E_i$may appear as vibrational, rotational orelectronic energy of the molecule.

If the photon $\hbar\omega_i$is scattered by a vibrationally excited molecule, it may

Gain energy and the scattered photon has a higher frequencyω_{as} as shown in (Fig. 3.1c),where

$$\hbar\omega_{as} = \hbar\omega_i + E_i - E_f, \quad E_f > E_i\,, \qquad (2.1b)$$

This "superelastic" photon scattering is called anti-Stokes radiation.

In the energy level scheme figure (2.1.b) the intermediate state$E_V = E_i + \hbar\omega_i$of the system "during" the scattering process is often formally described as a virtual level, which however, is not necessarily a "real" stationary Eigen state of the molecule. If the virtual level coincides with one of the molecular Eigen states, one speaks of the resonance Raman Effect. A classical description of the vibrational Raman Effect has been developed by Placek (Wolfgang Demtröder, 2008).

It starts from the relation

$$P = \mu_0 + \breve{\alpha}E \qquad (2.2)$$

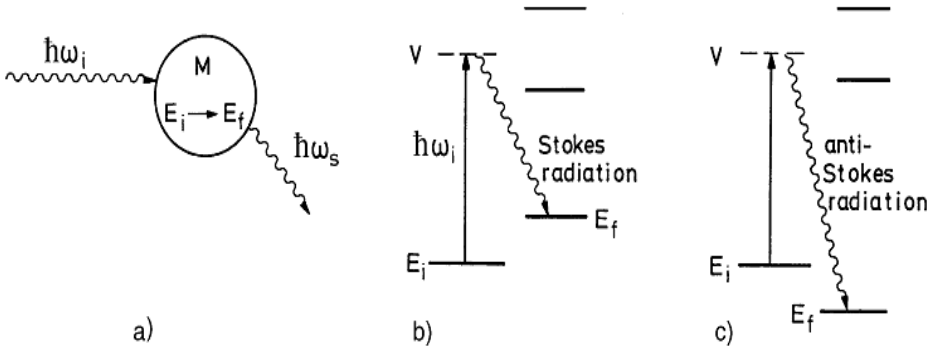

Figure (2.1) schematic level diagram of Raman scattering(Wolfgang Demtröder, 2008).

Between the electric field amplitude $E = E_0 cos\omega t$ of the incident wave and the dipole moment $\boldsymbol{p}$ of a molecule. The first term $\boldsymbol{\mu_0}$ represents a possible permanent dipole moment while $\tilde{\alpha}\,E$is the induced dipole moment. The polarizability is generally expressed by the tensor $\alpha_{ij}$of rank two, which dependson the molecular symmetry. Dipole moment and polarizability are functions ofthe coordinates of the nuclei and electrons. However, as long

as the frequency of the incident radiation is far off resonance with electronic or vibrational transitions, the nuclear displacements induced by the polarization of the electron cloud are sufficiently small. Since the electronic charge distribution is determined by the nuclear positions and adjusts "instantaneously" to changes in these positions, we can expand the dipole moment and polarizability intoTaylor series in the normal coordinatesq_n of the nuclear displacementsEq (2.3).

$$\mu = \mu(0) + \sum_{n=1}^{Q} \left(\frac{\partial \mu}{\partial q_n}\right)_0 q_n + \cdots, \qquad \alpha_{ij}(q) = \alpha_{ij}(0) + \sum_{n=1}^{Q} \left(\frac{\partial \alpha_{ij}}{\partial q_n}\right)_0 q_n + \cdots \quad (2.3)$$

Where $Q = 3N - 6$ (or $3N - 5$for linear molecules) gives the number of

Normal vibrational modes for a molecule with *N* nuclei, and $\mu(0) = \mu_0$and $\alpha_{ij}(0)$are the dipole moment and the polarizability at the equilibrium

Configuration $q_n = 0$. For small vibrational amplitudes the normal coordinates$q_n(t)$of the vibrating molecule can be approximated by

$$q_n(t) = q_{n0} \cos(\omega_n t) \quad (2.4)$$

Whereq_{n0} gives the amplitude, andω_n the vibrational frequency of the *n* th normal vibration. Inserting (2.4 and 2.3) into (2.2) yields the total dipole moment

$$\begin{aligned} P = \mu_0 + \sum_{n=1}^{Q} \left(\frac{\partial \mu}{\partial q_n}\right)_0 q_{n0} \cos(\omega_n t) \\ + \alpha_{ij}(0) E_0 \cos(\omega t) \\ + \frac{1}{2} E_0 \sum_{n=1}^{Q} \left(\frac{\partial \alpha_{ij}}{\partial q_n}\right)_0 q_{n0} [\cos(\omega + \omega_n)t \\ + \cos(\omega - \omega_n)t] \end{aligned} \quad (2.5)$$

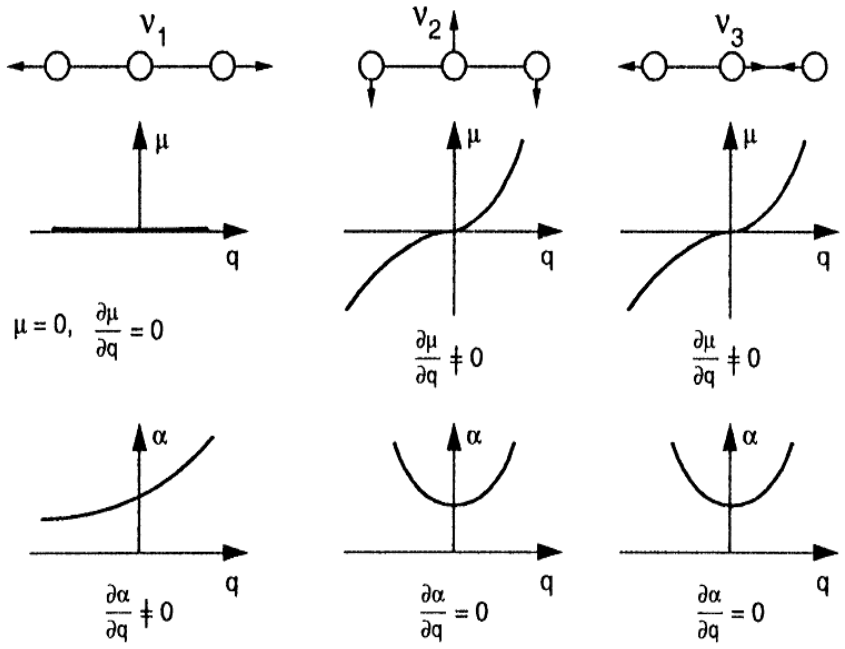

*Figure (2.2)*Dependence $\partial\mu/\partial q$of dipole moment and$\partial\alpha/\partial q$of polarizability on the normalvibrations of the CO_2 *molecule(Wolfgang Demtröder, 2008).*

The second term describes the infrared spectrum, the third term the Rayleigh scattering, and the last term represents the Raman scattering. In Fig. 2.2 the dependence of $\partial\mu/\partial q$and $\partial\alpha/\partial q$is shown for the three normal vibrations ofthe CO_2 molecule. This illustrates that $\partial\alpha/\partial q \neq 0$ for the bending vibration$\nu_2$and for the asymmetric stretchν_3. These two vibrational modes are called "infrared active." The polarizability change is $\partial\alpha/\partial q \neq 0$ only for the symmetricstretchν_1, which is therefore called "Raman active.

Since an oscillating dipole moment is a source of new waves generated at each molecule, that an elastically scattered wave at the

Frequency ω of the incident wave is produced (Rayleigh scattering) as are in elastically scattered components with the frequencies $\omega = \omega_n$(Stokes waves) and super elastically scattered waves with the frequencies$\omega + \omega_n$

(anti-Stokescomponents). The microscopic contributions from each molecule add up tomacroscopic waves with intensities that depend on the population $N(E_i)$ of the molecules in the initial level E_i, on the intensity of the incident radiation, and on the expression$\left(\frac{\partial \alpha_{ij}}{\partial q_n}\right) q_n$, which describes the dependence of thepolarizability components on the nuclear displacements.Although the classical theory correctly describes the frequencies$\omega \pm \omega_n$ofthe Raman lines, it fails to give the correct intensities and a quantum mechanical treatment is demanded. The expectation value of the component α_{ij} of thepolarizability tensor is given by

$$\langle \alpha_{ij} \rangle_{ab} = \int u_b^*(q) \alpha_{ij} u_a(q) dq \qquad (2.6)$$

Where the functions $u(q)$represent the molecular Eigen functions in the initiallevel***a***and the final level ***b***. The integration extends over all nuclear co-ordinates. This shows that a computation of the intensities of Raman lines are based on the knowledge of the molecular wave functions of the initial and final states. In the case of vibrational–rotational Raman scattering these are the rotational-vibrational eigenfunctions of the electronic ground state.

For small displacements q_n, the molecular potential can be approximated

By a harmonic potential, where the coupling between the different normal vibrational modes can be neglected. The functions $u(q)$are then separable intoa product

$$u(q) = \prod_{n=1}^{Q} \omega_n(q_n, v_n) \qquad (2.7)$$

of vibrational eigenfunction of the *n*th normal mode with$V_n$vibrational

Quanta. Using the orthogonality relation

$$\int \omega_n \omega_m \, dq = \delta_{nm} \,, \qquad (2.8)$$

Of the functions$\omega_n(q_n)$one obtains from (2.6 and 2.3).

$$\langle \alpha_{ij} \rangle_{ab} = (\alpha_{ij})_0 + \sum_{n=1}^{Q} \left(\frac{\partial \alpha_{ij}}{\partial q_n} \right)_0 \int \omega_n(q_n, v_a) q_n \omega_n(q_n, v_b) dq_n \quad (2.9)$$

The first term is a constant and is responsible for the Rayleigh scattering.

For non-degenerate vibrations the integrals in the second term vanish unless$v_a = v_b \pm 1$. In these cases it has the value$\left[\frac{1}{2}(V_a + 1)\right]^{\frac{1}{2}}$(Wolfgang Demtröder, 2008).

The basic intensity parameter of vibrational Raman spectroscopy is the derivative$\left(\frac{\partial \alpha_{ij}}{\partial q}\right)$which can be determined from the Raman spectra.

The intensity of a Raman line at the Stokes or anti-Stokes frequency $\omega_s = \omega \pm \omega_n$is determined by the population density $N_i(E_i)$in the initial Level$E_i(v, J)$by the intensity I_L of the incident pump laser, and by the Raman scattering cross section$\sigma_R(i \to f)$for the Raman transition $E_i \to E_F$.

$$I_s = N_i(E_i) \sigma_R(i \to f) I_L \quad (2.10)$$

At thermal equilibrium the population density$N_i(E_i)$follows the Boltzmanndistribution$N_i(E_i, v, J) = \frac{N}{Z} g_i e^{-E_i/KT}$, $N = \sum N_i$ $(2.11a)$

The statistical weight factors$\mathbf{g_i}$depend on the vibrational state $V = (n_1 v_1, n_2 v_2)$, the rotational state with the rotational quantum number J,the projection Konto the symmetry axis in the case of a symmetric top,

and furthermore on the nuclear spins *I* of the *N* nuclei. The partition function

$$Z = \sum_{I} g_i e^{-E_i/KT}, \qquad (2.11b)$$

is a normalization factor, which makes$\sum N_i(\upsilon, J) = N$ as can be verified byinserting (2.11b) into (2.11a).In case of Stokes radiation the initial state of the molecules may be the vibrational ground state, while for the emission of anti-Stokes lines themolecules must have initial excitation energy. Because of the lower populationdensity in these excited levels, the intensity of the anti-Stokes lines is lower by a factor $\exp\left(-\frac{\hbar\omega_\upsilon}{KT}\right)$(Wolfgang Demtröder, 2008).

2.3 Emission spectroscopy:

Theoretical explanation of emission spectroscopy led the way to the development of quantum mechanics. This form of spectroscopy examines the wavelength of photons emitted when an atom or molecule drops from a higher electronic state to a lower one and it is the structure of the sample that dictates the wavelength of the photons the shamble can absorb and emit. The mechanism by which atoms or molecules are excited sub classifies this type of spectroscopy further. For example if electromagnetic radiation is used, fluorescence spectroscopy can result. Protons can produce particle- induced x-Ray emission, and if heat is applied to a sample causing an increase in collisions between particles flame emission spectra can be detected. In fluorescence spectroscopy the absorption of a quantum of energy by the target molecule allows a transitions from the ground state to a higher electronic state in which there are several vibrational levels, collisions between the sample molecules can result in a loss of different quantum of energy as the molecules drop from one vibrational state to a

lower one within that particular electronic state. A further quantum of energy can be lost if the molecule subsequently drops to its ground state. The energy emitted during each of these events is different and so are the frequencies and wavelengths of the emitted light, two types of spectra can be obtained, where the excitation radiation has a signal. Constant wavelength the intensity of the emission is recorded and the spectrum produced is called an emission. If different wavelengths of excitation radiation are used a series of emission spectra can be recorded and the wavelength producing the maximum intensity of emitted radiation from each spectrum can be used to form an intensity profile for the specimen as a function of the excitation wavelength, this is called an excitation spectrum (Babara Stuart Wiely. 2003) **.**

At low concentration the intensity of fluorescence id considered to be directly proportional to the concentration of flourophore present. In florescence spectra the Raman signal is always seen at apposition which has a constant wave number difference relative to the excitation wave number. it has proved difficult to obtain standard spectra in fluorescence spectroscopy as the signal can be distorted in many ways. Factors related to instrumentation include variation in the intensity and wavelength of the light source. Alight which maintains the same intensity over all wavelengths has proved elusive as has a detecting system which maintains constant efficiency over time. Factors relating to the sample include photo decomposition, scattering of light by Raman and Rayleigh effects and variation in the intensity of the radiation throughout the sample with photons of energy emitted through fluorescence sometimes being absorbed (DR.H.Kaur,2001).

2.4 Infrared spectroscopy and Raman spectroscopy:

Infrared is an example of absorption spectroscopy. The transition between molecular vibrational levels within the mid-infrared range allowing Raman spectroscopy and mid-infrared spectroscopy to be complimentary in nature when used to probe biological molecules.

The two techniques have fundamental differences ; in IR the absorption effect as a result of a change in permanent molecular dipole moment where as in Raman spectroscopy it results from scattering of light due to and induced dipole present around the molecule.IR exploits the fact that certain molecules have unique frequencies at which they can vibrate or rotate. In molecules with little or no symmetry the IR and Raman spectra have peaks at similar position .as a goal understand the vibrational motion of a molecule can only be fully expressed by considering both IR and Raman spectra.

In infrared spectroscopy the incident radiation is polychromatic i.e. has a range of frequencies. It can only excite the molecule through vibrational transitions and absorption only occurs when the energy required by the molecule to move between the vibrational levels equals that of photons of the incident light. In Raman spectroscopy the incident radiation is monochromatic and the scattered radiation measured differs by one vibrational unit of energy from the incident radiation thus no match is required between the energy of the incident radiation and the energy difference between the ground and the excited states. Infrared absorption can be thought of as resulting from a direct resonance between the frequency of the incident radiation and the vibration frequency of that particular molecule. The increase in energy corresponds to the energy of the incident photon at the frequency at vibration resonance. This is a one

photon event in contrast to the changes that results as a result of Raman and Raleigh scattering which are considered as two photons events and require much higher radiation energy . Electromagnetic radiation can be characterized by its wavelength (λ). Energy is linearly related to frequency (υ) and wavenumber$\acute{\omega}$(DR.H.Kaur,2001).

The relationship between wavelength, frequency and energy (ΔE) is shwon bellow equations (1.22,1.25) also that of absorbance ,radiation intensity and transmission equation (1.26,1.24)

$$\lambda = {}^{c}/_{\nu} \qquad (1.26)$$

$$\nu = {}^{\Delta E}/_{h} \qquad (1.27)$$

$$\grave{\omega} = {}^{1}/_{\lambda} = {}^{\Delta \mathrm{E}}/_{hc} \qquad (1.28)$$

$$\Delta \mathrm{E} \propto {}^{1}/_{\lambda} \qquad (1.29)$$

Where C = speed of light ($3 \times 10^{8} ms^{-1}$)

h = plank constant ($6.626 \times 10^{-34} Js \; or \; 4.136 \times 10^{-15} \; eVs$)

$\acute{\omega}$Is wavenumber (cm^{-1})

Thus the heights energy absorption is associated with radiation of the shortest wavelength and highest frequency, the intensity of infrared absorption can be expressed in several ways.

Absorbance = A

Transmission =T

$$A = log10\left({}^{I_0}/_{I}\right) \qquad (1.30)$$

$$T = {}^{I}/_{I_0} \qquad (1.31)$$

$$T(\%) = 100\ \%T \quad (1.32)$$

$$A = log10\ {}^{1}/_{T} \quad (1.33)$$

Hence the I_0 is the intensity of the incident radiation and I is the intensity of the radiation after it had passed through the sample ,absorbance is governed by the Beer Lambert law

$$A = \varepsilon\ b\ k \quad (1.34)$$

Where:

ε = the molar Absorptivity ($Lmol^{-1}cm^{-1}$)

b = the cell length (cm)

k= the concentration of the sample in solution ($molL^{-1}$)

$$A = log10\left({}^{I_0}/_{I}\right) = \varepsilon\ b\ k \quad (1.35)$$

$$I = I_0 e^{-\varepsilon bk} \quad (1.36)$$

$$\frac{I_0}{I} = I_0 e^{-\varepsilon bk} \quad (1.37)$$

In infrared spectra it is conventional to plot percentage transmission against the wavenumber:

$$T(\%) = \left({}^{I_0}/_{I}\right) \times 100\% \quad (1.38)$$

Equation 1.33 and 1.34 show that percentage transmission is not directly proportional to concentration so in quantitative work absorbance is used in preference. IR spectroscopy is simple and reliable. It can be used for both

qualitative steady state and dynamic measurements. One practical of not is that aqueous solutions, the broad absorbance signal resulting from water must be subtracted out of spectra to allow simpler assessment (DR.H.Kaur, 2001).

2.5 Lasers in spectroscopy:

From 1960 onwards , the increasing a availability of intence,monochoromatic laser sources provide a tremendous impetus to a wide range of spectroscopic investigations, for branches of spectroscopy, other than Raman spectroscopy ,most laser sources may appear to have a great disadvantage, than of non-tunability. In regions of spectrum, particularly the IR, where tunable lasers are not readily available ways, ways have been devised for tuning, i.e shifting the atomic or molecular energy levels concerned until the transition being studied moves into coincidence with the laser radiation, this may be achieved by Applying an electric field to the sample and the technique is called laser stark spectroscopy. The corresponding technique using a magnetic field is that of laser magnetic resonance (laser Zeeman) spectroscopy (Peter F .Bernath, 2005).

2.5.1 Laser magnetic resonance spectroscopy:

The topic of laser magnetic resonance or MLR spectroscopy has growing importance as a method for obtaining structural and chemical information about free radicals.

The development of spectroscopic techniques in the region between the micro wave regions. with a high limit of about 300 GHz or 10 cm^{-1} , and grating IR spectroscopy, with a limit of about 6000 GHz or 200 cm^{-1} has been hampard by the lack of high power tunable source . the first really versatile sources of radiation in this region were the far IR lasers ,these

lasers operated on the rotational transitions of small molecules such as H_2O , D_2O or HCN excited in an electric discharge, and produced up to 0.1 watts of continuous coherent radiation in the 100 cm^{-1} region. Feasibility of this technique detect a weak rotational transition in O_2 using the HCN laser as a source ,similarly between this technique and the well-known electron paramagnetic resonance led to the title (Laser Paramagnetic Resonance) this description perhaps on the grounds of its unfortunate acronym, was soon replaced by (Laser Magnetic Resonance) after this initial observations progress was swift. The sensitivity of the technique was improved by several orders of magnitude by placing the spectroscopic absorption region within the laser cavity and the spectra of other stable magnetic molecules in this frequency range were observed (France F .Le Blanc.;et.al.,2004).

2.5.2 Nuclear laser spectroscopy:

Using advanced laser spectroscopy methods, nuclear ground state spins moments, charge radii, of radioactive nuclei can be determined. The optical techniques based on hyperfine structure splitting (HFS) or isotope shift measurments,yield model-independent information about nucleus. Various experimental methods and concepts are proposed to take advantage of exotic nuclei provided at low energy including spectroscopy on trapped highly-charged ions, which is a new approach for studies of nuclear and isotopic effects with high sensitivity (France F .Le Blanc.et.al. 2004).

2.5.2.1 Fine structure:

The spectra are organized into separate singlet and triplet manifolds states only with weak inter combination transitions connecting them.

Spin orbit- interaction causes many atomic lines to split into multiples such as the Na D lines or the six-line batten of the Ca D^3-P^3 transition at 442.5 - 445.6 nm. The splitting into multiples is called fine-structure. The transition elements lanthanides and actinides have very complex energy level patterns because of the many terms and levels arising from open *d* and *f* sub shells (N.Stone .I.E Tothill.et.al.,2010).

2.5.2.2 Hyperfine structure and hyperfine anomaly:

In atomic physics, hyperfine structure refers to small shifts and splitting in the energy levels of atoms, molecules and ions, due to interaction between the state of the nucleus and the state of the electron clouds.

In atoms, hyperfine structure arises from the energy of the nuclear magnetic dipole moment interacting with the magnetic field generated by the electrons and the energy of the nuclear electric quadruple moment in the electric field gradient due to the distribution of charge within the atom. Molecular hyperfine structure is generally dominated by these two effects, but also includes the energy associated with the interaction between the magnetic moments associated with different magnetic nuclei in a molecule, as well as between the nuclear magnetic moments and the magnetic field generated by the rotation of the molecule.

Hyperfine structure contrasts with fine structure, which results from the interaction between the magnetic moments associated with electron spin and the electrons' orbital angular momentum. Hyperfine structure, with energy shifts typically orders of magnitudes smaller than those of a fine-structure shift, results from the interactions of the nucleus (or nuclei, in molecules) with internally generated electric and magnetic fields.

This interaction between the nuclear electromagnetic multiple moments and the electromagnetic field produced by the orbital electrons is well described by first order perturbation theory (Woodgate, Gordon K. ,1999).

Assuming that the contribution of higher order moments is negligible, the hyperfine splitting energy is expressed as

$$w_f = {}^1/_2 \; kA + {}^3/_4 \, k(k+1) - I\,(I-1) - \frac{J(J+1)}{2I}\left(\frac{2I(2I-1)j}{(2J-1)}\right) B \ldots (1.39)$$

Where $K = F(F+1) - I(I+1) - J(J+1), J+1 > F > I+J$.
Hyperfine interaction constants A and B are proportional to the nuclear magnetic dipole moment and electric quadruple moment, respectively. For a more quantitative discussion, the magnetic hyperfine constant A is given by

$$A = \frac{\mu_I H(0)}{IJ}(1 + \varepsilon_{BW}) \qquad (1.40)$$

Where μ1 is the nuclear magnetic moment, and H0 is the magnetic field at the center of a nucleus by the orbital electrons; this field includes the effects of the reduced mass, the Breit – Rosenthal effect etc …the ε_{WB} is the quantity caused by the spatial distribution of nuclear magnetism and the variation of H over the nuclear volume.

$$\varepsilon_{WB} = \frac{\int \mu_I(r) H(r) dv}{\mu_I H(0)} - 1 \qquad (1.41)$$

Although one can measureε_{WB} directly in the case of a harmonic atom ,its difficult to discuss the ε_{WB} of an ordinary atom directly because ε_{WB} is very small (< 10^{-3}) and no precise wave functions of the electrons are available .Therefore the information of ε_{WB}should be obtained as the difference for different isotopes 1 and 2 based on the ratio of the hyperfine constant A_1

$$\frac{A_1}{A_2} = \frac{\mu_{I1} I_2}{\mu_{I2} I_1} \frac{1+\varepsilon}{1+\varepsilon} \qquad (1.42)$$

where(ε) consist of not only ε_{WB}but also other efects similarly for $H(0\ )$as mentioned above. Since$\varepsilon_1 \sim \varepsilon_2$ Are small one can write

$$\Delta^2 \equiv \varepsilon - \varepsilon_2 \approx \frac{\mathrm{A_1 \mu_{I2} \div I_2}}{\mathrm{A_2 \mu_{I1} \div I_1}} - 1 \qquad (1.43)$$

This quantity Δ^2 is called the hyperfine anomaly. In order to measure and study the distribution of nuclear magnetization, one should measure the A and the g1 factor independently with an accuracy of $\leq 10^{-5}$ (Y.Fukashiron.et.al.,1992).

2.5.3 Infrared laser spectroscopy:

For a molecule to show infrared a absorption it must possess specific feature i.e. an electric dipole moment of a molecule must change during the vibration. This is the selection rule for infrared spectroscopy.

The change in the dipole moment of a hetronuclear diatomic molecule

Is described an example of an infrared -active molecule, the dipole moment of such a molecules change as the bond expands and contracts. an example of an infrared inactive molecule is a homonuclear diatomic molecule because its dipole moment remains zero no matter how long the bond is. An understanding of molecular symmetry and group theory is important when initially assigning infrared bands (N.Stone, .I.E Tothill.et.al.,2010).

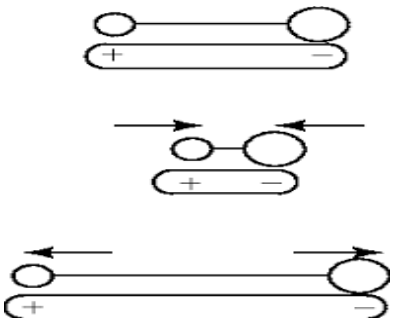

Figure (2.3) change in the dipolemoment of a heteronuclear diatomic molecule (John R. Ferraro, 2003).

Infrared absorptions are not infinitely narrow and there are several factors that can contribute to the broadening .for gases ,the Dopler effect, in which radiation source is moving towards or away from the observer, is a factor . There is also the broadening of bands due to the collisions between molecules. Another source of line broadening is the finite lifetime of the states involved in the transition. from quantum mechanics, when the Schrödinger equation is solved for a system which is changing with time , the energy states of the system don't have precisely defined energies and this leads to life time broadening. there is a relationship between the lifetime of an excited state and the band width of the absorption a associated with the transition to the excited state and this is a consequence of the Heisenberg uncertainty principle. This relationship demonstrates that the shorter the lifetime of a state, then the less well defined is its energy (N.Stone, .I.E Tothill.et.al.,2010)..

All molecules except mononuclear diatomic, have at least one allowed vibrational transition. Interestingly, even mononuclear molecules such as H_2 and N_2 have very week electric quadruple transitions. Vibrationally – excited emission of H_2 can be seen in shocked regions of molecular clouds in space and the vibration – rotation lines of N_2 can be seen in absorption through the earth's atmosphere using the sun as a source

vibrational transitions are thus a universal monitor of chemical composition. Infrared transitions however have some dis advantages. The most serious are those vibrational transitions tend to be relatively weak compared to pure rotational and electronic transition. The development of infrared lasers have helped to overcome this problem by increasing the sensitivity of infrared spectroscopy (N.Stone, .I.E Tothill.et.al.,2010).

Infrared spectroscopy of stable molecules is, in general more easily carried out with Fourier Transform spectrometers than with lasers except for very low concentrations or very high resolutions. Free radicals and other transient molecules have intrinsically low concentrations because of their great reactivity. The power of modern infrared laser spectroscopy is thus well illustrated with the study of transient species such as ions, free radicals and Van Der Waals molecules.

Rather than modify a line – tunable laser, it is simpler to tune a molecular transition into resonance with a fixed frequency laser using electric or magnetic field. The basic concepts uses a cell containing the molecule of interest inside a laser cavity and the molecular transition frequency is tuned by application of an electric or magnetic field. When the molecular transition is in resonance with the fixed - frequency laser there is a sharp drop in output power because of the extra loss inside the (D.A Cremer.; et.al. 2006).

2.5.4 Laser-Induced Breakdown Spectroscopy (LIBS):

LIBS are a sensitive technique for analyzing the chemical or atomic compositions of solid or liquid materials. Here a laser pulse is focused onto the surface of a solid or liquid material. Due to the high peak intensity, fast evaporation of a small volume in the focus of the laser pulse occurs. The gaseous plume ejected from the surface contains molecules, atoms and ions

contained in the focal volume. The fluorescence emitted by the excited species is collected by a lens, focused into an optical fiber and sent to the entrance slit of a spectrograph

(Fig1.5) if the detector at the exit of the spectrograph is time-gated, the spectra can be recorded at specific times after the generation

Of the plume. Since the plume cools during its expansion, the ions recombine to excited states of neutral atoms or molecules and the emission from these states is a measure of the concentration of the atoms in the sample. With moderate laser power, molecules can evaporate without fragmentation. This is particularly useful for investigations of biological samples or for inspecting tissues in vitro. When a second weak probe laser is used, it can cross the plume at different locations, where it generates spatially resolved laser-induced fluorescence,

This can be detected and analyzed. Using REMPI techniques, ionization of the neutral species can be achieved with subsequent mass-selective detection in a mass spectrometer (A.W. Miziolek, V. Paleschi.et.al., 2006).

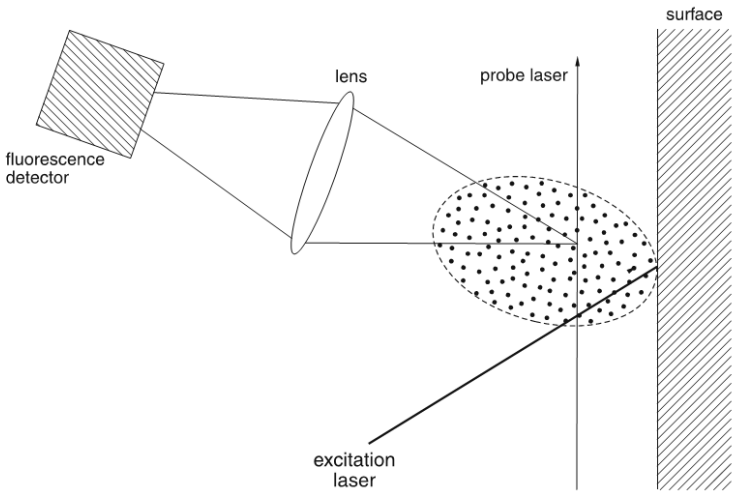

*Figure (2.4) Laser-induced breakdown spectroscopy (*Maher S. Amer, 2010).

2.5.5 Laser absorption spectroscopy:

Laser absorption spectroscopy operates on the principle that the amount of light absorbed by a sample is related to the concentration of the target species in the sample. Light of known intensity is directed through a gas sample cell and the amount of light transmitted through the sample cell is measured by a detector. If we assume incident light intensity

I_0 (x= 0, λ) and transmitted light intensity, I(x, λ) the Beer's law relates the transmitted light to the incident light and the absorption coefficient of the sample α(λ)

$$I(x\,,\lambda) = I_0 e^{-\alpha(\lambda)x} \qquad (1.44)$$

Where λ is the wavelength and x is the path length. Concentration is determined from the absorption coefficient.

Laser absorption spectroscopy (LAS) offers a promising new effective technique. The mid- infrared spectral range is ideal for tunable laser absorption spectroscopy (LAS) since most molecular gases possess strong characteristics fundamental rotational – vibrational lines. High resolution (LAS) can resolve absorption features of targeted molecules and selectively access optimal spectral lines at low (≤100 torr) pressure without interference from CO_2 and H_2O to achieve high levels of trace gas detection sensitivity and specificity. Avoiding H_2O and CO_2 interferences is particularly important in the development of biomedical gas sensors for breath analysis (Housten,Mathew R Mc Curdy.et.al., 2007).

Each gas has an absorption line at a unique wavelength, preferably free of interference of other gases in the sample cell. Equation (1-40) shows that the ability of a LAS – based sensor to detect a specific concentration depends on the path length through the absorbing medium. The strongest

molecular rotational – vibrational transitions which are desired to perform ultra-sensitive concentration measurements are in the mid – infrared (mid IR) spectral region. The usefulness of laser spectroscopy in this region is limited by the availability of reliable, tunable, contentious wave infrared laser sources. The most practical sources include lead salt diode lasers, coherent sources based on different frequency generation (DFG) optical parametric oscillators(OPOs) , tunable solid state lasers , and quantum and inter band cascade lasers. Sensors which utilize lead diode lasers are typically large in size and require cryogenic cooling because such lasers operate at temperature of $< 90C^0$ .DFG – based spectroscopic sources have recently been shown to be reliable and compact.

The recent advances quantum cascade (QC) and inter band cascade (IC) lasers fabricated by band structure engineering offer an attractive new source option for mid infrared absorption spectroscopy with ultra- high resolution and sensitivity. The most technologically developed mid infrared QC laser source to date is based on type – 1 inter sub band transition in Ga As / in AL AS hetero structure . More recently inter band cascade lasers (ICLs) based on type II inter band transition have been reported in the 3- 5 μmregion (Housten,Mathew R Mc Curdy.et.al., 2007)..

2.5.6 Laser Raman spectroscopy:

Raman spectroscopy is based on inelastic scattering of light by matter. The simplest way of explaining the classical or spontaneous Raman Effect is via an energy level diagram such as that depicted in figure 1.6

Let us assuming that the molecular system has two vibrational energy levels, the ground state n=0 and the excited state n= 1, which are separated by energy hv_m where hv_m is the frequency of the molecular vibration.

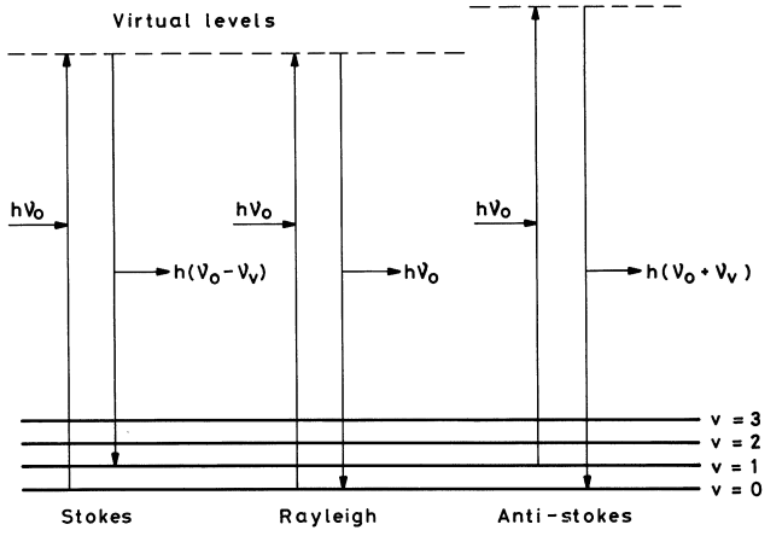

Figure (2.5)idealized model of Rayleigh scattering and Stokes and anti-Stokes Raman scattering (John R. Ferraro, 2003).

They include light with energy v_L induces transitions to virtual levels as shown. Returning to the initial state takes place in three different ways, namely by emitting light of frequencies$v_{L,}\ hv_L - hv_m\ ,\ hv_L + hv_m$

The elastic for Rayleigh scattering arises from a transition that starts and finished at the same vibrational energy level. The shifts to lower and higher frequencies are known as Stocks and anti-stocks Raman scattering respectively stokes Raman scattering arises from a transition that starts at the ground state vibrational energy level and finishes at a higher vibrational energy level. Whereas anti-stoke Raman scattering involves transition from a higher to lower vibrational energy level.

At the ambient temperatures, most molecules are in the ground state and thus the anti-stock transitions are less likely to occur than the stoke transitions, resulting in the stoke Raman scattering being more intense. For

this reason it is usually the stokes Raman spectrum that is routinely studied (John R. Ferraro, 2003).

2.6 Selection Rules for Raman Spectra:

To determine if the vibration is active in the Raman spectra, the selection

Rules must be applied to each normal vibration. Since the origins of Ramanspectra are markedly different than IR spectroscopy, their selection rules arealso distinctively different. According to quantum mechanics a vibration isRaman-active if the polarizabilityis changed during the vibration (John R. Ferraro, 2003).

To discuss Raman activity, let us consider the nature of the polarizability when a molecule is placed in an electric field (laser beam), it suffers distortion since the positively charged nuclei are attracted toward the negative pole, and electrons toward the positive pole(Fig. 2.6). This charge separation produces an induced dipole moment (*P*) given by

$$\boldsymbol{P = \alpha E} \qquad (2.12)$$

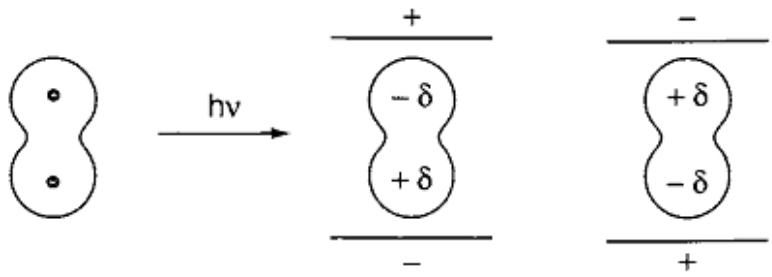

Figure (2.6)Polarization of a diatomic molecule in an electric field(John R. Ferraro2003)

In actual molecules, such a simple relationship does not hold since both ***P*** and ***E*** are vectors consisting of three components in the x, y and z directions Thus, Eq. (2.12) must be written as

$$
\begin{aligned}
p_x &= \alpha_{xx}E_X \quad \alpha_{xY}E_Y \quad \alpha_{xZ}E_Z \\
p_y &= \alpha_{Yx}E_X \quad \alpha_{YY}E_Y \quad \alpha_{YZ}E_Z \\
p_z &= \alpha_{Zx}E_X \quad \alpha_{ZY}E_Y \quad \alpha_{ZZ}E_Z
\end{aligned}
$$

In matrix form this is written,

$$
\begin{bmatrix} \boldsymbol{P_x} \\ \boldsymbol{P_y} \\ \boldsymbol{P_z} \end{bmatrix} = \begin{bmatrix} \boldsymbol{\alpha_{xx}} & \boldsymbol{\alpha_{xy}} & \boldsymbol{\alpha_{xz}} \\ \boldsymbol{\alpha_{yx}} & \boldsymbol{\alpha_{yy}} & \boldsymbol{\alpha_{yz}} \\ \boldsymbol{\alpha_{zx}} & \boldsymbol{\alpha_{zy}} & \boldsymbol{\alpha_{zz}} \end{bmatrix} \begin{bmatrix} \boldsymbol{E_X} \\ \boldsymbol{E_Y} \\ \boldsymbol{E_Z} \end{bmatrix}
$$

The first matrix on the right-hand side is called the polarizability tensor. Innormal Raman scattering, this tensor is symmetric

$\alpha_{xy} = \alpha_{yz}$, $\alpha_{xz} = \alpha_{zx}$And $\alpha_{yz} = \alpha_{zy}$

According to quantum mechanics, the vibration is Raman-active if one of these components of the polarizability tensor is changed during the vibration.In the case of small molecules, it is easy to see whether or not thepolarizability changes during the vibration. Consider diatomic molecules such as H_2or linear molecules such as CO_2

Their electron clouds have an elongated water melon like shape with circular cross-sections. In these molecules, the electrons are more polarizable (*a larger α*) along the chemical bond than in the direction perpendicular to it. If we plotα_i(α in the *i*-direction) from the center of gravity in all directions, we end up with a three- dimensional surface. Conventionally, we plot $1/\sqrt{\alpha i}$ rather than α_{ij}itself and call the resulting three-dimensional body a polarizability ellipsoid. Figure 2.4shows the changes of such an ellipsoid during the vibrations of the CO_2 molecule. In terms of the polarizability ellipsoid, the vibration is Raman-active if the size, shape or orientation changes during the normal vibration.

The size of the ellipsoid is changing in $\upsilon_1$vibration and $\upsilon_3$vibration, although the diagonal elements$\alpha_{xx}, \alpha_{yy}\ and\ \alpha_{zz}$**)** are changing simultaneously. Thus, it is Raman-active. The difference between the υ_1 and $\upsilon_3$is shown in Fig. 2.7

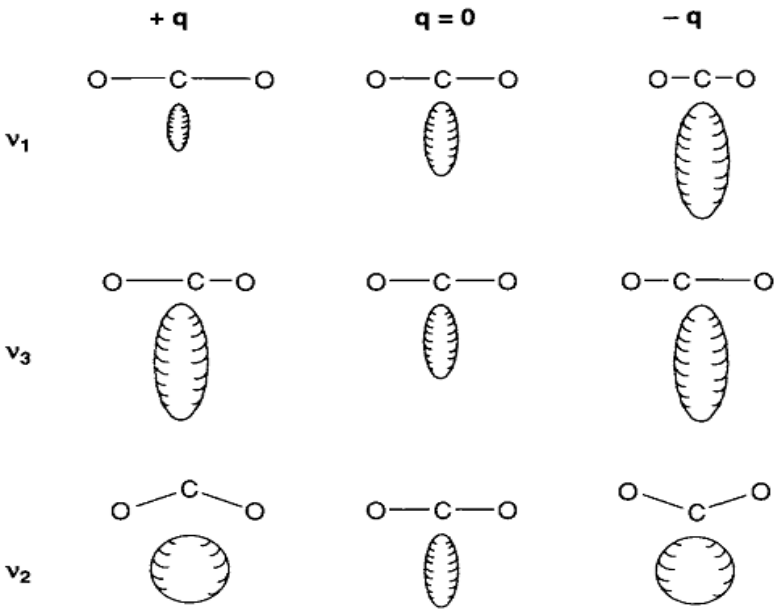

Figure (2.7)Polarizability ellipsoid for different normal vibration modes of CO2(John R. Ferraro2003).

Figure (2.8) illustrates the changes in the polarizability ellipsoid during the normal vibrations of the H_2O molecule. Its $\upsilon_1$vibration is Raman-active, as is the υ_1 vibration of CO_2. The υ_2 vibration vibration is also Raman-active because the shape of the ellipsoid is different at $+q$ and $-q$. In terms of the polarizability tensors $(\alpha_{xx}, \alpha_{yy}\ and\ \alpha_{zz})$are all changing with different rates. Finally, the υ_3 vibration is Raman-active because the orientation of the ellipsoid is changing during the vibration.

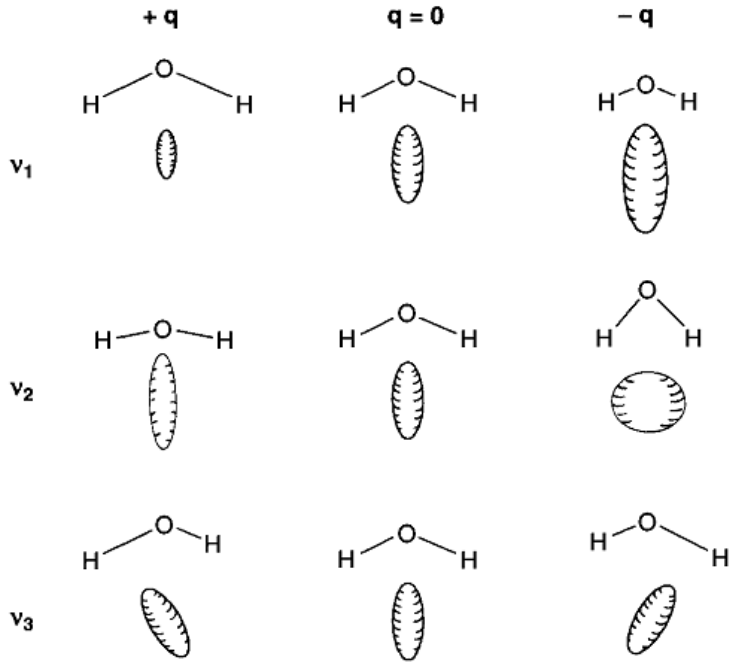

Figure (2.8) Changes in polarizability ellipsoid during normal vibrations of H_2O molecule((John R. Ferraro2003).

2.7 The DepolarizationRatios:

Depolarization ratios of Raman bands provide valuable information about the symmetry of a vibration that is indispensable in making band assignments. Figure 2.9 shows a coordinate system which is used for measurements of depolarization ratios. A molecule situated at the origin is irradiated from the y- direction with plane polarized light whose electric vector oscillates on the y z- plane (E_Z) . If one observes scattered radiation from the x- direction n and measures the intensity in the $y(I_y)$ and z (I_z) – directions using an analyzer the deplorization ratio(P_p) measured by polarized light (P) is defined by Eq(2.8)

$$\rho_P = \frac{I_\perp(I_Y)}{I_\parallel(I_z)}, \qquad (2.8)$$

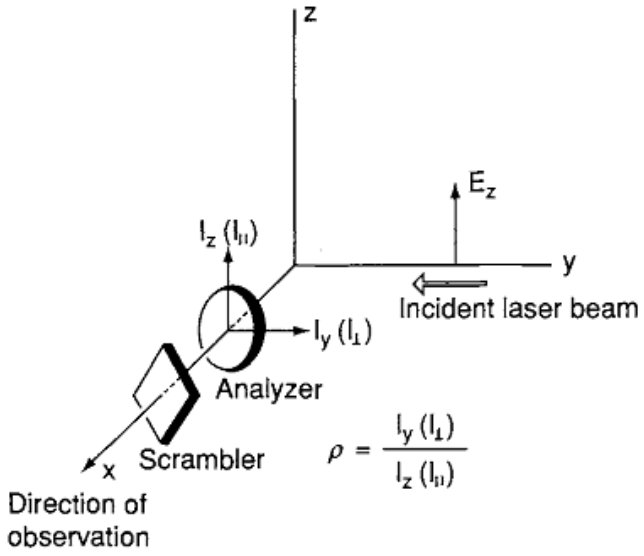

Figure (2.9) Irradiation of sample from the y-direction with plane polarized light, with the Electronic vector in thez-direction(John R. Ferraro2003).

In this case, the polarizer is not used because the incident laser beam is almost completely polarized in the z direction. If a premonochromator is placed in front of the laser, polarizer must be inserted to ensure complete polarization. The scrambler (crystal quartzwedge) must always be placed after the analyzer since the monochromator gratings show different efficiencies for perpendicular⊥ L and parallel ∥ polarized light.

For information on precise measurements of depolarization suppose that Suppose that atetrahedral molecule such as CCI_4 is irradiated by plane Polarized light (E_z). Then,the induced dipole also oscillates in The same yz-plane .If the molecule is performing the totally symmetric vibration, the polarizability ellipsoid is always sphere-like; namely, molecule is Polarized equally in every direction under such a circumstance,$I(I_Y) = 0$. Since the oscillating dipole emitting the radiation is confined to the xz-plane,thus $P_P = 0$such a vibration is called polarized (abbreviated as *p*).

In liquid and solutions, molecules take random orientations. Yet this conclusion holds since the polorizibility ellipsoidis spherical throughout the totally symmetric vibration.

If the molecule is performing anon totally symmetric vibration, thepolarizibility,ellipsoid changes its shape from a sphere to an ellipsoid during the vibration. Then the induced dipole would be largest along the direction of largest polarizibility,namely along one of the minor axes of the ellipsoid(John R. Ferraro,2003).

2.7.1 Determination of depolarization ratio:

The determination of depolarization ratio(*p*) is an important laidin studying Raman lines, the value of depolarization ratio indicates the symmetrical nature of the vibrations.Hence completely symmetric vibrationsyield polarized Raman lines while partially symmetric vibrations are deplorized.concider Raman spectrum of CCl_4 out of the five bandsat ,218,314,459,710 and 760 cm^{-1} ,only one at 459 cm^{-1} is polarizedfigure (2.10).so it corresponds to the completely symmetric vibration v_1 while the rest are depolarized and assigned to unsymmetrical vibrations .

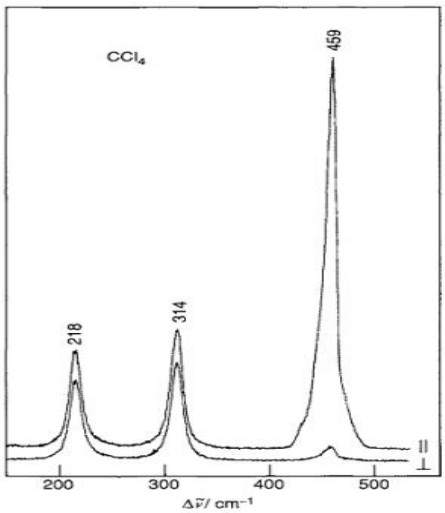

Figure (2.10) Raman spectrum of CCI_4 (500-200cm^{-1}) in parallel and perpendicular polarization (488nm excitation)(John R. Ferraro2003).

In the photographic method for the determination of deplorizationratio,a polarizer is placed in the beam of Raman scattered light, the upper half of which allows only the vertical component of the scattered light to pass and the lower half passes only the horizontal component. The intensities on the photographic plate can then be measured with a suitable microphotometer and the ratios determined(DR.H.Kaur,(2001).

2.8 Linear Laser Raman Spectroscopy:

The scattering cross sections in spontaneous Raman spectroscopy are verysmall, typically on the order of $10^{-30}cm^2$. The experimental problems of detecting weak signals in the presence of intense background radiation are by nomeans trivial. The achievable signal-to-noise ratio depends both on the pumpintensity and on the sensitivity of the detector. Recent years have broughtremarkable progress on the source as well as on the detector side (D.J. Gardkner ,1989).

The incident light intensity can be greatly enhanced by using multiple reflection cells, interacavity techniques or a combination of both.Figure 2.8depicts as an example of such advanced equipment a Raman spectrometer with a multiple-reflection Raman cell inside the resonator of an argonlaser. The laser can be tuned by the Brewster prism with reflecting backside(L_P + M) to the different laser lines (A. Weber, 1982).

A sophisticated system of mirrors CM collects the scattered light, which is further imaged by the lens L_1onto the entrance slit *S* of the spectrometer. A Dove prism DPTurns theimage of the line source by 90˚to make it parallel to the entrance slit (Wolfgang Demtröder, 2008).

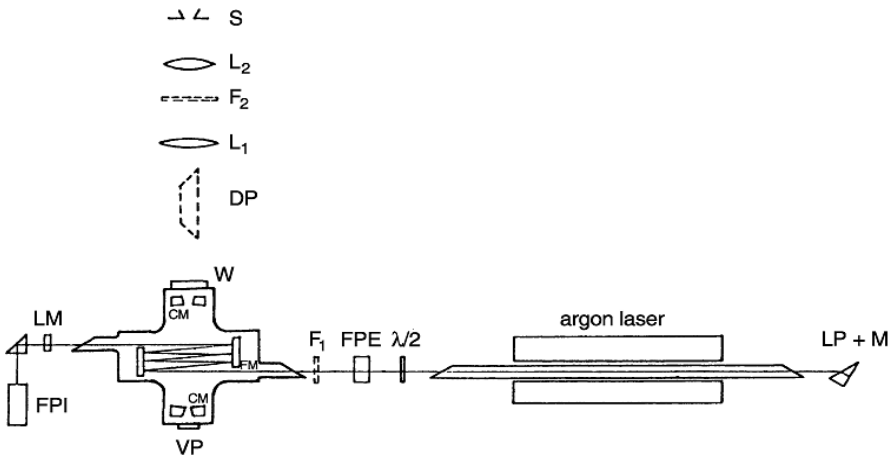

*Figure. (2.11)Experimental arrangement for intracavity Raman spectroscopy with an argon laser: CM, multiple reflection four-mirror system for efficient collection of scattered light; LM, laser-resonator mirror; DP, Dove prism, which turns the image of the horizontalminteraction plane by 90˚ in order to match it to the vertical entrance slit S of the spec-trograph; FPE, Fabry–Perot etalon to enforce single-mode operation of the argon laser; LP, Littrow prism for line selection (*John R. Ferraro2003*).*

2.9 Nonlinear Raman Spectroscopy:

When the intensity of the incident light wave becomes sufficiently large, the induced oscillation of the electron cloud surpasses the linear range.

This implies that the induced dipole moments **p** of the molecules

Are no longer proportional to the electric field **E** and it had to be generalized.The function ***p***(***E***) can be expanded into a power series of E^n (n=0,1,2,...), which is generally written as (2.12a)

$$P(E) = \mu + \tilde{\alpha}\, E + \tilde{\beta}\, E.E + \tilde{\gamma}\, E.E.E \qquad (2.13a)$$

Where α̃ is the polarizability tensor, $\tilde{\beta}$ is named hyper-polarizability,and $\tilde{\gamma}$ iscalled thesecond hyper-polarizability. The quantities α, β, and $\gamma$are tensorsof rank two, three, and four, respectively. In component notation(i =x, y ,z) can be written as (2.13b)

$$\mathrm{p_i}(E) = \mu_\mathrm{i} + \sum_{\mathrm{k}} \alpha_{ik}\, E_K + \sum_{K}\sum_{j} \beta_{ikj} E_K E_j + \sum_{k}\sum_{j}\sum_{I} \gamma_{ikjI} E_K E_j E_I \quad (2.13b)$$

This gives for the polarization $P = N_P$of a medium with N oriented dipoles(2.14c)

$$\mathrm{p_i}(E) = \epsilon_0 \left(\chi_i + \sum_{k} \chi_{ik} E_K + \sum_{K,j} \chi_{ikj} E_k E_j + \cdots \right) \qquad (2.13c)$$

For sufficiently small electric field amplitudes E the nonlinear terms in

(2.13a) can be neglected, and we then obtain $P = \mu_0 + \tilde{\alpha}\, E$ for the linear Raman Spectroscopy(JohnR.Ferro,et.al., 2006).

The nonlinear techniques represent coherent third-order processes

Analogous to saturation spectroscopy, polarization spectroscopy, or two-photonabsorption, because the magnitude of the nonlinear signal is proportional to the third power of the involved field amplitudes.

The advantages of these nonlinear Raman techniques are the greatly increased signal-to-noise ratio and thus the enhanced sensitivity, the higher spectral and spatial resolution, and in the case of the hyper-Raman spectroscopy, the possibility of measuring higher-order contributions of molecules in the gaseous, liquid, or solid state to the susceptibility (Z.Q. Tian, B. Ren ,2000) .

2.9.1 Stimulated Raman Scattering:

If the incident laser intensity $I_L$becomes very large, an appreciable fraction ofthe molecules in the initial state $E_i$is excited into the final state E_f and theintensity of the Raman-scattered light is correspondingly large. Under theseconditions we have to consider the simultaneous interaction of the molecules with two *EM* waves: the laser wave at the

Frequencyω and the Stokes waveat the frequency$\omega_s = \omega_L - \omega_V$or the anti-Stokes wave at$\omega_a = \omega_L + \omega_V$.Bothwaves are coupled by the molecules vibrating with the frequencies ω_V.This parametric interaction leads to an energy exchange between the pump wave and the Stokes or anti-Stokes waves. This phenomenon of stimulated Ramanscattering, which was first observed by Woodbury (Wolfgang Demtröder ,2008).

The Raman medium is taken as consisting of *N* harmonic oscillators

Per unit volume, which is independent of each other Because of the combined action of the incident laser wave and the Stokes wave, the oscillators experience a driving force $\boldsymbol{F}$ that depends on the total field amplitude $\boldsymbol{E}$

$$E(z,t) = E_L e^{i(\omega_L t - k_{sz})} + E_s e^{i(\omega_s t - k_{sz})} \qquad (2.14)$$

Wherewe have assumed plane waves traveling in thez-direction. The potentialenergy $W_{pot}$of a molecule with induced dipole moment $p = \alpha E$in an EMfield with amplitudeEis, according to (3.2, 3.3) with μ=0

$$\mathrm{W_{pot}} = -\mathrm{P.E} = -\alpha(\mathrm{q})\mathrm{E}^2 \qquad (2.15)$$

The forceF=−gradW_{pot} acting on the molecule gives

$$F(z,t) = +\frac{\partial}{\partial q}\{[\alpha(q)]E^2\} = \left(\frac{\partial \alpha}{\partial q}\right)_0 E^2(z,t) \qquad (2.16)$$

The equation of motion for the molecular oscillator with oscillation amplitude *q*,mass *m*, and vibrational eigenfrequency W_V is then

$$\frac{\partial^2 q}{\partial t^2} - \gamma \frac{\partial q}{\partial t} + \omega_V^2 q = \left(\frac{\partial \alpha}{\partial q}\right)_0 E^2/m\,, \qquad (2.17)$$

Whereγis the damping constant that is responsible for the linewidth$\Delta\omega = \gamma$of spontaneous Raman scattering. Inserting the complex ansatz

$$q = \frac{1}{2}\left(q_V e^{i\omega t} + q_V^* e^{-i\omega t}\right), \qquad (2,18)$$

into (3.22) we get with the field amplitude (2.19)

$$(\omega_V^2 - \omega^2 + i\gamma\omega\,) q_V e^{i\omega t} = \frac{1}{2m}\left(\frac{\partial \alpha}{\partial q}\right)_0 E_L E_S e^{i[(\omega_L - \omega_s)t - (k_L - k_s)z]}\,, (2.19)$$

Comparison of the time-dependent terms on both sides of (2.19) shows that$\omega = \omega_L - \omega_s$The molecular vibrations are therefore driven at the difference frequency$\omega_V = \omega_L - \omega_S$. Solving (2.19) for q_v yields

$$q_V = \frac{\left(\frac{\partial \alpha}{\partial a}\right)_0 E_L E_S}{2m[\omega_V^2 - (\omega_L - \omega_s)^2 + i(\omega_L - \omega_s)\gamma]} e^{-i(k_L - K_S)Z}\,, \qquad (2.20)$$

The induced oscillating molecular dipoles ***p*** (ω,z,t) result in a macroscopic polarization $P = NP$. According to (3.5), the polarization $P = P(\omega_s)$at theStokes frequencyω_s, which is responsible for Raman scattering, is given by

$$P_S = \frac{1}{2} N \left(\frac{\partial \alpha}{\partial q}\right)_0 qE. \qquad (2.21)$$

Inserting q from (2.19, 2.20) and E from (2.14) yields the nonlinear polarization

$$P^{NL}{}_S(\omega_s) = \frac{\left(\frac{\partial \alpha}{\partial a}\right)^2_0 E^2{}_L E_S}{4m[\omega_V^2 - (\omega_L - \omega_s)^2 + i(\omega_L - \omega_s)\gamma]} e^{-i(k_L - K_S)Z} \quad (2.22)$$

This shows that a polarization wave travels through the medium with amplitude proportional to the product$E_L^2 \cdot E_S$. It has the same wave vector $K_s$asthe Stokes wave and can therefore amplify this wave. The amplification canbe derived from the wave equation

$$\Delta E = \mu_0 \sigma \frac{\partial}{\partial t} E + \mu_0 \epsilon \frac{\partial^2}{\partial t^2} E + \mu_0 \frac{\partial^2}{\partial t^2} \left(\mathrm{p}^{\mathrm{NL}}{}_{\mathrm{s}}\right), \qquad (2.23)$$

For waves in a medium with the conductivity **σ**,where $\mathrm{P}^{\mathrm{NL}}{}_{\mathrm{S}}$

Acts as the driving term. For the one-dimensional problem (∂/∂y = ∂/∂x = 0) with the approximation $\mathrm{d}^2\mathrm{E}/\mathrm{dz}^2 \ll \mathrm{k}\ \mathrm{d}\ E\ /\ \mathrm{dz}$ and with(2.21), the equation for the Stokes wave becomes

$$\frac{dE_s}{dz} = -\frac{\sigma}{2}\sqrt{\frac{\mu_0}{\epsilon E_s}} + N\frac{K_S}{2\epsilon}\left(\frac{\partial \alpha}{\partial q}\right)_0 q_V E_L. \qquad (2.24)$$

Substituting$q_V$from (2.20) gives the final result for the case$\omega_V = \omega_L - \omega_S$

$$\frac{dE_s}{dz} = \left[-\frac{\sigma}{2}\sqrt{\frac{\mu_0}{\epsilon E_s}} + N\frac{\left(\frac{\partial\alpha}{\partial q}\right)_0^2 E^2{}_L}{4m\epsilon i\gamma(\omega_L - \omega_s)} \right] E_S = (-f+g)E_s \quad (2.25)$$

This becomes

$$E_S = E_S(0)e^{(g-f)z}. \qquad (2.26a)$$

The Stokes wave is amplified if the gain *g*exceeds the losses *f*.The amplification factor g depends on the square of the laser amplitude$E_L$and onthe term$\left(\frac{\partial\alpha}{\partial q}\right)_0^2$. Stimulated Raman scattering is therefore observed only ifthe incident laser intensity exceeds a threshold value that is determined bythe nonlinear term $\left(\frac{\partial\alpha_{ij}}{\partial q}\right)_0$ in the polarization tensor of the Raman-activenormal vibration and by the loss factor.

$f = \frac{1}{2}\sigma\left(\frac{\mu_0}{\varepsilon}\right)^{1/2}$.

According to (2.31), the Stokes intensity increases exponentially with the

Length z of the interaction zone. If, however, the pump wave is absorbed bythe medium, the pump intensity at the position zdecreases to

And the amplitude of the Stokes wave becomes for a medium with length *L*

$$E_S = E_S(0)e^{(g.L_{eff}-f.L)}. \qquad (2.26b)$$

While the intensity of anti-Stokes radiation is very small in spontaneous Raman scattering due to the low thermal population density in excited

Molecular levels, this is not necessarily true in stimulated Ramanscattering. Because of the strong incident pump wave, a large

fraction of all interacting molecules is excited into higher vibrational levels, and strong anti-Stokes radiation at frequencies$\omega_L + \omega_V$has been found.The driving term in the wave equation (2.23) for ananti-Stokes wave $\omega_a = \omega_L + \omega_V$is given by

$$P_{\omega a}^{NL} = \frac{1}{2} N \left(\frac{\partial \alpha}{\partial q}\right)_0 q_V E_L e^{i[(\omega_L - \omega_V)t - k_L]} \quad (2.27)$$

For small amplitudes $E_a << E_L$of the anti-Stokes waves, we can assume that the molecular vibrations are independent of Ea and can replace qv by its solution (2.25). This yields an equation for the amplification of $E_a$that is analogous to (2.29) for E_s

$$\frac{dE_a}{dz} = -\frac{f}{2} E_a e^{i(\omega_a t - k_a z)} + N_V \left[\frac{\omega_a \sqrt{\frac{\mu_0}{\epsilon}}}{8 m_V} \left(\frac{\partial \alpha}{\partial q}\right)_0^2\right] E_L^2 E_S^* e^{i(\omega_a t - k_a z)}, \quad (2.28)$$

WhereN_ν is the density of vibrationally excited molecule. This shows that, analogously to sum- or difference-frequency generation, a macroscopic wave can build up only if the phase-matching condition

$$K_a = 2K_L - k_s, \quad (2.29)$$

Can be satisfied. In a medium with normal dispersion this condition cannot be met for collinear waves. From a three-dimensional analysis, however, one obtains the vector equation

$$2K_L = 2K_S - k_a, \quad (2.30)$$

Which reveals that the anti-Stokes radiation is emitted into a cone whose axis is parallel to the beam-propagation direction Fig 2.9 The apex angle βofthis cone is obtained by multiplying (3.35) with k_a.

This is exactly what has been observed (Wolfgang Demtröder , 2008).

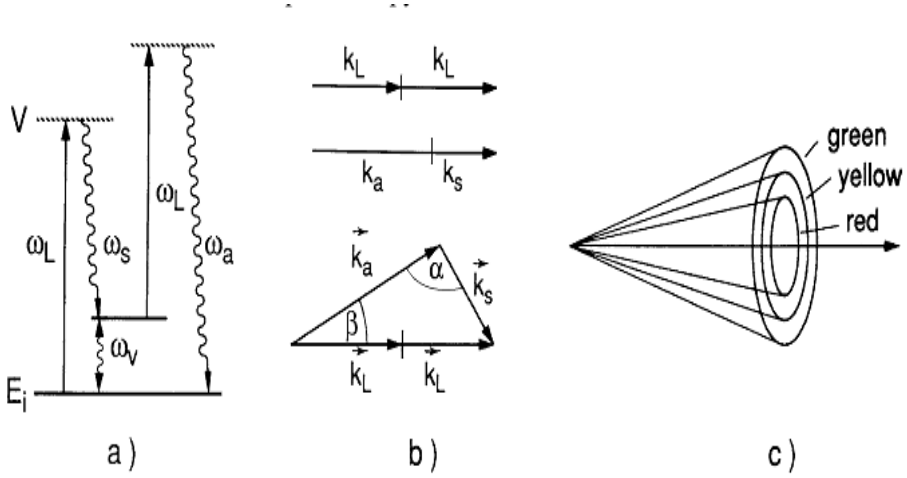

*Figure (2.12**)**.Generation of stimulated anti-Stokes radiation: (**a**) term diagram illustrating energy conservation; (**b**) vector diagram of momentum conservation for the collinear and noncollinear case; (**c**) radiation cone for different values of* $\boldsymbol{k}_S$ *showing red, yellow, and green rings of anti-Stokes radiation excited by a ruby laser at 694 nm*(Wolfgang Demtröder ,2008).

Briefly summarizing the differences between the linear (spontaneous)

And the nonlinear (induced) Raman effect:While the intensity of spontaneous Raman lines is proportional to the incident pump intensity, but lower by several orders of magnitude compared with the pump intensity, the stimulated Stokes or anti-Stokes radiation depend in a nonlinear way onI_P but have intensities comparable to that ofthe pump wave.

The stimulated Raman Effect is observed only above a threshold pump intensity, which depends on the gain of the Raman medium and the length of the pump region.

Most Raman-active substances show only one or two Stokes lines at the

Frequencies$\omega_s = \omega_L - \omega_V$in stimulated emission. At higher pump intensities, however, lines at the frequencies $\omega = \omega_L + n\omega_V$($n$=1,2,3),

Which do not correspond to overtones of vibrational frequencies, have

Beenobserved besides these Stokes lines. Because of the anharmonicity

of molecular vibrations, the vibrational levels in an anharmonic potential

Have energies $E_V = \omega_V\left(n+\frac{1}{2}\right) - x_k\hbar\left(n+\frac{1}{2}\right)^2$and therefore the sponta-neous Raman lines from vibrational overtones are shifted against$\omega_L$by

$\Delta\omega = n\omega_V - (n^2+n)x_K$,where$x_k$ represent the anharmonicity constants.

In Fig. 2.12is illustrated that these higher-order Stokes lines are generatedby consecutive Raman processes, induced by the pump wave, the Stokeswave, etc.

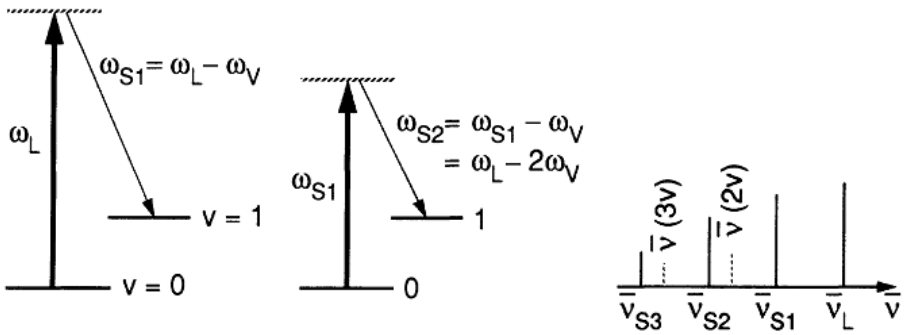

Figure (2.13) Level diagram for the generation of higher-order Stokes sidebands, which differ from the vibrational overtone frequencies (WolfgangDemtröder , 2008)

The linewidths of spontaneous and stimulated Raman lines depend on the linewidth of the pump laser. For narrow line widths, however, the width of the stimulated Raman lines becomes smaller than that of the spontaneous lines, which are Doppler-broadened by the thermal motion of the scattering molecules. A Stokes photon$\hbar\omega_s$, which is scattered into an angle φagainst

the incident laser beam by a molecule moving with the velocity**v**,has a Doppler-shifted frequency.

$$\omega_s = \omega_L - \omega_V - (K_L - K_S).v = \omega_L - \omega_V - \left[1 - \left(\frac{k_s}{k_L}\right) cos\phi\right] k_L.v \qquad (2.31)$$

In the case of spontaneous Raman scattering we have 0≤ φ≤ 2π,and

The spontaneous Raman lines show a Doppler width that is

$\left(\frac{K_S}{K_L}\right) = \left(\frac{\omega_s}{\omega_L}\right)$Times that of fluorescence lines atω_L. For induced Raman

Scattering$K_S \parallel\rightarrow cos\phi = 1$, and the bracket in (2.31) has the value

$$1 - \frac{K_S}{K_L}\omega_L \ll \ 1 \ if \ \omega_V \ll \omega_L \qquad (2.32)$$

The main merit of the stimulated Raman Effect for molecular spectroscopy may be seen in the much higher intensities of stimulated Raman lines.

During the same measuring time one therefore achieves a much better

signal-to-noise ratio than in linear Raman spectroscopy.

The experimental realization of stimulated Raman spectroscopy is based on two different Techniques:

1. Stimulated Raman gain spectroscopy (SRGS), where a strong pump laser at $\omega_L$is used to produce sufficient gain for the Stokes radiation atω_s. This gain can be measured with a weak tunable probelaser tuned to the Stokes wavelengths.

2. Inverse Raman spectroscopy (IRS), where the attenuation of the weak

Probe laser atω_1 is measured when the strong pump laser atω_2 is tuned

Through Stokes or anti-Stokes transitions, several high-resolution stimulated Raman spectrometers have been builtthat are used for

measurements of linewidths and Raman linepositions in order to gain information on molecular structure and dynamics.A good compromise for obtaining a high resolution and a large signal-to-noise ratio is to use a pulsed pump laser and a single-mode cw probe laser quasi-cw spectrometer,The narrow-band pulsed laser can be realizedby pulsed amplification of a single-mode cw laser . For il-lustration Fig. 2.14 shows a typical quasi-cw stimulated Raman spectrometer,where the wavelengths of the tunable dye laser are measured with a travelingMichelson wavemeter(Wolfgang Demtröder2008), (W. Kiefer ,2000).

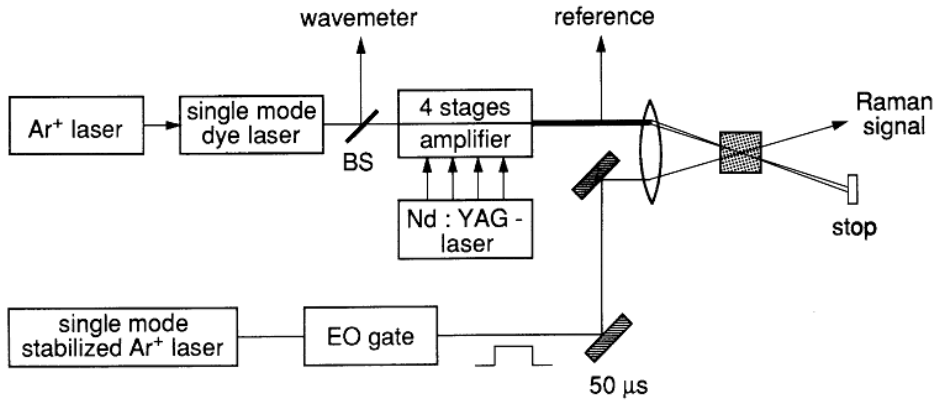

Figure (2.14)Schematic diagram of a stimulated Raman spectrometer with pulsed, amplifiedCW pump laser and a single-mode cw probe laser(Wolfgang Demtröder , 2008)

2.10 Coherent Anti-Stokes Raman Spectroscopy:

Despite the enormous intensities of stimulated Stokes and anti-Stokes

Waves, stimulated Raman spectroscopy has been of little use in molecular

Spectroscopy. The high threshold, which depends on themolecular density$N$, the incident intensity $I \propto E_L^2$, and the square of thesmall

polarizability term $\left(\frac{\partial \alpha_{ij}}{\partial q}\right)$limits stimulated emission toonly the strongest Raman lines in materials of high densities *N*.

The recently developed technique of coherent anti-Stokes Raman spectroscopy (CARS), however, combines the advantages of signal strength obtained in stimulated Raman spectroscopy with the general applicability ofspontaneous Raman spectroscopy(E.K. Gustafson,et.al.,1981),(W. Kiefer,1982).

In this technique two lasersare needed. The frequencies ω_1 andω_2 of the two incident laser waves are chosen such that their difference $\omega_1 = \omega_2 = \omega_V$coincides with a Raman-active vibration of the molecules under investigation. These two incident waves correspond to the pump wave$(\omega_1 = \omega_L)$ and the Stokes wave$(\omega_2 = \omega_S)$ instimulated Raman scattering. The advantage is that the Stokes wave atω_2 is already present and does not need to be generated in the medium.

Because of the nonlinear interaction, Stokes and anti-Stokes waves are generated. The waves ω_1 and $\omega_2$produce a large population density of vibrationally excited molecules by stimulated Raman scattering. These excited molecules act as the nonlinear medium for the generation of anti-Stokes radiation at$\omega_a = 2\omega_1 - \omega_2$by theincident wave with frequency ω_1. In a similar way, a Stokes wave with frequency $\omega_s = 2\omega_2 - \omega_1$ is generated by the incident waves at ω_1 andω_2. Since four waves are involved in the generation of the anti-Stokeswave, CARS is called a four wave parametric mixing process.

If the incident waves are at opticalfrequencies, the difference frequency

$\omega_R = \omega_1 - \omega_2$Small compared with $\omega_1$in the case of rotational–vibrational frequencies ω_R. In gaseous Raman samples the dispersion is generally

negligible over small ranges $\Delta\omega = \omega_1 - \omega_2$and satisfactory phase matching is obtained for collinear beams. The Stokes wave at$\omega_s = 2\omega_2 - \omega_1$and the anti-Stokes wave at$\omega_a = 2\omega_2 - \omega_1$ are then generated in the same direction asthe incoming beams Fig. (2.11b). In liquids, dispersion effects are more severe and the phase-matching condition can be satisfied over a sufficiently long coherence length only, if the two incoming beams are crossed at the phase-matching angle (Fig. 3.14c)(S.A. Akhmanov,et.al.1976).

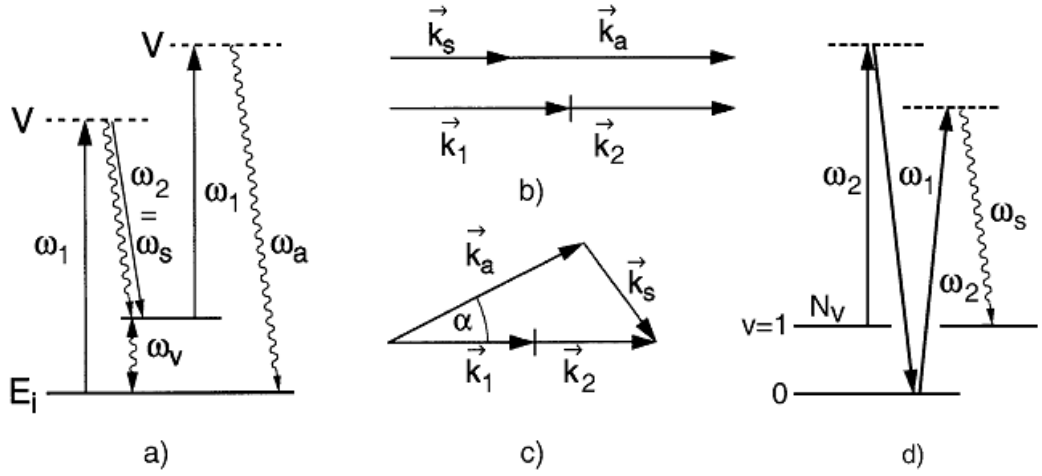

Figure (2.15)(a) Level diagram of CARS; (b) vector diagrams for phase matching in gaseswith negligible dispersion and (c) in liquids or solids with noticeable dispersion(Wolfgang Demtröder , 2008)

2.11Hyper-Raman Effect:

The higher-order terms β***EE,*** γ***EEE***in the expansion ***p(E)*** represent the hyper-Raman effect. We can expand β in a Taylor series in the normal coordinates $q_n = q_{n0}\cos(\omega_n t)$

$$\beta = \beta_0 + \sum_{n=1}^{2Q}\left(\frac{\partial\beta}{\partial q_n}\right)_0 q_n + \cdots, \qquad (2.33)$$

Assume that two laser waves $M\, qE_1E_{01}\cos(\omega_1 t - K_1 Z)$ and$E_2 = E_{02}\cos(\omega_2 t - K_2 t)$are incident on the Raman sample. From the third term in (2.18a) we then obtain with (2.14) contributions to *p(E)* due to β_0

$\beta_0 E^2{}_{01}\cos(2\omega_1 t)And\beta_0 E_{02}^2\cos(2\omega_2 t)$ (2.34)

Which give rise tohyper-Rayleigh scattering at frequencies $2\omega_1, 2\omega_2$and $\omega_1 + \omega_2$Fig. (2.13a). the term $\left(\frac{\partial\beta}{\partial q_n}\right) q_{n0}\cos(\omega_n t)$of inserted into (3.18a) yields contributions

$$P^{HR} \propto \left(\frac{\partial\beta}{\partial q}\right)_0 q_{n0}[\cos(2\omega_1 \pm \omega_n)\, t + \cos(2\omega_2 \pm \omega_n)\, t \qquad (2.35)$$

Which are responsible forhyper-Raman scattering Fig. (2.16b,c)(Wolfgang Demtröder , 2008)

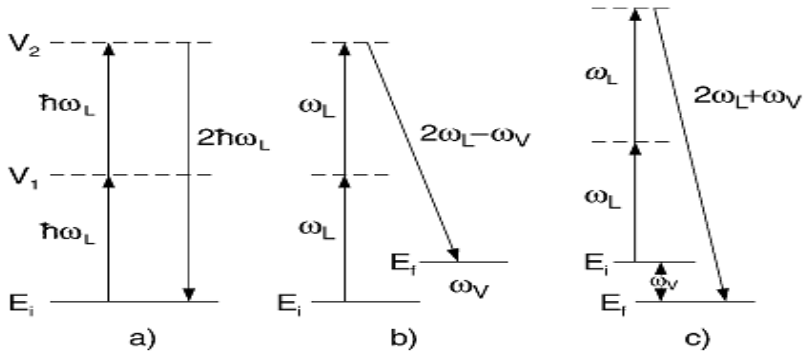

Figure (2.16)a–c.Hyper-Rayleigh scattering (a), Stokes hyper-Raman (b), and anti-Stokeshyper-Raman scattering (c) (Wolfgang Demtröder , 2008) .

Since the coefficients$\left(\frac{\partial\beta}{\partial q}\right)_0$are very small, one needs large incident intensities to observe hyper-Raman scattering. Similar to second-harmonic generation, hyper-Rayleigh scattering is forbidden for molecules with a center of inversion. The hyper-Raman effect obeys selection rules that differ from those of the linear Raman Effect. It is therefore very attractive to molecular spectroscopists since molecular vibrations can be observed in

the hyper-Raman spectrum that is forbidden for infrared as well as for linear Raman transitions. For example, spherical molecules such as CH_4 have no pure rotational Raman spectrum but a hyper-Raman spectrum, which was found by Maker.

The intensity of hyper-Raman lines can be considerably enhanced when

The molecules under investigation are adsorbed at a surface.

Because the surface lowers the symmetry and increases the induced dipole moments. Similar to the induced Raman Effect, the hyper-Raman effect can also beused to generate coherent radiation in spectral ranges where no intense lasersexist. One example is the generation of tunable radiation around 16μmbythestimulated hyper-Raman effect in strontium vapor (S. Nie, L.A. Lipscomb, 1991).

2.12 Types of Raman spectroscopy include:

The types of Raman spectroscopy include the following:

2.12.1 Resonance Raman spectra:

Resonance Raman (RRS) scattering occurs when the

Sample is irradiated with an exciting line whose energy corresponds to that of the electronic transition of a particular chromophoric group in a molecule. Under these conditions, the intensities of Raman bands originating in this Chromophore are selectively enhanced by a factor of 10 ^{3}t o 10^5. This selectivity is importantt not only for identifying vibrations of this particular chromosphere in acomplex spectrum, but also for locating its electronic transitions in an absorption spectrum.

Theoretically, the intensity of a Raman band observed at $V_0 \longrightarrow V_{mn}$is given By (2.9) (John R. Ferraro,2003).

$$I_{mn} = conistant.\, I_0.\,(\nu_0 - \upsilon_{mn})^4 \sum_{P\sigma} |(\alpha_{P\sigma})_{mn}|^2 \quad , (2.36)$$

Here, m and n denote the initial and final states,respectively,of the electronic Ground state. Although not expect in Eq. (2-9),**e** represents an electronic Excited state involved in Raman scattering I_o is the intensity of the Incident laser beam of frequency V_0.finally $(\alpha_{P\sigma})_{mn}$represent the change in polorizibility α caused by the moment transition, and p and σ are x ,y and z components of the polorizibility,tensors this term can be written as (2.10)

$$(\alpha_{P\sigma})_{mn}\frac{1}{h}\sum_{e}\left(\frac{M_{me}M_{en}}{\nu_{em}-\nu_0+i\Gamma_e}+\frac{M_{me}M_{en}}{\nu_{em}-\nu_0+i\Gamma_e}\right), \quad (2.37)$$

Where υ_{em} and υ_{en} are the frequencies corresponding to the energy differences Between the states subscribed and h is Planck's constant. M_{me},etc., are the Electric transition moments, such as(2.11)

$$M_{me} = \int \Psi_m^* \mu_\sigma \Psi_e \, d\tau \,, \quad (2.38)$$

HereΨ_m and $\Psi_e$are total wave functions of the **m** and **e** states, respectively,and**μ**is theσ component of the electric dipolemoment. Γ_eIs the band width Of the **e**th state, and the $i\Gamma_e$term is called the damping constant. In normal Raman scattering υ_0 is chosen so that

$\upsilon_0 \ll \upsilon_{em}$Namely, the energy of the Incident beam is much smaller than that of an electronic transition. Under Theseconditions, the Raman intensity is proportional to $(\upsilon_0 - \upsilon_{mn})^4$. As υ_0Approaches υ_{em},the denominator of the first term in the brackets of Eq(2.11) becomes very small, hence this term (resonance term) become so large that the intensity of the Raman at $\upsilon_0 - \upsilon_{mn}$increases inormously.this phenomenon is called Resonance Raman Scattering.(RRS) (JohnR.Ferro,et.al.,2006).

2.12.2 Surface-Enhanced Raman Scattering:

The intensity of Raman scattered light may be enhanced by several orders of magnitude if the molecules are adsorbed on a surface there are several mechanisms that contribute to this enhancement. Since the amplitude of the scattered radiation is proportional to the induced dipole moment

$$\boldsymbol{P_{ind} = \alpha . E}$$

The increase of the polarizability α by the interaction of the molecule with the surface is one of the causes for the enhancement. In the case of metal surfaces, the electric field *E*at the surface may also be much larger than that of the incident radiation, which also leads to an increase of the induced dipolemoment. Both effects depend on the orientation of the molecule relative tothe surface normal, on its distance from the surface, and on the morphology,in particular the roughness of the surface. Small metal clusters on the surface increase the intensity of the molecular Raman lines. The frequency of the exciting light also has a large influence on the enhancement factor. In the case of metal surfaces it becomes maximum if it is close to the plasma frequency of the metal. Because of these dependencies, surface-enhanced Raman spectroscopy has been successfully applied for surface analysis and also for tracing small concentrations of adsorbed molecules one example is the detection of explosive molecules such as TNT on porous gold surfaces where detection sensitivity down to 0.1 ppm could be achieved (Z.Q. Tian, B. Ren ,2000).

2.12.3 Raman Microscopy:

For the nondestructive investigation of very small samples, for example, partsof living cells or inclusions in crystals, the combination of microscopy and Raman spectroscopy turns out to be a very useful technique. The laser beam is focused into the sample and the Raman spectrum that is emitted

from the small focal spot is monitored through the microscope with subsequent spectrometer. This also applies to measurements of phase transitions in molecular crystals under high pressures. These pressures, which reach up to several GigaPascal, can be realized with moderate efforts in a small volume between two

Diamonds with area that are pressed together by a force *F* producing a pressure $p=F/A$. For example, with $F=10^3$Pa and$A=10^{-6}$cm^2, one obtains a pressure of $10^9 Pa$. The phase transitions lead to a frequency shift of molecular vibrations, which are detected by the corresponding shift of the Raman lines.One example of the application of this technique is the investigation of different phases of “fluid inclusions” in a quartz crystal found in the Swiss Alps.Their Raman spectra permitted determination of CO_2 as a gaseous inclusion and water as a liquid inclusion, and they showed that the mineral thought tobe $CaSO_4$ was in fact $CaCO_3$(S. Nie, L.A. Lipscomb,1991).

A typical experimental arrangement for Raman microscopy is shown in

Fig. 2.17 The output beam of an argon laser or a dye laser is focused

by a microscope objective into the micro sample. The backscattered Raman light is imaged onto the entrance slit of a double or triple monochromator,which effectively suppresses scattered laser light. A CCD camera at the exit of the monochromator records the wanted spectral range of the Raman radiation (L. Quin, Z.X. Shen,et.al.,1997).

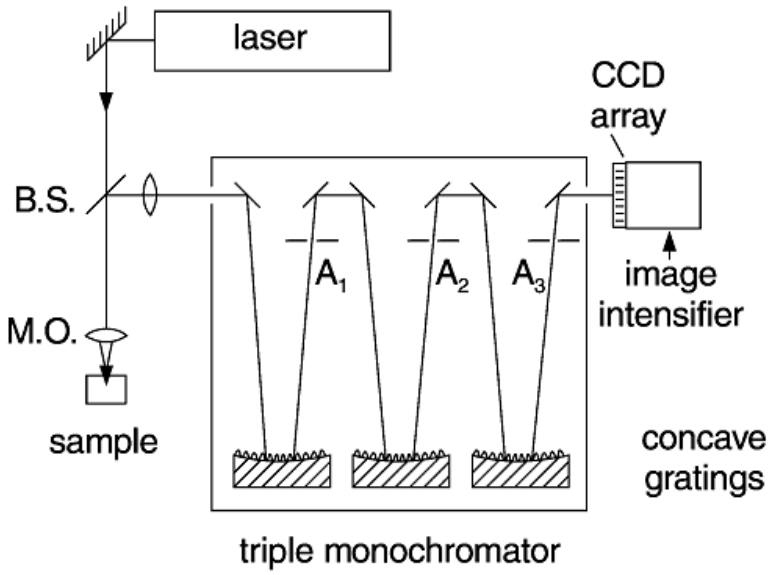

Figure(2.17) Raman microscopy with suppression of scattered laser light by a triple monochromator with three apertures Ai(Wolfgang Demtröder , 2008)

2.12.4 Time-Resolved Raman Spectroscopy:

Both linear and nonlinear Raman spectroscopy can be combined with time-resolved detection techniques when pumping with short laser pulses

Since Raman spectroscopy allows the determination of molecular parameters from measurements of frequencies and populations of vibrational and rotational energy levels, time-resolved techniques give information on energy transfer between vibrational levels or on structural changes of short-livedintermediate species in chemical reactions. One example is the vibrational excitation of molecules in liquids and the collisional energy transfer from the excited vibrational modes into other levels or into translational energy ofthe collision partners. These processes proceed on Picosecond to Femtosecondtime scales (W. Kiefer, 2000).

Time-resolved Raman spectroscopy has proved to be a very useful tool

to elucidate fast processes in biological molecules, for instance, to follow

the fast structural changes during the visual process where, after photoexcitation of rhodopsin molecules, a sequence of energy transfer processesinvolving isomerization and proton transfer takes place(M. Danfus, G. Roberts,1991).

2.12.5 High-Pressure Raman Spectroscopy:

The pressure technique involves a pressure device diamond anvil cell (DAC)that can transmit the pressure to the sample under study. If spectroscopic methods are chosen for diagnostic purposes, it is a requirement to use windows on the pressure device that are hard and transmit the irradiating light in the particular wavelength of the electromagnetic spectrum being studied. The window of choice for IR and Raman studies is type of diamond. It is the hardest material known and is transmissive for laser Raman studies.Additionally, it is an excellent thermal conductor as well. The pressure deviceMust be compact and fit into the sample compartment of the spectrometer.The DAC fulfills all of these criteria and has been extensively used since itsdiscovery by Weir and Van Valkenburg in 1959. The interface to the Ramanspectrometer is readily accomplished (unlike the IR experiment where beam condensers are required in the dispersive instrument, although presently this requirement is unnecessary in the Raman DAC experiment), and normal commercial Raman instrumentation can be used (John R. Ferraro,2003).

A few applications illustrating the pressure effects on materials using Raman spectroscopy as the diagnostic tool, like:

1. Phase Transitions in Solids.

2. Pressure Changes in Solid Coordination Compounds.

3. Evidence for Metallization of hydrogen at Mega bar Pressures.

2.12.6 Matrix-Isolation Raman Spectroscopy:

Technically, Raman spectroscopy is more difficult to apply to low-temperature matrices than IR spectroscopy for the following reasons: (1)

Since Raman signals are inherently weak, relatively high concentrations of the sample or relatively wide slit widths are required. The former may cause the formation of diametric and polymeric species, while the latter leads to the loss of resolving power of the monochromator. (2) If one increases the laser power to obtain stronger Raman signals, the matrix temperature will rise because of local heating by the laser beam, and this will accelerate the diffusion of solute molecules in the matrix. (1) and (2) can be circumvented if Raman spectra are obtained under resonance conditions. (3) The quality of the Raman spectra obtained depends on the quality of the matrix prepared;"clear matrices" give better results. (4) The matrix itself or oil contamination from the diffusion pump may cause fluorescence.

In some cases, matrix-isolation laser-Raman spectroscopy can be utilized to produce unstable species via laser photolysis and to measure their resonance Raman spectra simultaneously in the same matrix using the same laser (John R. et al., 2003).

2.12.7 Raman spectroelectrochemistry:

Raman spectroelectrochemistryis a field in which studies electro generated species on electrode surfaces, in electrode diffusion layers and bulk solutionby Raman spectroscopy. Thus, the surface-enhanced Raman scattering(SERS) is part of Raman spectroelectrochemistry. Here, we discuss Raman spectroscopic studies on electrogenerated species in bulk solution and in electrode diffusion layers. Since no enhancement from SERS is expected and

Since the concentrations of these electro generated species are rather low, it isimperative to take advantages of resonance Raman (RR) scattering ;

(a) Bulk solution: measured the RR spectrum of the tetracyanodimethane

Anion radical ($TCNQ^-$).

(b) Diffusion Layer: The RR spectrum of tetramer hyphenylenediamine$TMPD^+$, confined to the diffusion layer, was obtained by applying a square-wave voltage (repetition rate, 10 Hz)(John R. et al.,2003).

2.12.8 Two Dimensional Correlation Raman Spectroscopy:

The concept of two-dimensional (2D) correlation spectroscopy has been

Applied to a number of systems to separate overlapped bands, to make band as signments, and to study intensity variations of individual bands due toexternal perturbations. The first step is to measure a series of spectra (Raman)of a system by changing the external perturbation (temperature, pressure,concentration etc.). Then, a series of dynamic spectra are calculated bysubtracting a reference spectrum from each perturbed spectrum. An average of observed spectra is generally used as the reference spectrum (John R. et al., 2003).

2.12.9 Raman Imaging Spectrometry:

In Raman images, Raman spectra are measured at the various spatial

Locations. After all the data are collected, it is possible to display individual Raman spectra for each spatial location or to display a false color image based on the intensities at a selected Raman frequency.

The ability to obtain Raman images of chemical and biological samples is of great importance to the scientific community. The improvements and

Increased use of charge couple devices (CCD) for detection of Raman spectra has made such measurements practical. Imaging spectrometer used to measure Raman images of a biological system.

Two Dimensional correlation spectroscopy is highly effective in separating overlapped bands which cannot be resolved by conventional one-dimensional spectroscopy (John R. Ferraro, 2003).

2.13 Raman spectrometers:

Raman spectrometers are used to analyze light scattered by molecules. Major advantage of Raman spectroscopy is the high spatial resolution that can be obtained, typically of the order of 1μm (compared to approximately 10 μm with FTIR).in conventional Raman experiments the sample is illuminated by monochromatic light. The registration of the low intensity Raman scattering in the presence of strong Tyndale and Rayleigh scattering implies special requirements for Raman spectrometer, A Raman spectrometer has to combine very good filter characteristics for eliminating Rayleigh and Tyndall scattering with high sensitivity for detecting very weak Raman bands(G.Goulitz,et.al.,2003).

There are three types of Raman instruments:

1/ Raman grating spectrometer with single channel detectors

2/ FT-Raman spectrometer with near infrared excitation.

2/ Raman grating polychromaticwith multi-channel detector.

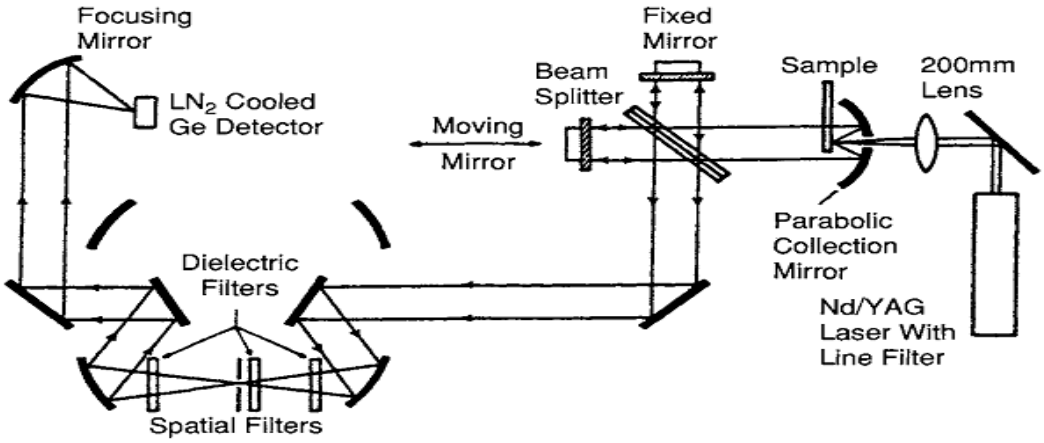

Figure (2.18) Ramanspectrometer(John R. Ferraro, 2003).

2.13.1 Instrumentation and Experimental Techniques:

Most Raman spectroscopic investigations have been performed on dispersive instruments. . However, Fourier transform(FT) techniques have Become increasing important as a means of reducing interference from fluorescence.

Four major components make up the commercially available Raman spectrometer these consist of the bfollowing**:**

The Excitation source which determine the Transmit limit of wavelength of light with enough power to produce Raman spectra, which is generally acontinuous wave (CW) laser, lasers are ideal excitation sources for Raman spectroscopy due to the following characteristics of the laser beam:

(a) Single lines from large CW Lasers can easily provide 1-2Wof power,and pulsed lasers produce huge Peak powers on the order of 10 – 100 MW.

(b) Laser Beams are highly monochromatic (bandwidth ~ $0.1cm^{1}$forAr^{+}laser),and Extraneous lines are much weaker. The extraneous lines can be eliminated easily by using notch filters or pre-monochromators.

(c) Most laser beams have small diameters (1-2mm),which can be reduced to 0.1 mm by using Simple lens systems.Thus all the radiant flux can be focused on a small sample, enabling fruitful studies of micro liquids (~μL) and crystals (~1mm^3).In the case of Raman microscopy sample areas as Small as ~2 μL in diameter can be studied.

(d) Laser beams are almost completely linearly polarized and are ideal for measurements of depolarization ratios.

(e) It is possible to produce laser beams in a wide wavelength Range by using dye lasers and other devices (John R. Ferraro, 2003).

2.13.2 Sample illumination:

Since the Raman scattering is inherently weak, the laser beam must be

Focused properly on to the sample and the scattered radiation collected efficiently.The focusing of the laser on to the sample can be readily achieved Because of the small diameter of the laser beam (~1mm).Excitation and Collection from the sample can be accomplished by using several optical configurations, such as the 90°and180°scattering geometries illustrated in. Collection optics consist of a nachromatic Lens system with a collecting lens and a focusing lens, as shown in an oblique illumination , angle is also a common configuration for illuminating the front surface of a shamble with incident laser beam at ~85° to the normal (John R. Ferraro,2003).

Wavelength selector can be classified into several categories, the simplest detective device is an interference filter, which depends on its two optically flat surfaces to generate constrictive interference and transmit an integer number of wavelengths corresponding to twice the thickness of the filter.

Interference filters are constructed for single wavelengths (wavelengths corresponding to this wavelength divided by integers also will have constructive interferences and be observed).

Variable wedge shaped interference filters are available for selecting desired wavelengths, however the spectral resolution of these devices is generally too large for Raman spectra. Recently acoustic and liquid crystal tunable filters have been used successfully for measuring Raman spectra and Raman spectral images.

Both prism and grating monochromators and spectrographs have been

Used extensively for measuring Raman spectra.While monochromators are Still the main stay of Raman instrumentation, FT-Raman has made considerable advancement in recent years and is now considered to be competitive With monochromators.

2.13.3 Detection:

Since Raman signals are inherently weak, the problems involved with detection and amplification are severe, Most of the very early work was performed with photographic detection using long exposure times. Furthermore, the Time to develop photographic plates and examine them with a micro photometer rendered Raman spectroscopy unfit as a routine technique. This situation has changed considerably since the development of strong laser Sources and sensitive detection techniques.

Several detections techniques are used, such as, Photon counting, photodiode array charged couple device (CCD), and indium -Gallium-Arsenide (In Ga As) detectors used for FT Raman instruments which required high sensitivity.

2.13.4 Interpretation of Raman spectrum:

Raman is interpreted by evaluating wavelength or frequency of the line, its intensity and state of polarization. These are then compared with spectra obtained for pure compounds. Like IR spectra, correlations exist between the presence of certain functional groups in a molecule and frequencies of certain Raman lines. Symmetrical vibrations are active in Raman spectrum but are inactive in IR spectrum. Hence these vibrations give sharp Raman lines, similarly covalently bonded inorganic compounds are Raman active. Some vibrations alter both the polorizibility and the dipole moment and hence will be seen in Raman spectra as well as IR spectra (DR.H.Kaur,2001).

2.13.5 The intensity of Raman peaks:

The intensity or power of Raman peaks depends on the following factors:

- Intensity of the source
- Concentration of the active group
- Polorizibility of the molecule

  In the absence of absorption, the power of Raman emission increases with the fourth power of the frequency of the source. Raman intensities are directly proportional to the concentration of the active species, where the concentration intensity relationship is logarithmic.

  Generally strong bands in the IR correspond to weak bands in the Raman spectrum and vice versa. This complementary nature of IR and Raman spectra is because electrical characteristics of the vibrations.

  The absolute intensity measurements of Raman lines are more difficult than that of IR lines.

The variables which affect the Raman intensity are of two types:

i. The variables dependent upon the nature of the sample
ii. The variables independent upon the nature of the sample

The former includes the refractive index of the sample and absorption of both exciting and scattered radiation by the sample. The variables independent of sample include the instrumentation conditions like, slit width, frequency response of the detector, time constant speed and variation in the transmittance of the instruments etc. due to these reasons, the intensity of the Raman line is usually measured in terms of arbitrary chosen 459cm^{-1} line of CCL_4 which is the most intense line among stokes and anti –stokes lines. The ratio of the intensity of Raman line and that of 459cm^{-1} line known as the scattering coefficient, the usual procedure is to scan 459cm^{-1}line of CCL_4 before and after the spectral trace of each sample. The recorded height of the sample peak is then divided by the averageheights of the two traces of CCL_4 peak. This gives the scattering coefficient which is a measure of the intensity of the Raman line (DR.H.Kaur, 2001).

2.14 Applications of Laser Raman Spectroscopy:

The primary object of Raman spectroscopy is the determination of molecular energy levels and transition probabilities connected with molecular transitions that are not accessible to infrared spectroscopy. Linear laser Raman spectroscopy, CARS, and hyper-Raman scattering have very successfully collected many spectroscopic data that could not have been obtained without other techniques. Besides these basic applications to molecular spectroscopy there are, however, a number of

scientific and technical applications of Raman spectroscopy to other fields, which have become feasible with the new methods discussed in the previous sections.

Since the intensity of spontaneous Raman lines is proportional to the density of molecules in the initial state, Raman spectroscopy can provide information on the population distribution and its local variation, and on concentrations of molecular constituents in samples. This allows one, for instance, to probe the temperature in flames or hot gases from the

Rotational Raman spectra and to detect deviations from thermal

Equilibrium (Wolfgang Demtröder ,2008).

With CARS the spatial resolution is greatly increased, in particular if BOXCARS is used. The focal volume from which the signal radiation is generated can be made smaller than $0.1mm^3$.

The local density profiles of reaction products formed in flames or discharges can therefore be accurately probed without disturbing the sample conditions (Wolfgang Demtröder, 2008).

Another example is the measurement of CARS spectra of water vapor in flames, which allowed one to probe the temperature in the post flame region of a premixed CH_4 air flame.

With a detection sensitivity of 10 to 100 ppm, CARS is not as good as

Some other techniques in monitoring pollutant gases at low concentrations but its advantage are the capability to examine a large number of species quickly by tuning the dye lasers.

Examples are temperature and concentration measurements of molecular nitrogen, oxygen, and methane in a high-temperature furnace up to 2000 K

[3.84], where the thermal radiation is much stronger than laser-induced fluorescence. Therefore CARS is the best choice because the detector can be placed far from the furnace.

A further example of the scientific application of CARS is the investigation of cluster formation in supersonic beams, where the decreasing the rotational and vibrational temperatures during the adiabatic expansion and the degree of cluster formation in dependence on the distance from the nozzle can be determined (Wolfgang Demtröder, 2008).

2.15 Raman IndustrialApplications:

Industrial applications of the Raman Effect have garnered intense interest since the introduction of FT-Raman instrumentation. Concurrent with FT-Raman instrumentation developments have been the fiber optics improvements and the advent of new detectors. These three factors have synergized and have led to the present interest in Raman spectroscopy. This has brought the Raman Effect from the laboratory and into the plant ، wherein situ measurements are now possible in a number of industrial environments (John R. Ferraro, 2003).

Raman spectroscopic investigation of CO_2clatharate formation,clatharate are cage like structures formed by water molecules under low temperature and high pressure conditions. Trapping of small gas guest molecule in the hydrogen bonded network of water molecules initiate the formation of clathrates. Interest in clathrates has increased recently science methane clathratesmay be potential natural gas source,and CO_2clathrates provides a way to relocate the atmospheric CO_2. CO_2clathrates also play important roles in the atmosphere of Mars and other planetary system.

Clathrates are comprised of 85 % mole water molecules and 15 mole % guest molecules. This composition makes their structure different from that of hexagonal ice.

There are characteristic differences in the stability and thermo dynamics properties between hexagonal ice and clathrates. Raman spectroscopy is used to follow the formation of CO_2clathratesat different pressure and to understand the kinetics of formations .the fermidiads of carbon dioxide show a change in the frequency and linewidth when carbon dioxide is incorporated in the clathrate cages. Monitoring the increase in the intensities ofthe Fermidiads over time provides information of the rates of formation ofclathrates under different pressure conditions.this direct relation between the ease the ease of formation of clathrates and increasing pressure is correlated with the presence of a guasi-liquied layer (Patric Benziher,2004).

2.16 Medical Raman Applications:

Due to recent advancements in instrumentation, Raman spectroscopy has

Become one of the most powerful tools in medical research. Such advancements include development of new lasers , FT-Raman spectroscopy, CCD Detectors ,confocal Raman microscopy, Raman imaging, fiber optic probes ،and computer software.In medical science is demonstrated by using selected examples such as skin. Nails and Hair

Also Lenses proteins,gal lstones and medical diagnosis (Y.Guan.E,et.al.,1999).

2.17 Raman Applications in Biology:

Applications of Laser Spectroscopy: Three aspects of laser spectroscopy are particularly relevant for biological applications. These are the high spectral resolution combined with high temporal resolution, and the high detection sensitivity. Laser light, focused into cells, also offers a high spatial resolution. The combination of LIF and Raman spectroscopy has proven very helpful in the determination of the structure of biological molecules, whereas time-resolved spectroscopy plays an essential

Role in the study of fast dynamical processes, such as the isomerization during photosynthesis or the formation of antenna molecules during the first steps of the visual process. Many of these spectroscopy techniques are based on the absorption of laser photons by a biological system, which brings the systeminto a non-equilibrium state. The time evolution of the relaxation processes thattry to bring the system back to thermal equilibrium can be followed by lasers pectroscopy (Wolfgang Demtröder, 2008).

2.18 Artificial sweeteners*:*

The fondness of humans for sweet food is inborn; studies have shown a preference for sweet-tasting nutrition in newborns. Therefore, mankind has always added sweet substances to their food. Recognizing our desire for sweet flavors, the food industry has developed and supplied sugar free alternatives designed to satisfy our cravings, referred to as sugar substitutes, artificial sweeteners, or non-nutritive sweeteners. Uses of sweeteners have largely increased in the past 20 years. Nowadays they occupy a large portion of commercial space on supermarket shelves worldwide. These products are available mainly for people who are diabetic or who are looking for low-calorie materials. Alternative

sweeteners are produced to be used in several products ranging from cookies to soft drinks, in order to satisfy the consumers. Where conventional sugars such as glucose, fructose, and sucrose are to be replaced by highly sweet alternatives, the fact that such alternatives often do not have the bulk that the conventional carbohydrates do, on account of their higher sweetening intensity per unit weight, must be borne in mind. Sweet substances are compounds with diverse chemical structures and sizes, for example, sugars (sucrose), sugar alcohols (xylitol), sulfonyl amides (saccharin), Peptides (aspartame), D-amino acids (D-tryptophan), and proteins (thaumatin) The worldwide demand for high-potency sweeteners is expected to increase, Especially with the new practice of combining different sweeteners. Amongst naturally derived sweeteners, stevia and liquorice root are likely to become prevalent sources of high-potency sweeteners for the growing natural food market in the future Sweeteners can be grouped in various ways. Sweetener potency is defined as the number of times that a sweetener is sweeter than sucrose, the potency of a sweetener is compared with sucrose mainly in the threshold levels of the sweetener and sucrose. Sugars and sugar alcohols, such as sucrose and xylitol, are low-potency sweeteners, whose sweetener potencies are about 1 and under. On the other hand, sweeteners which have a sweetener potency exceeding 10 are called high-potency sweeteners, Such as saccharin and aspartame. Interestingly, low-potency sweeteners, such as Sucrose, exhibit higher sweetness intensity than high-potency sweeteners at very High concentrations. That is why low-potency sweeteners are also called high intensity sweeteners table (2.1) shows the classification of sweeteners (Arpita Das, et.al. 2016).

2.18.1 Classification of sweeteners:

Sweeteners are classified according to their origin, table 2.1illustrate the types of sweeteners;

Table 2.1 Classification of sweeteners

Caloric	Natural	Sugars	Sucrose, glucose, dextrose, fructose, lactose,maltose,Naturalgalactoseandtrehalose, tagatose,Sucromalt
		Natural caloric sweeteners	Honey, maple syrup, palm or coco sugar, and sorghum syrup
	Artificial	Modified Sugars	High fructose corn syrup,caramel,inverted sugar.
		Sugar alcohols	Sorbitol, xylitol, mannitol, erythritolmaltitol,isomaltulose, lactitol, glycerol
Noncaloric	Natural	Noncaloric sweeteners	Luohanguo, stevia, thaumatin, pentadin, monellin, brazzein
	Artificial	Sweeteners	Aspartame, sucralose, saccharin, neotame, acesulfame K, cyclamate,neohesperidinDC,alitame, advantame

2.18.2 Natural and Artificial Sweetener:

Sweetener can be broadly divided into two categories, natural and artificial or synthetic sweetener. Natural sweetener can be further divided into saccharide andnonsaccharidesweeteners. Many other natural alternatives to sugar are available, though not widely used, despite the fact that natural nonrefined sugar alternatives potentially contain beneficial bioactive compounds, especially polyphenolic compounds, known and appreciated for their antioxidant properties. Some of these natural sugar alternatives include plant saps/syrups (e.g., maple syrup, agave nectar), syrups made from raw sugar and grains (e.g., molasses, barley malt, and brown rice syrup), honey, and fruit or vegetable sugars (e.g., date sugar, carrot).

Artificial sweeteners have been classified as nutritive and non-nutritive depending on whether they are a source of calories. The nutritive sweeteners include the monosaccharide polyols (e.g., sorbitol, mannitol, and xylitol) and the disaccharide polyols (e.g., maltitol and lactitol). They are approximately equivalent to sucrose in sweetness. The non-nutritive sweeteners, better known as artificial sweeteners,Include substances from several different chemical classes that interact with tasteReceptors and typically exceed the sweetness of sucrose by a factor of 30–13,000Times. Nutritive sweeteners (e.g., sucrose, fructose) are generally recognized as safe (GRAS) by the Food and Drug Administration (FDA), yet concern exist aboutIncreasing sweetener intakes relative to optimal nutrition and health(Arpita Das,et.al.,2016).

2.18.3 Health Aspects of Sweeteners:

Both nutritive and non-nutritive sweeteners have generated health concerns among health care providers and the public for many years. Concerns

related to safety of non-nutritive sweeteners are addressed primarily in animal studies. Artificial sweeteners are present in many food consumed by whole world. Their use is beneficial in that they provide sweetness, increasing the palatability of food without the added sugar and resulting calories, an important adjunct to weight loss and diet regimens. Most artificial sweeteners are not metabolized by the body and are therefore considered safe. However, scientists disagree about safety of these chemical additives and still studies in progress in the field of investigation the effect of the artificial additives on the cancer cells, because the metabolites of the "nonmetabolized" compounds have been shown to produce deleterious effects in mice, rats, and dogs (Arpita Das,et.al.,2016).

2.19 Literature Review:

Anna GraziaMignani, Leonardo Ciaccheri. Et.al in 2016 used Raman spectra, excited at 532 nm dispersiveschemes. These spectra provided fluorescence-free Raman signatures from which to identify the most significant peaks of the variousSweeteners (AccesulfameK($C4H4KNO4S$) ,Aspartame ($C14H_{18}N_2O_3$) ,Saccharin ($C_7H_4NNaO_3S$) ,Sorbitol ($C_6H_{14}O_6$) , Sucralose ($C_{12}H_{19}C_{l3}O_8$) , and Xylitol($C_5H_{12}O_5$), These peaks were also compared with ones obtained by means of computational analysis, in order to show the effect of the entire sweetener matrix. The spectroscopic data were then processed by means of chemometric analysis for distinguishing what kind of sweetener was present in a given sample. First, Principal Component Analysis was applied for the purpose of data dimensionality reduction and explorative investigation and provided good clustering depending on the type of sweetener. Next, the K-nearest neighbors method was used in order to assign the samples to predefined classes. An excellent identification in accordance with the type of high- or low-power sweetener was thus obtained. These results confirm the success of Raman

spectroscopy in attaining a straightforward analysis of intact food, with high potentials for its use as a non-destructive and "green" analytical method for quality control in the food industry (Arpita Das,et.al.,2016).

Marleen de Veij,a Peter Vandenabeele.et.al. In 2008 used Raman spectroscopy as direct and nondestructive technique in pharmaceutical analysis by focusing onPharmaceutical excipients that presented in food and Drugs in this article, which can serve as a reference for the interpretation of Raman spectra during drug analysis (including classical qualitative and quantitative pharmaceutical analysis, counterfeit tracing and process analytical technology (PAT) applications). The 43 analyzed excipients can be classified into seven categories: mono- and disaccharides (dextrose, lactitol, maltitol, sorbitol , xilytol, lactose and sucrose), polysaccharides (microcrystalline cellulose,methylcellulose (MC), carboxymethylcellulose (CMC), hydroxypropyl cellulose (HPC), hydroxypropylmethylcellulose (HPMC), wheat starch, maltodextrin, primojel, tragacanth and pectin), polyalcohols (propylene glycol, erythritol, xylitol, mannitol and sorbitol), carboxylic acids and salts (alginic acid, glycine, magnesium stearate, sodium acetate and sodium benzoate), esters (arachis oil, lubritab, dibutylsebacate, triacetin, Eudragit E100 and Eudragit RL100), inorganic compounds (calcium phosphate, talc, anatase and rutile (TiO_2), calcium carbonate,magnesium carbonate, sodium bicarbonate and calcium sulfate) and some unclassified products [gelatin, macrogol 4000 (polyethylene glycol (PEG), polyvinyl pyrrolidone and sodium lauryl sulfate (Marleen de Veij,et.al.,2008).

Nicoleta Tosa.et.al in 2012 studied some non-nutritive sweeteners such as aspartame, acesulfame-K, sodium cyclamate and sodium saccharin were simultaneously determined in ternary mixtures using FT-IR and EI-MS measurements. FT-IR method is based on direct measurements of the peak

height values and area centered on 1736 cm-1, 836 $cm^{-1,}$ 2854 cm^{-1} and 1050 cm^{-1} for aspartame, acesulfame-K, sodium cyclamate and sodium saccharin, respectively.

Mass spectrometry determinations show the characteristic peaks at m/z 91 and 262 for aspartame, m/z 43 and 163 acesulfame-K, m/z 83 and 97 for sodium cyclamate and m/z 104 and 183 for sodium saccharin. The results obtained by EI-MS in different formulations are in agreement with the FT-IR ones and provide also essential data concerning the purity grade of the components. It is concluded that FT-IR and EI-MS procedures developed in this work represent a fast, sensitive and low cost alternative in the quality control of such sweeteners in different ternary formulations (Nicoleta Tosa,et.al.,2012).

NiculinaPeica in 2009, by vibrational spectroscopy and theoretical modeling studied Identification and characterization of the Aspartame E951 artificial food sweetener, a very well-known dipeptide sweetener, approximately 150–200 times sweeter than sugar, is widely used in a variety of applications, especially in soft drinks. A drawback of E951 is its relatively low stability at high pH values and athigh temperatures, thereby limiting its use. The changes observed in the very strong bands from the 1600 cm^{-1} to 300 cm^{-1} spectral region, characteristic to the υ(CO) mode coupled with the NH bending mode, allows to establish the species present in the Raman and SERS solutions at different concentrations and pH values. More exactly, a molecule protonation at the amino group was detected on going from basic to acidic pH values. The DFT calculated geometry, harmonic vibrational modes and Raman scattering activities of E951 were in good agreement with the experimental data and helped establish its SERS behavior on silver surfaces. According to the DFT calculations performed, E951 can give rise to an intermolecular hydrogen

bonding network, with lengths in the same range as the hydrogen bonds in the peptide unit moieties (NiculinaPeica, 2009).

Anna G. Mignani a, Leonardo Ciaccheri a, Andrea A.et.al in 2014 used Raman spectroscopy excited at 1064 nm was used to measure a selection of artificial sweeteners that are commonly used in low calorie diets. Aqueous solutions with different sweetener concentrations in the 5%-30% w/w range were analyzed, and aMultivariate data processing of spectroscopic data was used to building a classification map. This map showed an excellent clustering according to the sweetener composition, indicating excellent potentials of Raman spectroscopy for the assessment of food quality, the study shows the results of Raman spectroscopy in the most significant 300-1600 cm-1 band of all sweetener solutions with minimum and maximum concentration, as expected, every type of sweetener has a different Raman spectrum, like a signature, depending of the own composition as fellows Sorbitol main peak is at (876) cm^{-1}, Erythritol main peaks are at (867,1046,700) cm^{-1} , Dextrose main peaks at (517, 446, 424, 1126) cm^{-1}. Sucrose main peaks are at (838, 547, 525, 638) $cm^{-1}$and Maltodextrin the main peaks are at (481, 937, 863) cm^{-1}(Anna G. Mignani a, 2014).

P.Ramesh and S. Gunasekaran in (2018) studied the Structural, Spectroscopic Investigation and Quantum Chemical Calculation studies on Methyl L-α aspartyl –Lphenylalaninate (Aspartame) for pharmaceutical Application using The Fourier transform infrared (FTIR-ATR) and FT-Raman spectra of Methyl L-α aspartyl -L-Phenyl alaninate have been recorded in the range of 4000-400cm-1 and 4000-50cm-1 respectively . A detailed interpretation of the vibrational spectra of this compound has been made based on the calculated potential energy distribution (PED). Then the vibrational FTIR and FT-Raman spectra of Aspartame were recorded

and compared with the computed vibrational wavenumbers. The fundamental assignment has been made on the basis of the calculated Potential Energy Distribution. The molecular structural parameters like bond length, bond angle, vibrational frequencies of the fundamental modes and thermodynamic properties has been determined using DFT-B3LYP calculations with 6-31G(d,p) basis set (P.Ramesh, S., 2018).

Ismail HakkiBoyaci.Etal in 2015 used Dispersive and FT-Raman spectroscopic methods in food analysis as a powerful technique for molecular analysis of food samples. A fingerprint spectrum can be obtained for a target molecule by using Raman technology, as specific signals are obtained for chemical bonds in the target. In this way, food components, additives, processes and changes duringshelf life, adulterations and numerous contaminants such as microorganisms, chemicals and toxins, can also be determined with or without the help of chemometric methods. The studies included in this review show that Raman spectroscopy has great potential for food analyses. In this review, we aim tobring together Raman studies on components, contaminants, raw materials, and adulterations of various food, and attempt to prepare a database of Raman bands obtained from food samples (Ismail Hakki Boyaci2015).

HARPREET KAUR KHURANA.Etal in 2008 used Multibounce Attenuated Total Reflectance Fourier Transform Infrared Spectroscopy and Chemometrics for Determination of Aspartame in Soft DrinksFourier transform infrared (FTIR) Spectroscopy with attenuated total reflectance sampling accessory and partial least-squares regression (PLS) was used for rapid determination of aspartame in soft drinks. On the basis of spectral characterization, the highest $R2$ value, and lowest PRESS value, the spectral region between 1600 and 1900 cm-1 was selected for quantitative

estimation of aspartame. The potential of FTIR spectroscopy for aspartame quantification was examined and validated by the conventional HPLCMethod. Using the FTIR method, aspartame contents in four selected carbonated diet soft drinks were found to average from 0.43 to 0.50 mg/mL with prediction errors ranging from 2.4 to 5.7% when compared with HPLC measurements. The developed method also showed a high degree of accuracy because real samples were used for calibration, thus minimizing potential interference errors. The FTIR method developed can be suitably used for routine quality control analysis of aspartame in the beverage-manufacturing sector, (HARPREET KAUR KHURANA.Etal, 2008).

SylwesterMazurek, Roman Szostak in 2011, used Analytical Methods

Efficient methods are proposed herein for the quantification of aspartame in commercial sweeteners. These methods are based on a treatment of Raman data with partial least squares (PLS), principal component regression (PCR) and counter-propagation artificial neural networks (CP-ANN) methods. For the

three chemometric techniques used, the relative standard errors of prediction (RSEP) calculated for calibration and validation data sets were on the order of 1.8‑2.2%. Four commercial preparations containing between 17% and 36% of aspartame by weight were evaluated by applying the developed models. Concentrations ound from the Raman data analysis agree perfectly with the results of the UV‑Vis reference analysis, with the recoveries in the 98.7‑100.8%, 98.6‑101.1% and 97.8‑102.2% ranges for the PLS, PCR and CP-ANN models, respectively. The proposed procedures can be used for routine quality control during the production of commercial aspartame sweetenersQuantification of aspartame in

commercial sweeteners by FT-Raman spectroscopy (SylwesterMazurek.Etal (2011)).

Sergio Armenta, Salvador Garrigues.Etal. in 2004used spectroscopic technique for Sweeteners determination in table top formulations using FT-Raman Spectrometry. A partial least squares (PLS) Fourier transform Raman spectrometry procedure based on the measurement of solid samples contained inside standard glass vials, has been developed for direct and reagent-free determination of sodium saccharin and sodium cyclamate in table top sweeteners. A classical 22 design for standards was used for calibration, but this system provides accuracy errors higher than 13% w/w for the analysis of samples containing glucose monohydrate. So, an extended model incorporating glucose monohydrate (23 standards) was assayed for the determination of sodium saccharin and sodium cyclamate in all the samples. Mean centering spectra data pre-treatment has been employed to eliminate common spectral information and root mean square error of calibration (RMSEC) of 0.0064 and 0.0596 was obtained for sodium saccharin and sodium cyclamate, respectively. A mean accuracy error of the order of 1.1 and 1.9% w/w was achieved for sodium saccharin and sodium cyclamate, in the validation of the method using actual table top samples, being lower than those obtained using an external monoparametric calibration. FT-Raman provides a fast alternative to the chromatographic method for the determination of the sweeteners with a three times higher sampling throughput than that obtained in HPLC. On the other hand, FT-Raman offers an environmentally friendly methodology which eliminates the use of solvents. Furthermore, the stability of samples and standards into chromatographic standard glass vials allows their storage for future analysis thus avoiding completely the waste generation.ometricanalysis(Sergio Armenta .etal 2004).

Da-you Fu .Etal in 2014 used Fast detection of illegal sweeteners in liquor and wine by laser Raman spectroscopy, Efficient method was proposed for the qualitative detection of 6 illegal sweeteners in commercial liquor and wine by laser Raman spectroscopy. The method was based on the comparative analysis of Raman spectrogram of pure sweeteners and alcohol samples. For the 6 kinds of sweeteners tested, saccharin sodium, acesulfame potassium impurity and cyclamate, were present as additives in the samples. The results showed that the proposed method was fast and simple with high repeatability and sensitivityto determine the peaks of the pure Sodium cyclamate, Acesulfame potassium imputity, Aspartame, Saccharin sodium, stevioside and Neotame, the Raman shift of which was revealed obviously, were at 3075 cm^{-1} and 3058 cm^{-1} of Raman spectra were strongly expressed in saccharin sodium, aspartame and neotame, because of the stretching vibration of C-H in aromatic compound, and the signal of 1598cm-1 was powerful because of C=C. The signals of 1295cm^{-1},1162 cm^{-1}, 1147 cm^{-1}, 1062 cm^{-1} and 1036 cm^{-1}were obvious in acesulfame potassium impurity, cyclamate and saccharin sodium owing to the structure of SO_2. And also there existed 1023 cm^{-1}and705 cm^{-1}(because of C=S) in saccharin sodium and 2968$cm^{-1}$and 2853 cm^{-1}(because of CH_2) in cyclamate and stevioside(Da-you Fu .Etal ,2014).

Chapter Three

Experimental part

3.1 Introduction:

This chapter describes the experimental part including the materials, equipment and methods, in Raman technique, a continuous wave laser irradiate small amount of material under the test directly.

The material used were three different typesof commercial artificial sweeteners: Tropicana slim, Stevania and süssina from Khartoum markets:

Table (3.1) classifications of Materials

Sample	Stevania	Tropicana	Süssina
Country of manufacture	Saudi Arabia	Indonesia	Austria

3.2 Preparation of the samples:

Firstly small amount of the solid powder from the three samples were put directly on the glass substrate without preparation.

Secondly 5 g from the three samples were taken and dissolved into boiling $100C^0$ mineral water (25mL) in addition, 25mL of HCl (3.1 pH)added to the mixture .

In order to illustrate the ability of Raman spectroscopy and to determine the compositions of the commercial artificial sweeteners, Laser Raman spectroscopy model Horiba LabRAM HR 3Dhas been used.

3.3 The experimental setup:

The experimental setup used in this work was arranged as shown in figure (3.1).

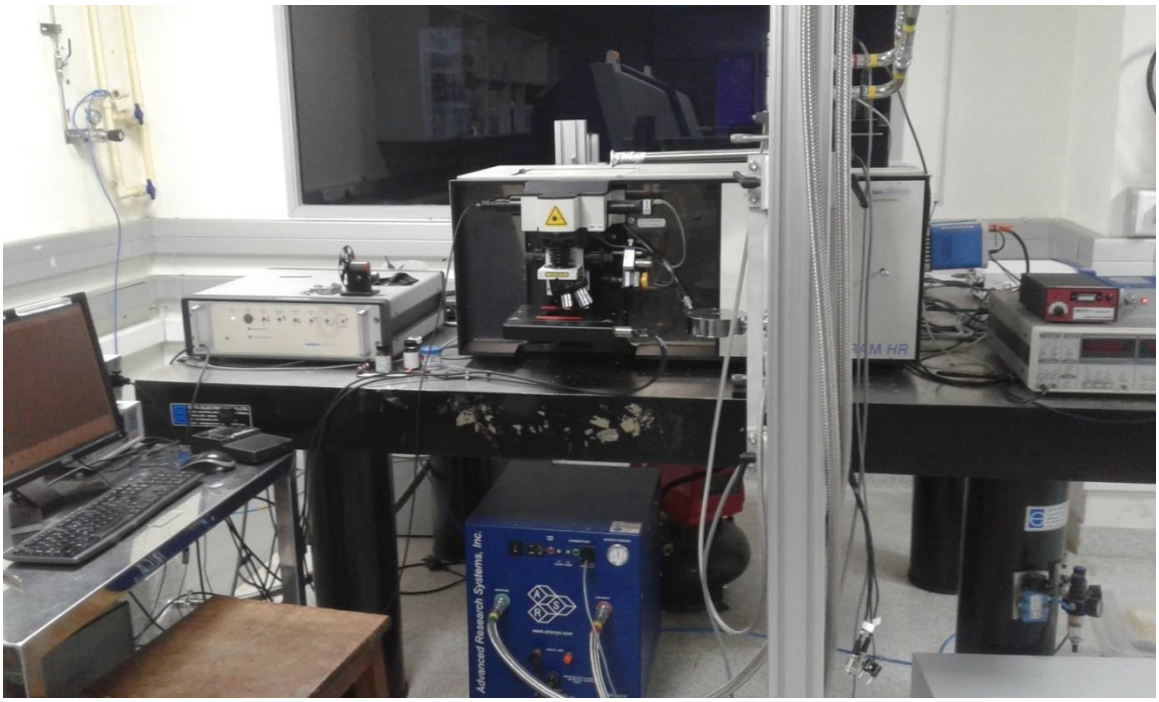

Figure (3.1) the experimental setup

3.4 Laser Raman spectrometer:

Laser Raman spectrometer model Horiba LabRAM HR 3D was used in this work to record Raman spectra of the samples its useful instrument for the identification of wide range of substances in physics and chemistry laboratories. Its straight forward nondestructive technique requiring no sample preparations and involve illuminating a sample with monochromatic light and using spectrometer examine the light scattered by the sample the specifications and the parameters of Horiba LabRAM HR 3D are listed in table 3.1.

Table (3-2) Specification and parameters of laser Raman Spectrometer Horiba LabRAM HR 3D

Specifications	Unit	VIS 532 nm 3000 g/mm	NIR 785 nm 1800 g/mm
Laser Class	-	3B	-
Spectral Dispersion / Resolution	cm-1 / pix	< 0.13	< 0.12
Spatial resolution XY	µm	0.5 / 0.25 100X NA 0.95	0.8 / 0,5 100X NA 0.95
Confocal depth resolution (typical / best)	µm	1.5 / 0.8 100X NA 0.95	2 / 1.5 100X NA 0.95
PhotoLuminescence Spectral range	nm	220 - 2100 (achromatic, no change of optics required)	
High wavenumber cut-off3	cm^{-1}	Up to 30 000	
Low wavenumber cut-off	cm^{-1}	Down to 5	
Imaging speed	ms/sp	Down to 0.75	
Deep cooled Spectroscopic Multichannel Detector	Front Illuminated UV coated EMCCD	1600 x 200 pixel 16 x16µm² pixel size	
Dark Current at -60°C	e-/pixel/s	<0.002	
Dimensions (Width x Depth x Height)	Mm	1300 x 1194 x 473	
Laser Type		Continuous wave	

The schematic diagram of the Horiba LabRAM HR 3D is shown in figure 3-2

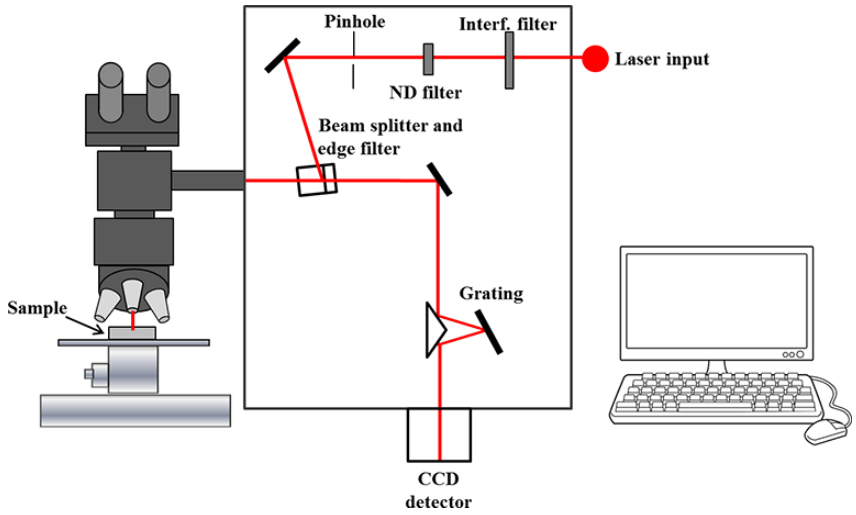

Figure (3.2) The schematic diagram of the Horiba LabRAM HR 3D spectrometer

3.4.1 Monochromator:

The optics structure of the mohnochromator is shown in figure 3-2. S1 is the entrance slit, M1is the collimating lens, and G is the diffraction grating. The diffracted beam is reflected by mirror M2 to the exit slit S2 where there is photomultiplier(PMT). When the grating is rotated, a spectrum message is transformed by the PMT into a current pulse which is enlarged and counted by photocounter and sent into the computer for processing. Then the spectrum distribution curve is displayed on the screen of the monitor. The best imaging position can be found by observing intensity of some Raman lines scanned by the monochromator.

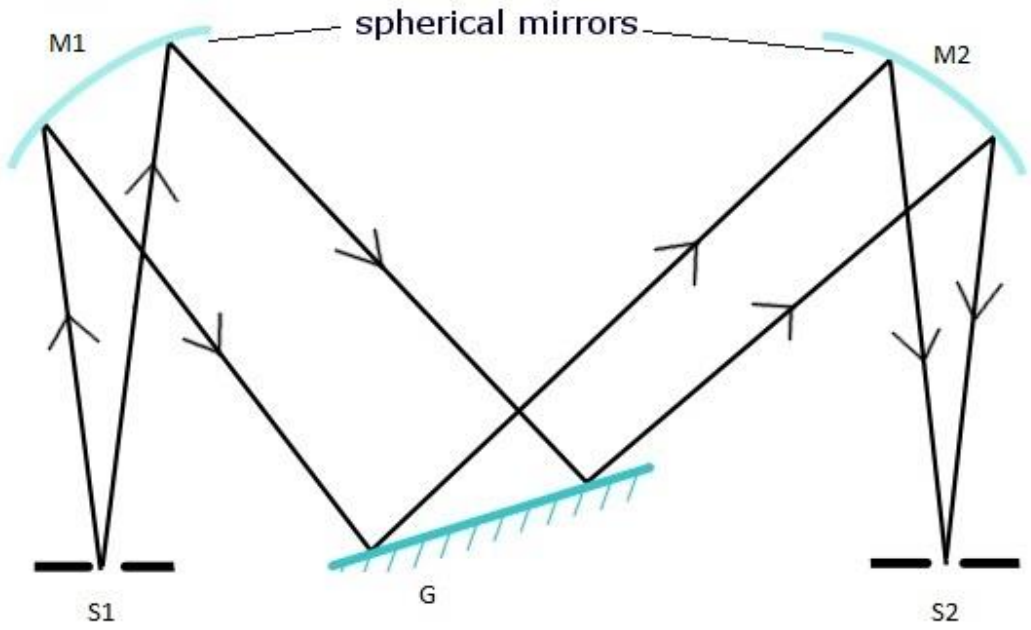

Figure (3.3) the optics structure of the monochromator

3.4.2 Laser used:

A diode pumped solid state green (DPSS) laser is used in the instrument as excitation light source. Its wavelength is 532 nm and it emits power up to 50 mW where its output beam is polarized one.

3.4.3 Polarization Measurements:

When conducting the experiment of polarametric measurement, two polarizers should be placed into the external path.

3.4.4 Probe systems:

Raman scattering light is very week and its intensity is less than $1\times 10^{-6}$of the incidents light, i.e., even less than the thermal noise of PMT. So it is impossible to extracting the signal submerged in the thermal noise by measuring the current directly.

Tacking advance of the feature the current output signal of the PMT naturally discrete under weak light ; the method of the photon counting can extract the weak signal submerged in the background noise by means of pulse height discrimination and digitization technique .beside analog testing technique such as lock in amplifier ,it avoids by and large the effects of high voltage direct current creep age of the PMT thermal noise ratio;its less affected by the PMT drifting and its gain variation ;the output is impulse signal which can be directly input to acomputer for processing without A/D conversion.

When the weak light irradiates the photocathode every incident photon entices the photocathode to shoot an electron by some probability, which is called quantum efficiency. These photoelectrons multiplied by the multiplier system and lastly form a current pulse in the anode loop, and forms of voltage pulse by load resistance, which is called a one-photon pulse .beside photoelectron pulse, her are heat emission electrons of the photocathode. The pulses formed on the anode by heat electrons are lower because the probability of heat electrons to be multiplied is less than photoelectrons, Furthermore, there is the pulse formed by the heat emission of the photo cathode.

Chapter Four

Results and discussion

4.1 Introduction:

The purpose of this study was to characterize and identify the components of the commercial artificial sweeteners using Laser Raman Spectrometer model Horiba LabRAM HR 3D . The three artificial sweeteners samples were collected from the Sudanese markets. The results of the investigation are presented and discussed in this chapter. The end of this chapter was main conclusions and recommendations are presented**.**

4.2 Results and analysis of Raman spectra of the samples:

Figure 4.1 shows the Raman spectrum of the sample Tropicana slim powder in the range from 50 to 1500 cm^{-1}.

It shows clear peaks and by comparison with the vibrations recorded in some references, it was found that these vibrations are attributed to the sorbitol molecules and some components of other materials as listed in Table 4. 1

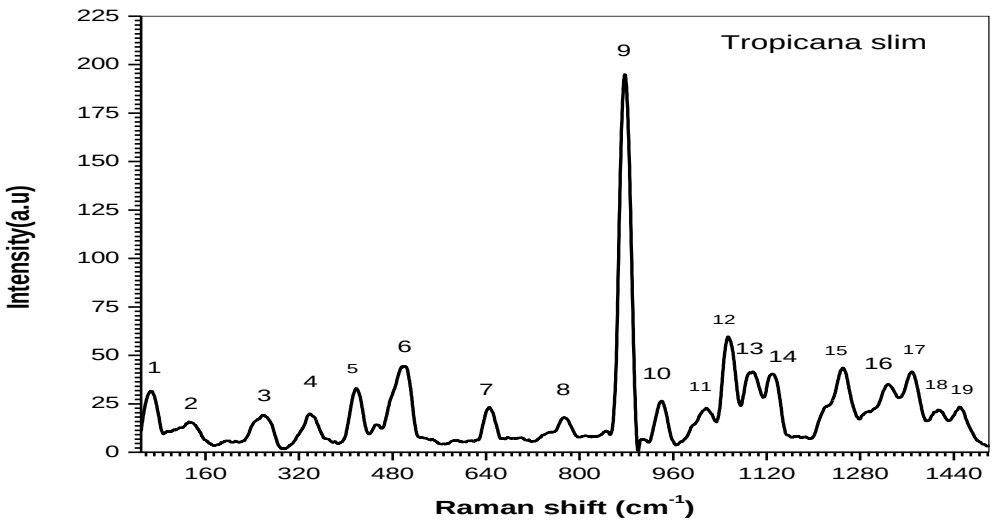

Figure (4.1) Raman spectrum of Tropicana slim powder in the range from 50 to 1500 cm^{-1}

Table 4.1 the analyzed data of Raman spectrum of (Tropicana slim) from 50 to 1500cm^{-1}

Peak NO	Raman shift (cm^{-1})	Intensity (au)	Assignment	Reference
1	61.0	32.2	Skeldef	(NiculinaPeica,2009)
2	134.0	16	υ(O–Ag–O)	(NiculinaPeica,2009)
3	263.0	19.3	Sorbitol	(Marleen de Veij,a Peter,;et.al.,2008) , (Anna.GraziaMignani,.et al,2016)
4	342.0	20	Sorbitol	(Marleen de Veij,a Peter,;et.al.,2008) , (Anna.GraziaMignani,.et al,2016)
5	415.0	33.5	O–H bending	(Marleen de Veij,a Peter,;et.al.,2008)
6	499.0	45.1	Skeletal deformation	(Yuan.Xiaojuan,;et.al.,2010)
7	642.1	23.8	Skeletal 5-ring Deformation	(Marleen de Veij,a Peter,;et.al.,2008) , (Anna.GraziaMignani,;et al,)
8	773.0	18.5	twist CH_3 Ring Stretching	(G.Mahalakshmi1,;et.al.,2016) , (Ewen S.,Geoffery D., 2005),

9	876.0	195.4	Skeletal vibration and C–H twisting	(Marleen de Veij,a Peter,;et.al.,2008) , (Anna.GraziaMignani,.et al,2016)
10	936.0	27.3	C–H bending and C–C stretching	(Marleen de Veij,a Peter,;et.al.,2008) , (Anna.GraziaMignani,.et al,2016)
11	1019.0	23.2	C–NH_2 stretching	(Yuan.Xiaojuan,;et.al.,2010)
12	1056.0	60.2	C–O stretching and O–H bending	[(Marleen de Veij,a Peter,;et.al.,2008) , (Anna.GraziaMignani,;et al,2016)
13	1091.0	41.7	C–C stretching and O–H bending	(Marleen de Veij,a Peter,;et.al.,2008) , (Anna.GraziaMignani,.et al,2016)
14	1134.5	41.3	C–O and C–C stretching, and O–H bending	(Marleen de Veij,a Peter,;et.al.,2008) , (Anna.GraziaMignani,.et al,2016)
15	1253.0	44.6	C_3-H_{14}& C_6-H_{17} Rocking	(Anna.GraziaMignani,.et al,2016), (Caiqin Han Yue Yao,;et.al,2017)
16	1325.0	35.4	C-H deformation	(Anna.GraziaMignani,;et al,2016),

17	1369.0	42.4	symmetrical carboxylate Stretching vibration.	(Marleen de Veij,a Peter,;et.al.,2008)
18	1411.0	22.5	CH_2 , CH_3	(Nafie.A.Almuslet,;et.al.,2016)
19	1446.0	23	C–C stretching	(Marleen de Veij,a Peter,;et.al.,2008),(Yuan.Xiaojuan,;et.al.,2010), (Alicia Beatriz Brizuela a.;et.al.,2012)

Figure 4.2 shows the Raman spectrum of the sample Tropicana slim powder in the range from 2500 to 3500 cm^{-1}.

It shows clear peaks and by comparison with the vibrations recorded in some references, it was found that these vibrations are attributed to some components of other materials as listed in Table 4.2

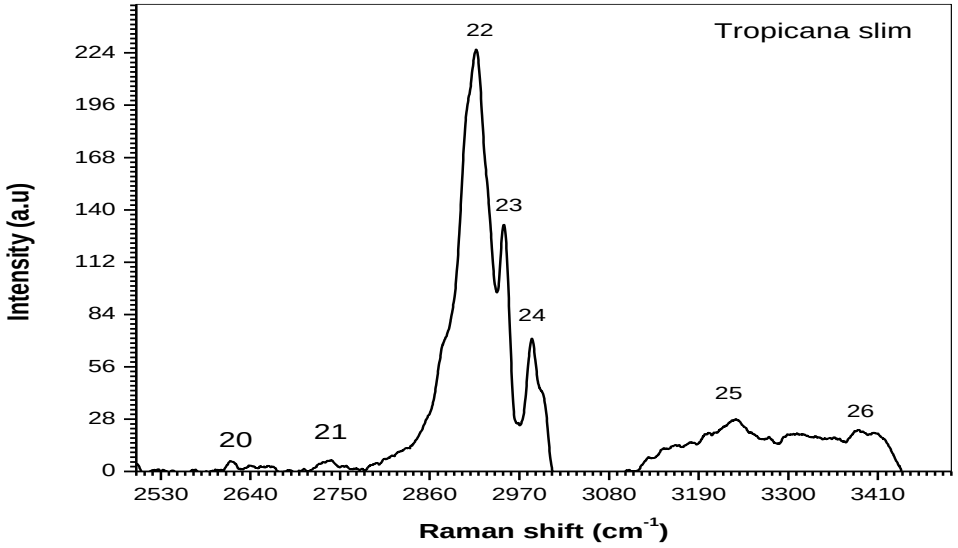

Figure (4.2) Raman spectrum of Tropicana slim powder in the range from2 500 to 3500 cm^{-1}

Table 4.2 the analyzed data of Raman spectrum of (Tropicana slim) from 2500 to 3500cm^{-1}

Peak NO	Raman shift (cm^{-1})	Intensity (au)	Assignment	References
20	2622.1	5.7	H-bonds	(NiculinaPeica, 2009)
21	2742.0	5.7	υs(C2H2)	(NiculinaPeica, 2009)
22	2918	233.4	ν CH	(P.Ramesh, S. Gunasekaran, 2018)
23	2950.1	133.1	ν CH	(P.Ramesh, S. Gunasekaran, 2018)
24	2986.0	71.8	O-H	(Vaclav Ranc, ZdenkaMarkova.;etal., 2014)
25	3238.1	28.3	-	-

26	3300.2	21.4	N–H O–H Modes of protein and lactose.	(Vaclav Ranc, ZdenkaMarkova.;etal., 2014), (Ismail HakkiBoyaci.;et.al.,2015), (Susanne Brunsgaard Hansen,2000)

Figure 4.3 shows the Raman spectrum of the sample Tropicana slim solution in the range from 500 to 2500 cm^{-1}.

It shows clear peaks and by comparison with the vibrations recorded in some references, it was found that these vibrations are attributed to some components of other materials as listed in Table 4.3

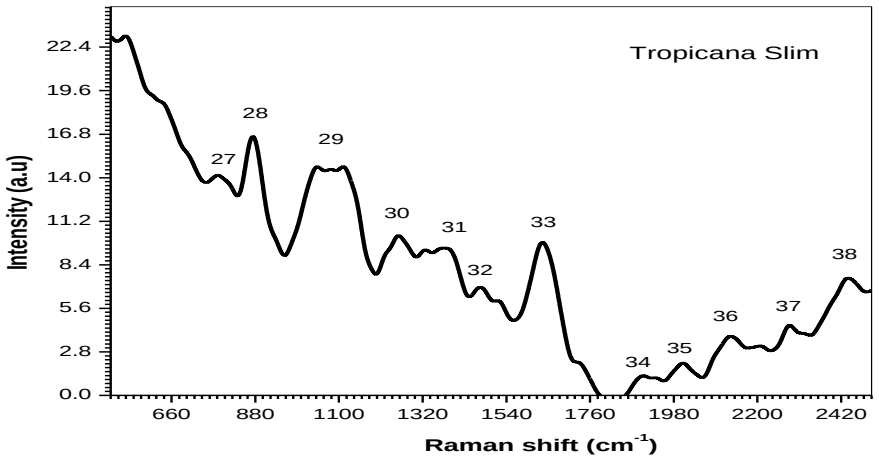

Figure (4.3)Raman spectrum of Tropicana slim powder dissolved in boiling mineral water and HCl acid (PH3.1) in the range from 500 to 2500 cm^{-1}

Table 4.3 the analyzed data of Raman spectrum of the dissolved (Tropicana slim) from 500 to 2500cm^{-1}

Peak No	Raman shift(cm^{-1})	Intensity(au)	Assignment	References
27	773.7	14	Ring Stretching	(Marleen de Veij,a Peter,;et.al.,2008),(Caiqin Han Yue Yao,;et.al,2017)
28	876.0	16.7	Skeletal vibration and C–H twisting	(Marleen de Veij,a Peter,;et.al.,2008), (Anna GraziaMignani.;et al., 2016)
29	1084	14.8	C–H bending and C–C C–O stretching	(Anna GraziaMignani.;et al., 2016)
30	1257	10.3	Amide III (random), thymine	(Marleen de Veij,a Peter,;et.al.,2008)
31	1384	9	V (COO)-	(Yuan Xiaojuan.;et.al.,2010)
32	1467	6	C-H bending	(IsmailHakkiBoyaci.;et.al., 2015)
33	1632	9	Asymmetric NH_2 deformation	(Yuan Xiaojuan.;et.al.,2010)
34	1901	-	-	-
35	2002	2	- -	-
36	2133.1	3	Azide	(Nafie.A.Almuslet,;et.al.,2016)

37	2285.3	4	-	-
38	2435	7	-	-

Figure 4.4 shows the Raman spectrum of the sample stevianapowder in the range from 50 to 1700 cm^{-1}.

It shows clear peaks and by comparison with the vibrations recorded in some references, it was found that these vibrations are attributed to the sorbitol molecules and some components of other materials as listed in Table 4. 4.

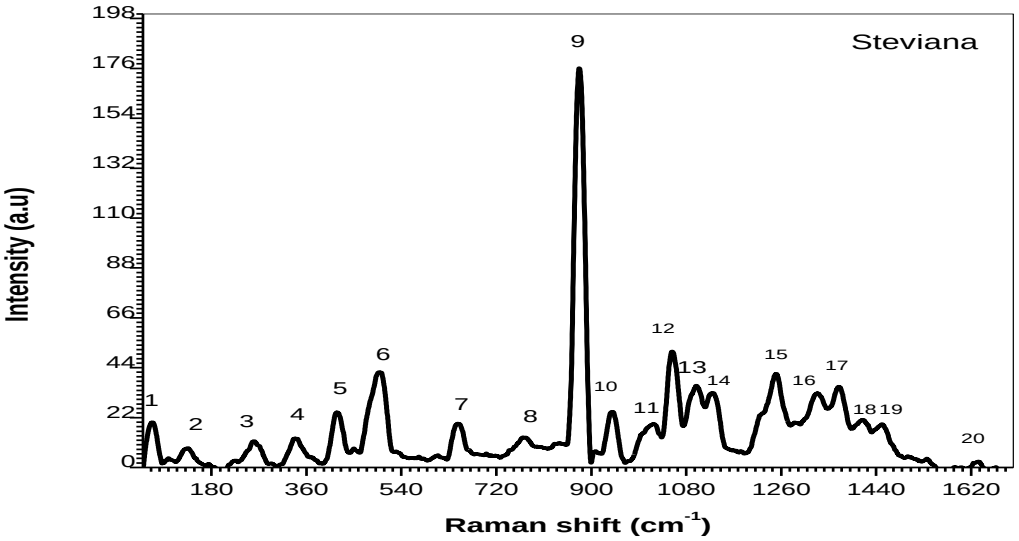

Fig (4.4) Raman spectrum of steviana powder in the range from 50 to 1700 cm^{-1}

Table (4.4) the analyzed data of Raman spectrum of (steviana) from 50 to 1700cm^{-1}

Peak No	Raman shift (cm^{-1})	Intensity (au)	Assignment	Reference
1	67	20.5	Skeldef	(NiculinaPeica, 2009)
2	140.0	9.4	υ(O–Ag–O)	(NiculinaPeica, 2009)
3	263.0	12.1	sorbitol	(Marleen de Veij.; et.al. 2008),(ArpitaDas.;et.al., 2016).
4	342.0	13.6	C–O–C sorbitol	(Marleen de Veij.; et.al. 2008),(ArpitaDas.;et.al., 2016).
5	416.3	25.6	O–H bending	(Marleen de Veij,a Peter Vandenabeele.;et.al.,2008),(ArpitaDas.;et.al., 2016).
6	500.0	42.7	disulphide bridges	(Marleen de Veij,a Peter Vandenabeele.;et.al.,2008),(P.Ramesh, S. Gunasekaran, 2018)
7	640.0	20.7	Skeletal 5-ring deformation	(Marleen de Veij,a Peter Vandenabeele.;et.al.,2008),(P.Ramesh, S. Gunasekaran, 2018)
8	773.0	14.3	twist CH3 Ring Stretching	(Anna GraziaMignani.;et.al.,2016),(G. Mahalakshmi..et.al.,2016)
9	876.0	176	Skeletal vibration and C–H twisting	(Marleen de Veij,a Peter Vandenabeele.;et.al.,2008), (ArpitaDas.;et.al., 2016).

10	940.0	25.7	C–C stretch of peptide backbone	(Marleen de Veij,a Peter Vandenabeele.;et.al.,2008), (ArpitaDas.;et.al., 2016).
11	1019	20.3	C–NH2 stretching	(Yuan Xiaojuan.;et.al.,2010)
12	1056.0	52	C–O stretching and O–H bending	(Marleen de Veij,a Peter Vandenabeele.;et.al.,2008), (ArpitaDas.;et.al., 2016).
13	1093.0	36.7	C–C stretching and O–H bending	(Marleen de Veij,a Peter Vandenabeele.;et.al.,2008), (ArpitaDas.;et.al., 2016).
14	1134.4	33.8	C–O and C–C stretching, and O–H bending NH_2 twisting	(Marleen de Veij,a Peter Vandenabeele.;et.al.,2008), (ArpitaDas.;et.al., 2016),(Yuan Xiaojuan.;et.al.,2010)
15	1250.0	60.5	Amide III	(Marleen de Veij,a Peter Vandenabeele.;et.al.,2008)
16	1325.0	42.2	CH2 wagging	(Marleen de Veij,a Peter Vandenabeele.;et.al.,2008),(Yuan Xiaojuan.;et.al.,2010)

17	1361.0	36.9	tryptophan amino acid	(Marleen de Veij,a Peter Vandenabeele.;et.al.,2008), (P.Ramesh, S. Gunasekaran, 2018)
18	1411.5	21.4	CH_2 , CH_3	(Maher S. Amer , 2010),(Ewen S. ,Geoffery D, 2005)
19	1446	20	CH_2 bending C−H –CH_3	(A.W. Miziolek.;et.al.,2006),(Marleen de Veij.;et.al.,2008),(P.Ramesh, S. Gunasekaran, 2018)
20	1632	3.4	Asymmetric NH_2 deformation	(Yuan Xiaojuan.;et.al.,2010)

Figure 4.5 shows the Raman spectrum of the sample stevianapowder in the range from 2700 to 3500 cm^{-1}.

It shows clear peaks and by comparison with the vibrations recorded in some references, it was found that these vibrations are attributed to some components of other materials as listed in Table 4.5.

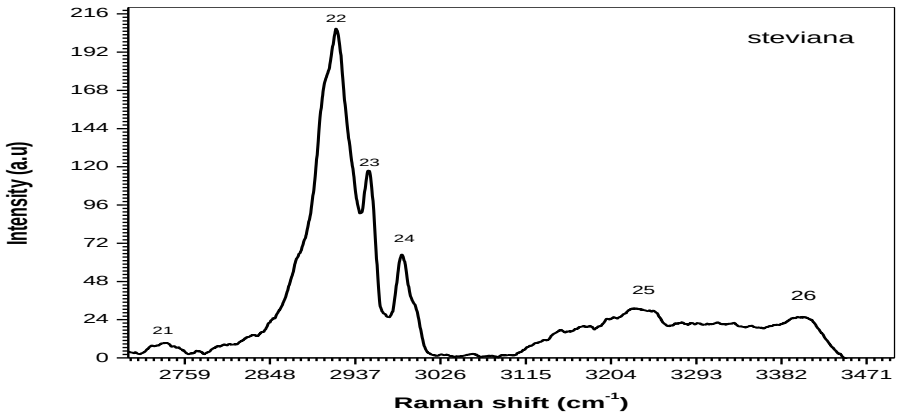

Figure (4.5) Raman spectrum of steviana powder in the range from 2700 to 3500 cm-1.

Table 4.5 The analyzed data of Raman spectrum of (steviana) from 2700 to 3500cm^{-1}

Peak NO	Raman shift (cm^{-1})	Intensity (au)	Assignment	Reference
21	2740.5	10.9	--	--
22	2918.2	207.0	ν CH	(P.Ramesh, S. Gunasekaran, 2018)
23	2955.7	117.9	Stretching (C_6H_2,C_5H)	(NiculinaPeica, 2009),(P.Ramesh, S. Gunasekaran, 2018)
24	2975.1	65.5	ν CH	(P.Ramesh, S. Gunasekaran, 2018)
25	3202	32	Stretching (CH_3)	(NiculinaPeica, 2009),
26	3406	26.5	N-H or O-H	(Susanne Brunsgaard Hansen, 2000)

Figure 4.6 shows the Raman spectrum of the sample steviana solution in the range from 500 to 2500 cm-1.

It shows clear peaks and by comparison with the vibrations recorded in some references, it was found that these vibrations are attributed to Magnesium Carbonate and some components of other materials as listed in Table 4.3

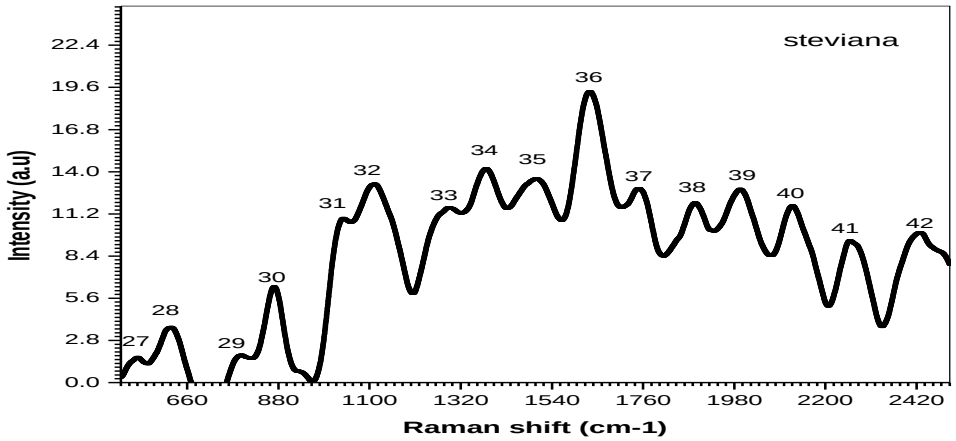

Figure (4.6)Raman spectrum of steviana powder dissolved in boiling mineral water and HCl acid (PH3.1) in the range from 500 to 2500 cm^{-1}.

Table 4.6 The analyzed data of Raman spectrum of the dissolved (steviana)from 500 to 2500cm^{-1}

Peak No	Raman shift (cm^{-1})	Intensity (au)	Assignment	Reference
27	540.0	1.7	disulphide bridges	(Ismail HakkiBoyaci.;et.al.,2015)
28	620	3.7	-	-
29	773.0	1.8	twist CH_3	(Marleen de Veij.;et.al.,2008),(G. Mahalakshmi1.;et.al.2016)
30	876	6.4	Skeletal vibration and C–H twisting	(Marleen de Arpita)،(Veij.;et.al.,2008 Das.;et.al.,2016)
31	1040	11	C–C and C–O stretching and O–H bending	(Marleen de Veij.;et.al.,2008),(Arpita Das.;et.al.,201)
32	1117	13.2	Magnesium carbonate	(Marleen de Veij.;et.al.,2008)
33	1298.4	11.6	C–N stretching and C–H bending	(Arpita Das.;et.al.,2016)
34	1382	14.2	V $(COO)^{--}$	(Yuan Xiaojuan.;et.al.,2010)
35	1506.0	13.6	Amide II	(Yuan Xiaojuan.;et.al.,2010)
36	1632	19	Asymmetric NH_2 deformation	(Nafie.A.Almuslet,;et.al.,2016)
37	1749	13	C = O stretching N–H bending	(Vaclav Ranc, ZdenkaMarkova.;e.tal., 2014),(IsmailHakkiBoyaci.;et.al., 2015)
38	1885	12	-	-
39	1994	12	-	-
40	2121.0	11.8	sothiocyanate	(Nafie.A.Almuslet,;et.al.,2016)
41	2254.0	11	Diazoniu	(Nafie.A.Almuslet,;et.al.,2016)
42	2433	10	-	-

Figure 4.7 shows the Raman spectrum of the sample süssina powder in the range from 50 to 1500 cm^{-1}.

It shows clear peaks and by comparison with the vibrations recorded in some references, it was found that these vibrations are attributed to the sorbitol, Aspartame and saccharine molecules and some components of other materials as listed in Table 4. 1

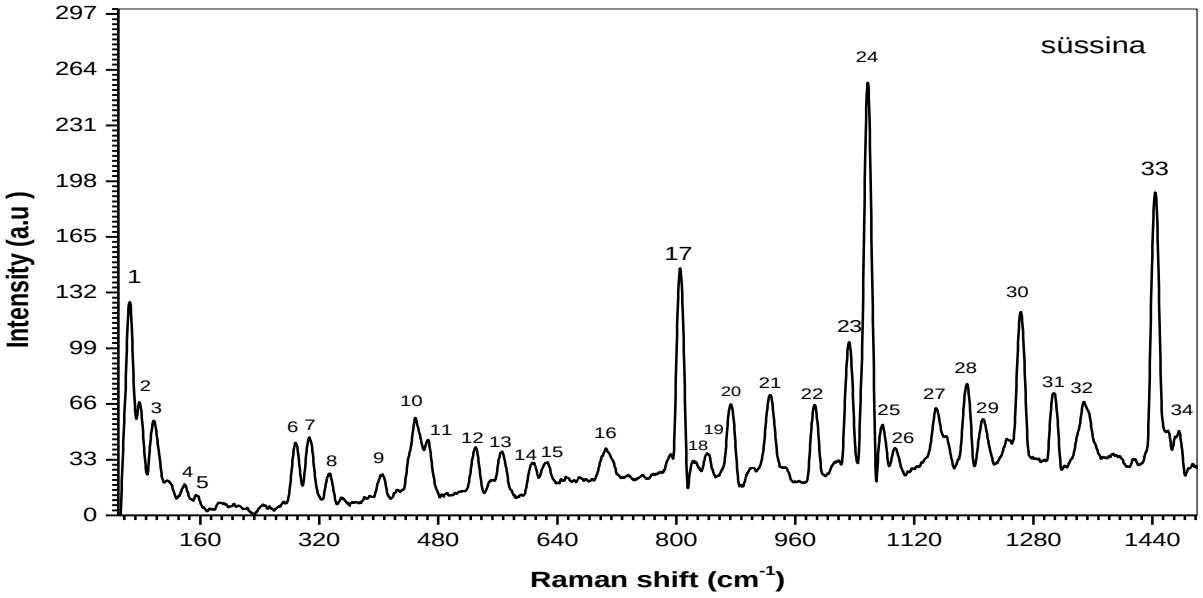

Figure (4.7) Raman spectrum of (süssina) powder in the range from 50 to 1500cm^{-1}.

Table 4.7The analyzed data of Raman spectrum of (süssina)from 50 to 1500cm^{-1}

Peak No	Raman shift (cm^{-1})	Intensity (au)	Assignment	Reference
1	67.0	127.8	Skeldef	(NiculinaPeica , 2009)
2	78.2	68.5	-	-
3	97.3	57	-	-
4	140.0	19.3	Stretching (O–Ag–O)	(NiculinaPeica , 2009)
5	153.7	13.2		
6	288.0	44	C-CH_3sci	(G. Mahalakshmi1, R. Suganya.et.al.,2016),

7	306.0	47.3	Torsion (N_2OH)	(Alicia Beatriz Brizuela, 2012), (Ismail HakkiBoyaci.;et.al.,2015)
8	334.0	25	-	-
9	405.0	24.9	--	-
10	451.4	58.8	β OCC + γ NCCC	(P.Ramesh, S. Gunasekaran,2018)
11	467.3	45.8	-	-
12	530.0	41.0	C – CL	(Nafie A. Almuslet.;et.al.,2016)
13	566.0	39.1	Amide VI	(G. Mahalakshmi1, R. Suganya.;etal.,2016)
14	608.5	31.8	-	-
15	622.4	31.8	Aryl ring deformation and C–H bending	(Yuan Xiaojuan.;et.al.,2010)
16	711.0	40.7	Skeleton deformation	(Yuan Xiaojuan.;et.al.,2010)
17	805.0	147	O-P-O	(Evelin Witkowska1.;et.al.,2016)
18	843	37	C – O – C	(Nafie A. Almuslet.;et.al.,2016)
19	818.0	33.5	Aryl C–H wagging	(Arpita Das.;et.al.,2016)
20	876	66.3	Skeletal vibration and C–H twisting	(Yuan Xiaojuan.;et.al.,2010), (Marleen de Veij.;et.al.,2008)
21	919.5	71.8	C–H bending and C–C stretching	(Yuan Xiaojuan.;et.al.,2010)
22	982.0	67	melamine	(Ismail HakkiBoyaci.;et.al.,2015)

23	1032.0	103.4	(Aryl ring deformation)mannitol	(Marleen de Veij.;et.al.,2008), (Y.Fukashiron.;et.al.,1992)
24	1154.0	257	Ring Stretching sodium saccharin	(Yuan Xiaojuan.;et.al.,2010)
25	1093.3	41.3	C–C stretching and O–H bending	(Yuan Xiaojuan.;et.al.,2010), (Marleen de Veij.;et.al.,2008)
26	1154.0	40.8	Aryl ring deformation and C–H bending C–C stretching	(Yuan Xiaojuan.;et.al.,2010), (Ismail HakkiBoyaci.;et.al.,2015)
27	1196	64.0	ν OC + β HOC+ β HNC+ β HCC	(Ismail HakkiBoyaci.;et.al.,2015)
28	1210.0	78.6	amide III	(Ismail HakkiBoyaci.;et.al.,2015)
29	1267.4	57.1	C–H symmetric rock	(Ismail HakkiBoyaci.;et.al.,2015)
30	1300.0	72.5	C–N stretching and C–H bending	(Ismail HakkiBoyaci.;et.al.,2015), (Arpita Das.;et.al.,2016)
31	1360	68.2	C_3H,C_2H_2	(NiculinaPeica , 2009), (Ismail HakkiBoyaci.;et.al.,2015), (A. Weber, 1982)
32	1445.0	66.8	C–C stretching	(G. Mahalakshmi1, R. Suganya.;etal.,2016)
33	1475	192.5	*ν*(CC) stretching vibrations ν(CN) in-plane vibrations	(Marleen de Veij.;et.al.,2008)

Figure 4.8 shows the Raman spectrum ofsüssina sample in the range from 2600 to 3500 cm^{-1}.

It shows clear peaks and by comparison with the vibrations recorded in some references, it was found that these vibrations are attributed to some components of other materials as listed in Table 4.8

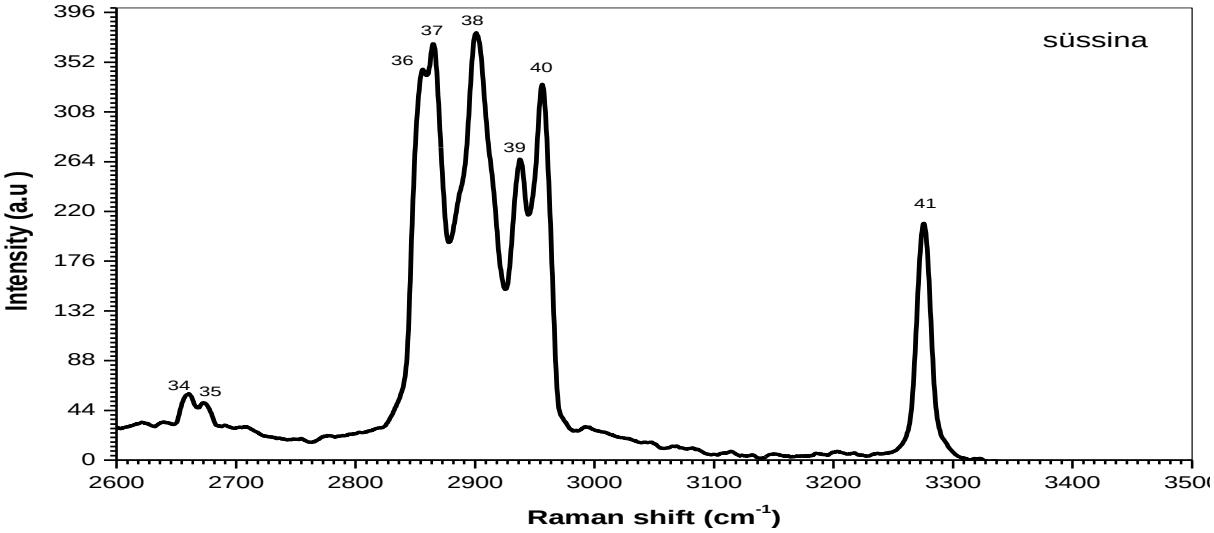

Figure (4.8) Raman spectrum of (süssina) powder in the range from 2600 to 3500 cm-1.

Table 4.8 The analyzed data of Raman spectrum of (süssina) from 2600 to 3500cm^{-1}

Peak No	Raman shift (cm^{-1})	Intensity (au)	Assignment	Reference
34	2677	60.8	H-bonds	(Marleen de Veij.;et.al.,2008)
35	2673.1	52.3	H-bonds	(NiculinaPeica , 2009), (Marleen de Veij.;et.al.,2008)
36	2852	347.4	ν CH	(P.Ramesh, S. Gunasekaran,2018)
37	2864	370.4	-	-

38	2885	380	(O−H stretch)	(Alicia Beatriz Brizuela, 2012), (Vaclav Ranc.;et.al.,2014)
39	2936	267	-	-
40	2952	333.1	ν CH	(P.Ramesh, S. Gunasekaran,2018)
41	3276.1	210.8	Alkyne	(Nafie A. Almuslet.;et.al.,2016)

Figure 4.9 shows the Raman spectrum of the sample süssina solution in the range from 500 to 2500 cm^{-1}.

It shows clear peaks and by comparison with the vibrations recorded in some references, it was found that these vibrations are attributed to some components of other materials as listed in Table 4.9.

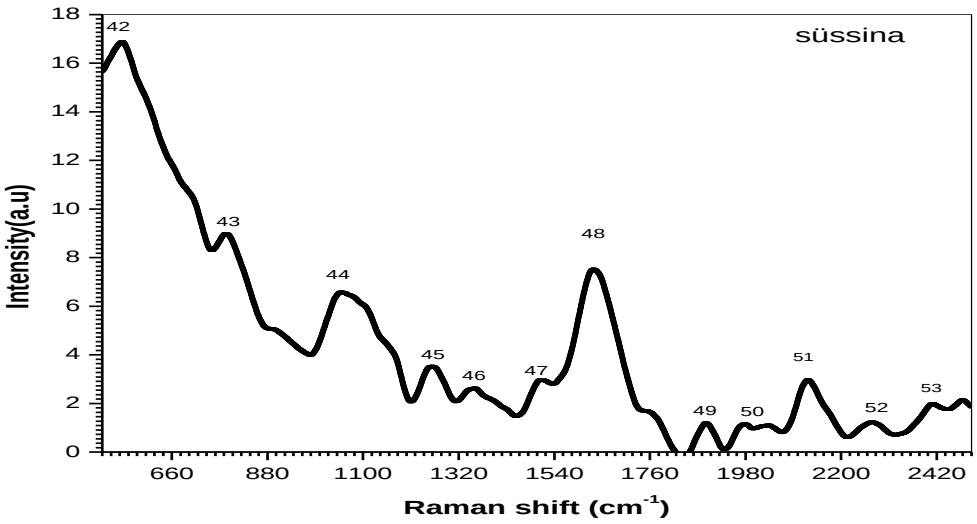

Figure (4.9) Raman spectrum of dissolved (süssina) in boiling mineral water and HCl acid (PH 3.1) in the range from 500 to 2500 cm^{-1}.

Table 4.9 the analyzed data of Raman spectrum of the dissolved (süssina) from 500 to 2500cm^{-1}.

Peak No	Raman shift(cm^{-1})	Intensity(au)	Assignment	Reference
42	540.0	16	disulphide bridges	(Marleen de Veij.;et.al.,2008)
43	785.0	9	twist CH_3	(G. Mahalakshmi1, R. Suganya.et.al.,2016),
44	1056	6	C–O stretching and O–H bending	(Yuan Xiaojuan.;et.al.,2010)
45	1271	3	Torsion HCCN + torsion HCCO	(P.Ramesh, S. Gunasekaran,2018),(NiculinaPeica , 2009)
46	1350	2.6	-	-
47	1513	3	lycopene	(Marleen de Veij.;et.al.,2008)
48	1632	7	Asymmetric NH_2 deformation	(G. Mahalakshmi1, R. Suganya.;etal.,2016)
49	1899	1.1	C = C	(Nafie A. Almuslet.;et.al.,2016)
50	2121	1.2	sothiocyanate	(Nafie A. Almuslet.;et.al.,2016)
51	2275	2.9	-	-
52	2413	1.3	-	-
53	2408	2.0	-	-

4.3 Discussion:

From the previous results shown in figures (4.1 to 4.9) through the analysis of the six samples of the artificial sweeteners (Tropicana slim, Steviana and süssina) has been done using laser Raman spectrometer model model Horiba LabRAM HR 3D with wavelength 532 nm and output power of 6 mW in the range from 50 to 4000 cm^{-1} successfully without fluorescence ,the results showed that , the vibrational modes at the wavenumbers ; (263.0, 342.0, 415.0, 599.0, 642.0, 773.0, 1446 , 876.0 , 936.0 , 1054.0 , 1091.0 , 1129.4 , 1250.0, 1325.0 , 1369) cm^{-1} which are attributed to the sorbitol ($C_6H_{14}O_6$) molecules appeared in all the powder samples(Tropicana slim ,Steviana and süssina) with different intensities, this results agree with work of (Marleen de Veij,a Peter Vandenabeele,etal;.2008).

Also the results showed that C–H (Skeletal vibration and twisting modes) at the wavenumber (876.0cm^{-1}) which is attributed the main peak of the sorbitol ($C_6H_{14}O_6$) appeared in (Tropicana slim, Steviana and süssina) with different intensities (195.4, 176, and 66.3) (au), respectively also C-H_3(Twist ring stretching)at the wavenumber (733.0 cm^{-1}) appeared in Tropicana slim and steviana with intensities (18,5 , 14,3) respectively.

Vibrational modes (Aryl ring deformation and C–H bending) at wavenumbers (622.4, 818.0) cm^{-1} appeared in the powder samples (süssina) which are attributed to the artificial Aspartame molecules ($C_{14}H_{18}N_2O_3$).

Vibrational modes (Aryl ring deformation and C–H bending) wavenumbers at (711.0 , (1054.0 main peak) ,1032 , 1300.0) cm^{-1} appeared in the powder sample (süssina) which are attributed to the artificial saccharine molecules ($C_7H_4NNaO_3S$) with intensities (40.7 ,257.0 , 103.0 and 72.0) respectively , this agree with the work of (Anna G. Mignani a, Leonardo Ciaccheri, etal;.2014).

It was found that in the sample (Tropicanaslim solution), the intensity of the sorbitol molecules at the wavenumber (876 cm^{-1}) decreased from (195 au to 16.7 au) , and the intensity of the wavenumber at (773cm-1) decreased from (18.5 au to 14.0 au) due to the interaction with acid . The Raman peak of the magnesium carbonate molecule at the wavenumber (1117cm^{-1}) did not appear in all solid samples, while it appeared in the dissolved sample Steviana with intensity (13.2 au) due to the reaction with the acid and the mineral water, The mineral water contains magnesium in its ingredients in the product manual, because of the interaction with acid with the carbohydrate of the sweeteners it constructed new bonds of magnesium carbonate molecule.

These results is in a good agreement with the work of (Marleen de Veij,a Peter Vandenabeele,etal;.2008) , and (NiculinaPeica, 2009).

4.4 conclusions:

The following specific conclusions can be remarked:

- The (Tropicana slim) powder sample has high intensity of natural pure sorbitol and it doesn't contain any toxic artificial sweeteners, and in the dissolved sample it has very low intensity of the sorbitol.
- The (steviana) powder sample also has high intensity of natural pure sorbitol and it doesn't contain toxic artificial sweeteners, and in the dissolved sample appeared the magnesium carbonate molecules with low intensity.
- In the (süssina) powder sample appeared the molecules of the toxic artificial sweetener Aspartame and saccharine with high intensity.

4.5 Recommendations:

The following are recommended for future work:

- Further research on the other types powder and soluble of sweeteners especially in the sundaes markets.
- Studying the effect of high temperature on the artificial sweeteners structure.
- Studying the effect of Acids and Bases in the presence of high temperature on the structure of the artificial sweeteners.
- Sudanese authorities should control and banned the export of the artificial sweeteners and concentrate on the natural sweeteners.

References:

Ayden R.wood and Don McNaughtonOnashUni, (2008)"Resonance Raman Spectroscopy of Erythrocytes" University Melbourne. Victorya.John Wiley and Sons.Australya.

John R. Ferraro, Kazuo Nakamoto and Chris W. Brown, (2003)." Introductory Raman Spectroscopy" second edition Elsevier.

J.MichalHollas, (2004) "Modern Spectroscopy" .University of Reading fourth edition, John Wiley and sons England.

DR.H.Kaur,(2001). "Spectroscopy" First edition.

Maher S. Amer, (2010). "Raman Spectroscopy, Fullerenes and Nanotechnology " Russ Engineering Center, Wright State University, Dayton, OH 45435, USA.

Peter F .Bernath, (2005) "Spectra of atoms and molecules "Second edition .By Oxford University Press.Oxford University.

Wolfgang Demtröder , (2008) "Laser Spectroscopy Vol. 2: Experimental Techniques". Springer-Verlag Berlin Heidelberg.ISBN 978-3-540-74952-3.

Babara Stuart Wiely, (2003)"Infrared Spectroscopy Fundamental and applications". Weily.ISBIN:0-470-85427-8(HB).

France F .Le Blanc, D.Lunney, M.SeWtzCern,ACnrsOrsay,(2004) " Laser Spectroscopy for the study of nuclear properties"Switzerland

N.Stone, .I.E Tothill and Mr. Thomas,(2010)." Raman Spectroscopy of Biological tissue for application in Optical diagnosis of malignancy" Crenfield University.

Woodgate, Gordon K, (1999). Elementary Atomic Structure.Oxford University Press.*ISBN978-0-19-851156-4.*

Y.Fukashiron, H Sunauhi, S.Hyashibe T. shinozuka,(1992)."Nuclear Laser Spectroscopy using A laser Microwave double resonance method with an ion trap" .Tohoku University.Sendai.*Cycletron and Radioisotope Center Japan*.

D.A Cremers, L.J. Radziemski , (2006) "Handbook of Laser-Induced Breakdown Spectroscopy Wiley, New York .

A.W. Miziolek, V. Paleschi, I. Schechter, (2006)" Laser-Induced Breakdown Spectroscopy" Cambridge Univ. Press, Cambridge.

Housten,Mathew R McCurdy.YuryBakhirkin.GerardWysocki.Rafa.Lewiki and Frank K Tittle.(2007)" Recent advances of laser spectroscopy based techniques for applications in Breath analysis"RiceUniversity.JOURNAL OF BREATH RESEARSH Quantum Institute,USA.

D.J. Gardner ,(1989) "Practical Raman Spectroscopy" Springer, Berlin, Heidelberg, New York.

A. Weber ,(1982)" High-resolution rotational Raman spectra of gases" Heyden, London.

JohnR.Ferro,KauzoNakamoto and chrisWBrown,(2006)" Introductory Raman Spectroscopy" Fourth edition Elsevier.

Z.Q. Tian, B. Ren , (2000) "Progress in Surface Raman Spectroscopy" Univ. Press, Xiaman, China.

E.K. Gustafson, J.C. McDaniel, R.L. Byer ,(1981) "CARS measurement of velocity in a supersonic jet. IEEE. J. Quantum Electron.

W. Kiefer, (2000) ‘Nonlinear Raman Spectroscopy: Applications’. In:Encyclopedia of Spectroscopy and Spectrometry Academic, New York.

S.A. Akhmanov, A.F. Bunkin, S.G. Ivanov, N.I. Koroteev, A.I. Kourigin, I.L. Shumay ,(1976) "Development of CARS for measurement of molecular parameters" Springer, Berlin, Heidelberg.

S. Nie, L.A. Lipscomb, N.T. Yu,(1991) "Surface-enhanced hyper-Raman spectroscopy Appl. Spectroscopy.

Z.Q. Tian, B. Ren , (2000) "Progress in Surface Raman Spectroscopy" Univ. Press, Xiaman, China.

L. Quin, Z.X. Shen, S.H. Tang, M.H. Kuck,(1997)"The modification of a spectrometer into a micro-Raman spectrometer".

M. Danfus, G. Roberts,(1991) "Femtosecond transition state spectroscopy and chemical reaction dynamics.

G.Goulitzand .Vo.Din,Weinhein,(2003) "Hand Book of spectroscopy ".Edited.Weily-Verlag GmbH and KgaA.

PatricBenziher, (2004) " Athesis of Raman Spectroscopic Investigation of CO_2clathratesFormation" Theohio State University by Patric.

Y.Guan,E.N.Lewis,andLW.Levin, (1999)"Biomedical applications of Raman spectroscopy Tissue differentiation and potential clinical usage,"in"Analytical Applications of Raman Spectroscopy". Oxford, England.

Arpita Das and RunuChakraborty,(2016) ,an Introduction to Sweeteners, Kolkata, India.

Marleen de Veij,a Peter Vandenabeele,etal ,(2008), Reference database of Raman spectra of pharmaceutical excipients, journal of Raman Spectroscopy.

NicoletaTosa, Zaharie Moldovan and IoanBratu,.et.al., (2012), Simultaneous Determination Of Some Artificial Sweeteners In Ternary Formulations By FT-IR And EI-MSAmerican Institute of Physics.

NiculinaPeica,(2009), Identification and characterization of the E951 artificial food sweetener by vibrational spectroscopy and theoretical modelling,Journal of Raman Spectroscopy.

Anna G. Mignani a, Leonardo Ciaccheri.et.al (2014) , Raman spectroscopy for distinguishing the composition of table-top artificial sweeteners, Elsevier.

P.Ramesh, S. Gunasekaran,(2018), Structural, Spectroscopic Investigation and Quantum Chemical Calculation studies on Methyl L-α aspartyl –Lphenylalaninate (Aspartame) for pharmaceutical Application, International Journal of ChemTech Research.

Yuan Xiaojuan, GuHuaimin, Wu Jiwei,(2010), Surface-enhanced Raman spectrum of Gly-Gly adsorbed on the silver colloidal surface, Journal of Molecular Structure,ELSEVIR.

G. Mahalakshmi1, R. Suganya2,etal,(2016), Determination of Structural and Vibrational Spectroscopic Properties of 4-Amino-2, 2, 6, 6- tetramethylpiperidine using FT-IR and FT-Raman Experimental Techniques and Quantum Chemical Calculations, International Journal of Science and Research (IJSR).

EwenS. ,Geoffery D., (2005), Modern Raman Spectroscopy, John Wiely and Sons,Ltd.ISBN 0-471-49668-5.

Nafie A. Almuslet and Mohammed A. Yousif, (2016), Identification Of Groundwater Components In Western Part Of Saudi Arabia Using Raman Spectroscopy, Journal of Multidisciplinary Engineering Science and Technology (JMEST).

Alicia Beatriz Brizuela a, Ana Beatriz Raschietal,(2012), Theoretical structural and vibrational properties of the artificial sweetener sucralose, Elsevier B.V.

NiculinaPeica,(2009), Identification and characterization of the E951 artificial food sweetener by vibrational spectroscopy and theoretical modelling,Journal of Raman Spectroscopy.

Vaclav Ranc, ZdenkaMarkova,etal,(2014) , Magnetically Assisted Surface-Enhanced Raman Scattering Selective Determination of Dopamine in an Artificial Cerebrospinal Fluid and a Mouse Striatum Using Fe3O4/Ag Nanocomposite, American Chemical Society.

Ismail HakkiBoyaci,abHavvaT¨umayTemiz,etal., (2015), Dispersive and FT-Raman spectroscopic methods in food analysis, Royal society of chemistry.

Anna G. Mignani a, Leonardo Ciaccheri(2014)Raman spectroscopy for distinguishing the compositionof table-top artificial sweeteners,ScienceDirect.Elsevier.

Susanne Brunsgaard Hansen, (2000), The Application of Raman Spectroscopy for Analysis of Multi-Component Systems, Hvalsø, Denmark.

Caiqin Han Yue Yao, Wen Wang Lulu, Qu Layne Bradley Shulin Sun YipingZhao(2017), Rapid and Sensitive Detection of Sodium Saccharin in Soft Drinks by Silver Nanorod Array SERS Substrates, Sensors and Actuators B.

G. Mahalakshmi1, R. Suganya2,etal,(2016), Determination of Structural and Vibrational Spectroscopic Properties of 4-Amino-2, 2, 6, 6- tetramethylpiperidine using FT-IR and FT-Raman Experimental Techniques and Quantum Chemical Calculations, International Journal of Science and Research (IJSR).

Vaclav Ranc, ZdenkaMarkova,etal,(2014) , Magnetically Assisted Surface-Enhanced Raman Scattering Selective Determination of Dopamine in an Artificial Cerebrospinal Fluid and a Mouse Striatum Using Fe3O4/Ag Nanocomposite, American Chemical Society.

HARPREET KAUR KHURANA(2008), Application of Multibounce Attenuated Total Reflectance Fourier Transform Infrared Spectroscopy and Chemometrics for Determination of Aspartame in Soft Drinks *J. Agric. Food Chem.,* Vol. 56, No. 3, 2008 783.

SylwesterMazurek.Etal (2011) Quantification of aspartame in commercial sweeteners by FT-Raman spectroscopy, Food Chemistry 125 (2011) 1051‑1057.

Sergio Armenta.Etal .(2004), Sweeteners determination in table top formulations using FT-Raman spectrometry and chemometric analysis, AnalyticaChimicaActa 521 (2004) 149–155.

Da-you Fu .Etal (2014), Fast detection of illegal sweeteners in liquor and wine by laser Raman spectroscopy, Advanced Materials Research Vols. 960-961 (2014) pp 32-38.